

PERFORMANCE ANALYSIS OF GPS ATTITUDE DETERMINATION IN A HYDROGRAPHIC SURVEY LAUNCH

J. P. R. MARREIROS

March 1998



**TECHNICAL REPORT
NO. 191**

PREFACE

In order to make our extensive series of technical reports more readily available, we have scanned the old master copies and produced electronic versions in Portable Document Format. The quality of the images varies depending on the quality of the originals. The images have not been converted to searchable text.

PERFORMANCE ANALYSIS OF GPS ATTITUDE DETERMINATION IN A HYDROGRAPHIC SURVEY LAUNCH

Joao Paulo Ramalho Marreiros

Department of Geodesy and Geomatics Engineering
University of New Brunswick
P.O. Box 4400
Fredericton, N.B.
Canada
E3B 5A3

March 1998

© Paulo Marreiros, 1997

PREFACE

This technical report is an unedited reproduction of a report submitted in partial fulfillment of the requirements for the degree of Master of Engineering in the Department of Geodesy and Geomatics Engineering, September 1997. The research was supervised by Dr. David Wells, and it was supported by Fisheries and Oceans Canada, by the Hydrographic Office of the Portuguese Navy, and by the Natural Sciences and Engineering Research Council of Canada.

As with any copyrighted material, permission to reprint or quote extensively from this report must be received from the author. The citation to this work should appear as follows:

Marreiros, J. P. R. (1998). *Performance Analysis of GPS Attitude Determination in a Hydrographic Survey Launch*. M.Eng. report, Department of Geodesy and Geomatics Engineering Technical Report No. 191, University of New Brunswick, Fredericton, New Brunswick, Canada, 140 pp.

DEDICATION

This report is dedicated to Fátima, my wife, and to Beatriz, my daughter.

For their encouragement and patience.

ABSTRACT

Attitude determination for hydrographic applications, using simultaneous GPS phase measurements from three antennas, has been investigated in this report. Two main issues were addressed: the first deals with GPS carrier phase ambiguity resolution and the second deals with attitude determination from GPS measurements.

Real time attitude determination is required for a number of applications such as hydrographic surveying with multibeam echosounders. Therefore, a technique capable of determining the ambiguities from a single epoch of data within the time interval defined by successive GPS outputs, has been implemented. This technique is a derivation of the least squares search method, extended to use the known baseline length between antennas to reduce the ambiguity search space. The performance of this technique has been evaluated using field data, for an antenna spacing of 2.0 and 4.5 metres. The results indicate that the carrier phase ambiguities were successfully solved, for all the data span, when using dual frequency data from a single epoch. This shows that the technique used is reliable and can be applied to real time attitude determination.

GPS attitude was computed using direct determination of heading, pitch and roll. GPS derived attitude measurements were compared with commercial motion sensor data collected onboard a hydrographic survey launch. This comparison indicates that GPS attitude parameters can be determined with an accuracy of 0.07 degrees for a 4.5 metres baseline length, and 0.20 degrees for 2.0 metres baseline.

ACKNOWLEDGMENT

I thank the Hydrographic Office, Portuguese Navy, for providing the opportunity to undertake this work.

I am particularly indebted to my supervisor, Dr. David Wells, for his support, orientation and helpful comments throughout this investigation, and during my studies at the University of New Brunswick.

The constructive recommendations of the Examining Board have been appreciated and have helped to improve the final version of this report.

I wish to thank the Canadian Hydrographic Service for providing equipment and resources for the collection of the data. Here I would like to thank André Godin and Stephen Parsons, not only for helping in collecting data, but also for the friendship and exciting exchange of ideas.

TABLE OF CONTENTS

	Page
DEDICATION	ii
ABSTRACT	iii
ACKNOWLEDGMENT	iv
TABLE OF CONTENTS	v
LIST OF TABLES	ix
LIST OF FIGURES	x
LIST OF SYMBOLS	xiii
LIST OF ABBREVIATIONS	xvi
1. INTRODUCTION	1
1.1. Motivation	3
1.2. Investigation Procedure	4
1.3. Contributions of this Report	5
1.4. Report Outline	6
2. GPS ATTITUDE DETERMINATION TECHNIQUES	9
2.1. Coordinate Systems Used in Attitude Determination	9
2.2. Definition of Attitude	11
2.3. Parameterization of the Attitude	12
2.4. The Concept of Attitude Determination Using GPS Measurements	14
2.5. Attitude Determination Using the Attitude Matrix	16
2.5.1. Determination of the Attitude Matrix	17
2.6. Attitude Determination Using a Least Squares Approach	19
2.7. Direct Determination of Pitch, Roll and Heading	20

3. COMPENSATION OF SHIP ATTITUDE FOR MULTIBEAM SONAR

SURVEYS	24
3.1. Multibeam Sonar Principles	24
3.2. Depth and Position Errors in MBES	28
3.3. Influence of Attitude Errors in Depth Determination	30
3.4. Influence of Attitude Errors in Position Determination	32
3.5. Attitude Measurement	34
3.5.1. Heading Determination	35
3.5.1.1. Magnetic Compass	35
3.5.1.2. Gyrocompass	36
3.5.2. Inertial Sensors	37
3.5.3. Combining Inertial Sensors in Orthogonal Triads	38
3.5.3.1. GPS Input	41
3.5.4. Inertial Navigation Systems	44
3.5.5. GPS Integrated with Inertial Navigation Systems	46

4. GPS CARRIER PHASE AMBIGUITY RESOLUTION

4.1. Carrier Phase Observation Equations	50
4.1.1. Undifferenced Carrier Phase	50
4.1.2. Carrier Phase Single Differences Between Receivers	52
4.1.3. Carrier Phase Double Differences	53
4.1.4. The Question of Simultaneity	55
4.2. Least Squares Ambiguity Search	57
4.2.1. Ambiguity Search with a Fixed Baseline Length	60
4.2.2. Selection of Primary Satellites	63
4.2.3. Validation of the Estimated Solution	64

5. FACTORS AFFECTING THE ACCURACY OF ATTITUDE

DETERMINATION WITH GPS	68
5.1. Measurement Errors	68

5.1.1. Receiver Specific Errors	68
5.1.2. Antenna Phase Centre Variation and Imaging	71
5.1.3. Carrier Signal Multipath	73
5.1.3.1. Carrier Signal Multipath Detection and Minimization Techniques	75
5.2. Operational Factors	78
5.2.1. Structural Flexing	79
5.2.2. Baseline Length	79
5.2.3. Satellite Number and Geometry	80
5.2.4. Antenna Configuration	82
6. FIELD DATA	84
6.1. Equipment Used	84
6.1.1. Ashetch Z12	85
6.1.2. POS/MV 320	86
6.2. Equipment Installation	87
6.2.1. GPS Antennas	87
6.2.2. Inertial Motion Unit	89
6.3. Data Logging	90
6.4. Problems and Solutions	92
6.4.1. Time Tag	92
6.4.2. Data Gaps	93
6.4.3. Interpolation	93
7. DATA PROCESSING AND RESULTS	97
7.1. Processing GPS Carrier Phase Measurements	97
7.1.1. Using PNAV	98
7.1.2. Instantaneous Ambiguity Resolution	99
7.1.2.1. Using Single Frequency Data	100
7.1.2.1. Using Dual Frequency Data	101

7.2. Comparison between POS/MV 320 and GPS Attitude Measurements . . .	108
8. CONCLUSION	112
8.1 Summary and Discussion	112
8.2 Conclusions	114
8.3 Suggestions for Further Research	116
REFERENCES	117
APPENDIX A - Transformation Between Euler Angles and Pitch, Roll and Heading	124
APPENDIX B - Vessel Attitude Plots	128
APPENDIX C - Vessel Trajectory	131
APPENDIX D - Satellite Configuration	133
APPENDIX E - Attitude Results for the Comparison Between GPS and POS/MV 320	136
VITA	141

LIST OF TABLES

	Page
6.1 Hydrographic launch characteristics	84
6.2 Periods of observation with data from all sensors	91
7.1 Single frequency instantaneous ambiguity resolution results	100
7.2 Dual frequency instantaneous ambiguity resolution results	101
7.3 Processing time and number of epochs versus baseline length error	104
7.4 Comparison between POS/MV 320 and GPS	110

LIST OF FIGURES

	Page
2.1 Attitude parameters used in marine navigation	12
2.2 Determination of the attitude of antenna baselines in the LCS, using GPS measurements	16
2.3 Antenna configuration for direct determination of pitch roll and heading	21
3.1 Calculation of soundings in a MBES	26
3.2 Sensors used in a MBES system onboard	27
3.3 Sensitivity of depth to roll measurement errors	31
3.4 Sensitivity of sounding position to heading errors	33
3.5 Triad of inertial sensors	39
3.6 Accelerometer roll axis misaligned with centripetal acceleration	42
3.7 Block diagram of a motion sensor	43
3.8 Simplified block diagram of a strapdown INS	45
3.9 GPS/INS open loop and closed loop mechanization	48
4.1 The problem of no simultaneity at transmission	56
4.2 Flowchart of the least squares ambiguity searching technique	60
6.1 Antenna layout onboard	88
6.2 Data collection periods for the POS/MV and GPS Ashtech antennae	91
6.3 Error due to linear interpolation of heading, pitch and roll	95
6.4 Error due to cubic spline interpolation of heading, pitch and roll	96

7.1	Frequency distribution of the variance factor	103
7.2	Frequency distribution of the ratio between the two smallest variances	103
7.3	Baseline length derived from GPS measurements	107
7.4	Heading, pitch and roll differences between POS/MV 320 and GPS attitude measurements	109
A.1	Rotations of the BCS to coincide with the LCS	125
A.2	Spherical triangles of rotations	125
B.1	Heading, pitch and roll measured by the POS/MV 320 during period 1	128
B.2	Heading, pitch and roll measured by the POS/MV 320 during period 2	129
B.3	Heading, pitch and roll measured by the POS/MV 320 during period 3	130
C.1	Vessel trajectory for period 1	131
C.2	Vessel trajectory for period 2	132
C.3	Vessel trajectory for period 3	132
D.1	Satellite configuration for period 1	133
D.2	Satellite configuration for period 2	134
D.3	Satellite configuration for period 3	134
D.4	Total number of satellites and PDOP	135
E.1	Velocity, rate of change of heading and attitude differences between POS/MV 320 and GPS during period 1	136
E.2	Velocity, rate of change of heading and attitude differences between POS/MV 320 and GPS during period 2	137
E.3	Velocity, rate of change of heading and attitude differences between POS/MV 320 and GPS during period 3	138
E.4	Rate of change of heading and heading differences, plot 1	139

E.5 Rate of change of heading and heading differences, plot 2	139
E.6 Rate of change of heading and heading differences, plot 3	140
E.7 Rate of change of heading and heading differences, plot 4	140

LIST OF SYMBOLS

- γ - Instantaneous angle between the heading and the tracking of the vessel.
- $\nabla\Delta$ - Double difference operator.
- $\Delta\rho$ - Differential range measurement.
- Δ_I - Difference between ionospheric delays experienced by two carrier signals.
- ΔR - GPS antennae baseline vector.
- δ - Vector of corrections to the parameters in a least squares adjustment.
- δD - Error in the baseline length measurement.
- ε - GPS carrier phase random measurement noise.
- θ - MBES beam incidence angle measured from the vertical.
- Λ - Geodetic longitude.
- λ - GPS carrier phase wavelength.
- ρ - Geometric range between GPS satellite and receiver.
- $\dot{\rho}$ - Geometric range rate between GPS satellite and receiver.
- $\hat{\sigma}_0^2$ - A posteriori variance factor.
- σ_0^2 - A priori variance factor.
- σ - Standard deviation of the beam angle measurement
- $\chi_{df, 1-\alpha}^2$ - Chi-square percentile for df degrees of freedom and the significance level $1-\alpha$.
- ψ - Heading angle.
- Φ - Geodetic latitude.
- φ - Measured GPS carrier phase in units of cycles.
- A - Design matrix.
- a - GPS satellite frequency offset.
- a_c - True centripetal acceleration affecting the vessel.
- a_r - Centripetal acceleration measured by the roll axis of the vessel.
- B - Bandwidth in hertz.
- C - Covariance matrix.
- c - Speed of light in the vacuum.

$C N_0$ - Carrier to noise ratio in a one Hertz bandwidth.
 D - Distance between GPS antennas.
 d - Depth measured from the MBES transducer.
 dt - GPS satellite or receiver clock error.
 e - Direction cosine to GPS satellite.
 f - GPS signal carrier frequency.
 f_D - Doppler frequency.
 h - GPS satellite or receiver hardware delay.
 I - GPS carrier phase ionospheric delay.
 k - Boltzmann's constant ($1.380662 \cdot 10^{-23} \text{ JK}^{-1}$).
 L - Lower triangular matrix resulting from Cholesky decomposition.
 l - Vector of observations.
 M - GPS carrier phase multipath error.
 N - GPS carrier phase ambiguity in units of cycles.
 $nint()$ - Nearest integer operator.
 ns - Number of visible GPS satellites.
 P - Pitch angle.
 P_t - Thermal noise power.
 R - Roll angle.
 r - Slant range from the MBES transducer to a point on the seafloor.
 r_0 - Position vector of the LCS origin, expressed in WGS84 coordinates.
 r_{LCS} - Position vector in LCS coordinates.
 r_{WGS84} - Position vector in WGS 84 cartesian coordinates.
 T - GPS carrier phase tropospheric delay.
 Te - Temperature in degrees Kelvin.
 Tr - Attitude matrix.
 T_E - Rotation matrix about the east axis of the LCS.
 T_U - Rotation matrix about the up axis of the LCS.
 v - Vector of residuals.

w - Misclosure vector.

y - Multibeam sonar across track distance.

LIST OF ABBREVIATIONS

BCS - Body Coordinate System.
BIH - Bureau International de l'Heure.
CPD - Carrier Phase Differential GPS.
CTP - Conventional Terrestrial Pole.
DoD - U.S. Department of Defense.
GDOP - Geometric Dilution of Precision.
GPS - Global Positioning System.
IHO - International Hydrographic Organization.
IMU - Inertial Measurement Unit.
INS - Inertial Navigation Systems.
LCS - Local Coordinate System.
MBES - Multibeam Echosounder.
r.m.s. - root mean square.
S/N - Signal-to-Noise Ratio.
TRS - Terrestrial Reference System.
TWTT - Two Way Travel Time.
UTC - Universal Time Coordinated.
VRU - Vertical Reference Unit.
WGS-84 - World Geodetic System 1984.

Chapter 1

INTRODUCTION

This report investigates the performance of the NAVSTAR Global Positioning System (GPS) for attitude determination of a hydrographic survey launch. The issues affecting the use of GPS for attitude determination addressed in this report can be divided into two areas. The first deals with the GPS signal itself and carrier phase ambiguity resolution. The second issue deals with the determination of attitude from GPS measurements.

The main principle in obtaining attitude from GPS is the determination of baseline vectors between antennas mounted on the vehicle. Due to the short baselines used, common mode errors between satellites and receivers can be eliminated or greatly reduced. Thus, accuracy at the millimetre level in the baseline vector can be achieved. To achieve this accuracy, carrier phase is the only GPS measurement that can be used. The main difficulty in using carrier phase measurements is the resolution of the unknown integer number of cycles, designated as the phase ambiguity.

In a marine environment, the ship can never be static even if it is anchored in the harbor, therefore, the technique of static initialization on the ground cannot be used. On-the-fly ambiguity resolution is required at the beginning of the mission as well as when cycle slips occur on most of the satellites simultaneously. Some kinematic positioning methods resolve the carrier ambiguity on-the-fly but require a period of data collection at the beginning of mission or when a loss of signal occurs in order to produce a valid

solution. Such periods of initialization may impose severe restrictions to efficiently execute the mission if frequent loss of signal occurs. In kinematic applications the solution is required in real time and the processing time should be less than the observation update rate. Therefore, a key requirement in real time kinematic attitude determination with GPS is the instantaneous resolution of the carrier phase ambiguities. The term “instantaneous” will be used as meaning that ambiguities are to be solved using data of a single epoch within the time interval given by the data rate. The first objective of this study is to instantaneously determine the relative positioning vector between two closely spaced antennas mounted aboard a small hydrographic launch.

Once the carrier phase ambiguities are solved, attitude parameters can be determined from differential range measurements or from vector observations. This report briefly describes attitude determination techniques using GPS measurements. No attempt has been made, however, to evaluate the performance of each technique. Such a study has been done previously by Lu et al. [1993] and Mowafy [1994]. Furthermore, the number of available GPS receivers used for data collection were limited to three, and their respective coordinates in a body reference frame were not measured, which imposes some restrictions on testing some attitude determination methods.

The second objective of this study is to assess the accuracy of attitude results from a three antenna GPS attitude sensor. This was achieved by assessing the compatibility of the three-antenna GPS attitude results with attitude measurements using a commercial GPS aided Inertial Navigation System (INS).

1.1 Motivation

Hydrographic surveying with MBES has many advantages, when compared with conventional single beam echosounders. Unlike single beam echosounders, MBES are designed for 100% coverage of the seafloor with a wide swath. In order to produce valid and accurate depth soundings, MBES require the measurement of ship's orientation, namely pitch, roll and heading. To obtain the full MBES bathymetric accuracy possible, a high precision motion sensor should be used.

Although developed as a means for navigation, GPS can be used as a source of directional information taking advantage of the submillimetre accuracy of carrier phase measurements. In the marine field this technology has applications in navigation (GPS heading), to aim antennas or other directional devices (weaponry) and eventually any application requiring precise directional measurements, given the trend in lowering the cost, size, weight and power of GPS technology.

The use of a standalone GPS attitude system for motion compensation of MBES is constrained by its limited update rate (less than 10 Hz) which leads to an insufficient sampling of the attitude parameters. Modern motion compensation of MBES uses a dual antenna GPS integrated with an INS [Applied Analytics, 1996a; Seatex, 1996b]. The function of the dual antenna is to measure heading and provide position and velocity updates to control the error of the INS. To effectively produce accurate results that can be used in real time, carrier phase ambiguities must be solved instantaneously.

The accuracy of a dual antenna GPS/INS motion sensor, as stated by the

manufacturer, should be tested under the dynamic conditions for which the system was designed. Such a test can be done by comparing results from a dual antenna GPS/INS system, with a standalone GPS attitude sensor, since the accuracy of GPS attitude results can be predicted by propagating the error of carrier phase measurements.

1.2 Investigation Procedure

The investigation procedure followed for this report was developed to evaluate the viability of using GPS as an attitude sensor for a hydrographic survey launch. This consisted of collecting data, processing carrier phase measurements to determine baseline vectors, and comparing GPS attitude results with a commercial GPS/INS attitude sensor.

Field data were collected in a hydrographic survey launch using three GPS Ashtech Z12 receivers. The survey launch was equipped with a MBES which has an ancillary motion sensor POS/MV 320 [Applied Analytics, 1996a].

The processing of GPS carrier phase measurements was done using PNAV software (Precise Differential GPS Navigation and Surveying), which is a precision trajectory package providing post-processed positions. PNAV can provide centimetre level accuracy on-the-fly [Ashtech, 1993]. Such software, however, was not developed for attitude determination, does not allow the use of geometric constraints to accelerate and improve carrier phase ambiguity resolution, and does not solve the ambiguities using data from a single epoch. For this reason a computer program was written in C++ language, using the algorithm described by Lu and Cannon [1994] to efficiently and instantaneously determine

the baseline vector using carrier phase measurements.

Once the baseline vectors were determined, attitude measurements were computed and compared with attitude measurements measured by the POS/MV 320.

1.3 Contributions of this Report

The contributions of this research can be summarized as follows:

- The methods used to measure attitude for motion compensation of MBES are described.
- Although GPS attitude determination in a marine vessel has been tested in a number of previous works, this report confirms the ability of GPS to measure ship's attitude.
- GPS attitude results are compared with a new motion sensor used for motion compensation of modern MBES.
- The least squares ambiguity search method [Hatch, 1990] with a fixed baseline length [Lu and Cannon, 1994] was implemented in a computer program used to determine the relative position vector between two antennas.
- The influence of baseline length error bound in the definition of the ambiguity search space was tested. Experimental results show that an error bound too small may cause instantaneous ambiguity resolution to fail, due to GPS carrier phase measurement errors.
- The ability of solving GPS carrier phase ambiguity using data from a single epoch was investigated. This report clearly demonstrates that, for small baselines,

instantaneous ambiguity resolution is possible and reliable when using dual frequency observations and more than six satellites are being tracked.

1.4 Report Outline

Chapter 1 has been an introductory section outlining the framework of this study. This chapter has introduced the motivation behind the investigation and sketched the investigation procedure followed. The contributions of this report have been elucidated and the structure of the written work has been described.

Chapter 2 briefly reviews fundamental aspects of attitude determination from GPS measurements. This chapter specifies the coordinate systems used in attitude determination with GPS, defines the term “attitude” and describes alternative methods of attitude parameterization. Next, the concept of attitude determination using GPS measurements is introduced. Finally, attitude determination techniques are briefly described. This includes the use of the attitude matrix, the least squares approach and direct determination of pitch, roll and heading.

Chapter 3 defines the accuracy requirements and attitude measurement techniques used for marine motion compensation. The multibeam sonar principles are introduced and the various error sources in multibeam sonar surveys are described with emphasis on attitude measurement errors. The last section briefly describes marine motion sensors. This includes heading sensors, inertial sensors and GPS integrated with INS, which is the sensor used in this research to compare with the standalone GPS attitude system.

Chapter 4 is focused on instantaneous ambiguity resolution using a least squares technique. GPS carrier phase observable and its observation equations are introduced and the question of simultaneity between two receivers tracking the same satellites is addressed. The least squares ambiguity resolution technique is described, as well as an efficient method of determining the search space on a sphere defined by the known baseline length between two antennas [Lu and Cannon, 1994]. The problems of satellite selection and validation of the estimated solution are also addressed.

Chapter 5 describes the main factors affecting accuracy of attitude determination from a multi-antenna GPS. These factors were divided into measurement errors and operational factors. The first category comprises receiver specific errors, antenna phase center variation and multipath propagation. The second category addresses operational factors such as baseline length, structural flexing, satellite geometry and antenna configuration.

Chapter 6 deals with the collection of field data onboard a hydrographic survey launch. The chapter describes the equipment used, its installation aboard and data collection methodology. The last section deals with time tagging of data from different sensors, gaps in the data set and interpolation.

Chapter 7 describes the processing of the data collected on the field. The processing was done in two steps. First, GPS carrier phase measurements were used to derive the relative position vector between antennas and the performance of instantaneous ambiguity resolution is analyzed. Second, relative position vectors were used to determine the vessel's attitude, which was then compared with interpolated POS/MV 320 measurements.

Chapter 8 contains the conclusions of this report, where a summary is given as well as a discussion of the issues that were raised during this investigation. The chapter ends with suggestions for future research in this field.

Chapter 2

GPS ATTITUDE DETERMINATION TECHNIQUES

This chapter describes different techniques that can be used for attitude determination using GPS measurements. These techniques are: computation of Euler angles using the attitude matrix, least squares estimation of Euler angles and direct estimation of heading pitch and roll. The chapter starts by specifying the coordinate systems used in attitude determination with GPS, defining the term “attitude” and describing alternative methods of attitude parameterization. Then, the concept of attitude determination using GPS measurements is introduced. Finally, each attitude determination technique is briefly described.

2.1 Coordinate Systems Used in Attitude Determination

In this section we introduce three coordinate systems used in attitude determination with GPS. These coordinate systems are the Terrestrial Reference System (TRS), the Local Coordinate System (LCS) and the Body Coordinate System (BCS).

The definition of a TRS must account for the motion of the rotation axis of the earth with respect to the crust. The TRS used by the U.S. Department of Defense (DoD) for GPS positioning is the World Geodetic System (WGS-84). The axes and origin of this coordinate system are defined as follows [Leick, 1995]:

- Origin: at the centre of mass of the earth.

- Z axis: pointing towards the Conventional Terrestrial Pole (CTP) as defined by the Bureau International de l'Heure (BIH), predecessor of the International Earth Rotation Service, for the epoch 1984.0.
- X axis: intersection of the reference meridian plane and the equatorial plane defined by the CTP, where the reference meridian is the meridian of Greenwich, defined by the BIH for the epoch 1984.0.
- Y axis: completes a right handed system, and lies in the equatorial plane defined by the CTP.

The definition of the LCS used in this report corresponds to the Local Geodetic System as defined by Vanicek and Krakiwsky [1986]:

- Origin: at a reference point in the rigid body.
- Z axis or U: defined as the outward ellipsoid normal.
- X axis or N: points in the North direction, tangent to the ellipsoidal meridian, in the plane of the ellipsoidal horizon.
- Y axis or E: points towards the East direction in the plane of the ellipsoidal horizon.

There are many possible realizations of the BCS. The most common convention consists of an orthogonal triad of axes which are oriented as follows for convenience:

- Origin: identical to the LCS. This eliminates the need to determine the shift vector between the two origins.
- z axis: the same orientation as for the U axis of the LCS, when the roll and pitch angles are equal to zero.

- x axis: parallel to the longitudinal axis of the vessel, pointing towards the bow.
- y axis: pointing to starboard.

With this definition the BCS coincides with the LCS, when the vessel is pointing north and roll and pitch angles, as defined in section 2.2, are equal to zero.

2.2 Definition of Attitude

The attitude of a rigid body is defined as its orientation in space with respect to a well defined and stable coordinate system [Mowafy, 1994]. A rigid body is a system of mass points with finite dimensions, such that the distance between all pairs of points remain constant under rotations and translations [Goldstein, 1950].

The configuration of a rigid body can be specified by a coordinate system attached to the body structure. This coordinate system is defined by the BCS. With this coordinate system the position of each particle of the rigid body is invariant in time. The orientation of the BCS with respect to a well defined coordinate system of the external space defines the attitude of the rigid body.

In a marine environment is important to define the attitude of a rigid body with reference to a locally level coordinate system, defined by the LCS. Using nautical terminology, the attitude of a marine vessel is described by heading, pitch and roll.

Heading, pitch and roll are defined as follows (see figure 2.1):

heading (ψ): the angle between the north axis of the LCS and the projection of the x axis of the BCS on the horizontal plane. It is positive in clockwise direction when

viewed from the upward direction of the z axis of the BCS. Yaw is an orientation angle defined in the horizontal plane, as heading, but instead of being referenced to the N axis, usually refers to variations from a nominal, averaged or planned heading.

- pitch (P): the elevation angle of the x axis of the BCS from the LCS xy plane. It is positive when the positive part of the BCS x axis is tilted above the LCS xy plane.
- roll (R): the elevation of the y axis of the BCS from the LCS xy plane. It is positive when the positive part of the BCS y axis is tilted below the LCS xy plane.

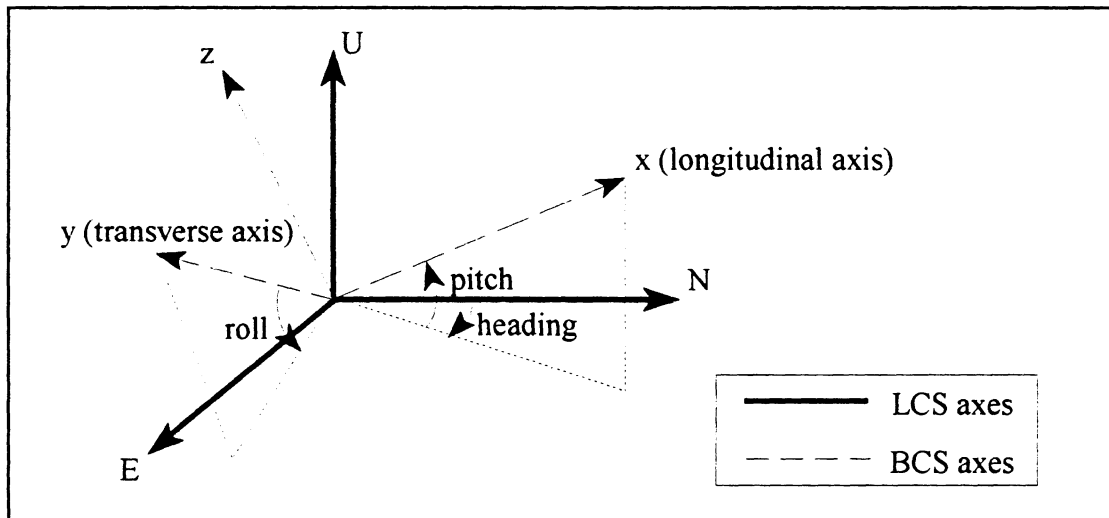


Figure 2.1 - Attitude parameters used in marine navigation.

2.3 Parameterization of the Attitude

The determination of the orientation of the BCS with relation to the LCS requires nine parameters, which can be regarded as the elements of a 3×3 matrix, called the attitude

matrix [Wertz, 1978]. The attitude matrix is a real orthogonal matrix. Its elements are not all independent, and theoretically, it is based on only three independent parameters. The attitude matrix is often called the direction cosine matrix because of its elements are the cosine of the angle between a BCS coordinate axis and a LCS coordinate axis.

Parameterization of the attitude can also be done in other ways. Among the methods used to represent a three axis attitude are the Cayley axis/angle, the Euler symmetric parameters (quaternions) and the Euler angles [Wertz, 1978].

From all the alternative attitude representations, the Euler angle representation is the one with most geometrical significance, and which is most often used in attitude determination with GPS [Roth and Singh, 1986; Graas and Braasch, 1992; Lu et al., 1994; Cohen, 1996]. Euler angles can be described as three rotation angles around each of the three coordinate axes, or alternatively as first and third rotations about the same axis and a second rotation about one of the other axes. There are twelve possible sequence of rotations, each one with a distinct transformation matrix form [Wertz, 1978].

Euler angles, determined from the attitude matrix are often called heading, pitch and roll. This is misleading since these terms do not have the same meaning as the attitude parameters defined in section 2.2. The attitude matrix is the matrix product of three elementary rotation matrices which describe successive rotations about each of the axes of the BCS. Thus, the Euler angles after each rotation refer to the new orientation of the BCS with respect to the LCS. Roll, pitch and heading Euler angles are dependent on the sequence of rotation used. To be compatible with heading, pitch and roll as defined above, Euler angles must be corrected. The most commonly used sequence of rotations is heading,

then pitch and then roll, for the transformation of LCS to BCS coordinates (Tate-Bryant sequence of rotation [Applied Analytics, 1996b]). In this case the Euler “heading” and “pitch” angles are the same as defined in section 2.2, and only the Euler “roll” angle needs to be corrected according to the following equation, as derived in Appendix A, where R_E stands for Euler “roll” angle:

$$\tan(R) = \frac{\tan(R_E)}{\cos(P)} \quad (2.1)$$

Equation (2.1) is equivalent to one presented by Mowafy [1994] using a different derivation process than the one described in Appendix A. Equation (2.1) shows that the difference between the Euler roll angle and the roll angle is dependent on pitch and roll magnitudes. For small angles (less than five degrees) the difference between the two angles is less than 0.02° . As the angles grow, however, the difference increases and can reach the degree level.

The requirement for roll accuracy for multibeam applications is much more demanding than for heading or pitch, as described in section 3.3. Care must be taken to make sure the correct attitude angle is given by the output of the motion sensor of a MBES.

2.4 The Concept of Attitude Determination Using GPS Measurements

The principle of determining orientation of an antenna baseline from GPS measurements, as sketched in figure 2.3, uses the satellites as reference points with known positions. By measuring ranges between the antennas, the relative positions of the antennas

are determined in WGS-84 coordinates. These relative positions are sufficient to determine the baseline orientation with reference to the WGS-84. To obtain baseline orientation with reference to a LCS, the relative antenna positions must be transformed to LCS coordinates. One of the antennas can be selected as the origin of the LCS and its WGS-84 coordinates can be determined using GPS methods. In this case, the LCS is re-defined for each epoch, since its origin and orientation depends on the geodetic position of the reference point of the platform. The antenna baseline in LCS coordinates can be obtained by using the following transformation equation:

$$\vec{r}_{WGS84} = T_U(\Lambda - 180)T_E(\Phi - 90)\vec{r}_{LCS} + \vec{r}_0 \quad (2.2)$$

where r_{WGS84} is the position vector in WGS 84 Cartesian coordinates,

r_{LCS} is the position vector in LCS coordinates,

T_U is the rotation matrix about the up axis of the LCS,

T_E is the rotation matrix about the east axis of the LCS,

Λ is the geodetic longitude,

Φ is the geodetic latitude,

r_0 is the position vector of the LCS origin, expressed in WGS84 coordinates.

In GPS attitude determination, the BCS coordinates are known a priori and LCS coordinates are derived from GPS measurements. The transformation between LCS and BCS coordinates is unknown. This transformation is the attitude matrix, which is required to derive attitude parameters.

A GPS attitude system is composed of multiple antennas. At least two noncolinear

baselines are required in order to determine the attitude matrix. More details about the determination of the attitude matrix and derivation of attitude parameters are given in section 2.5.

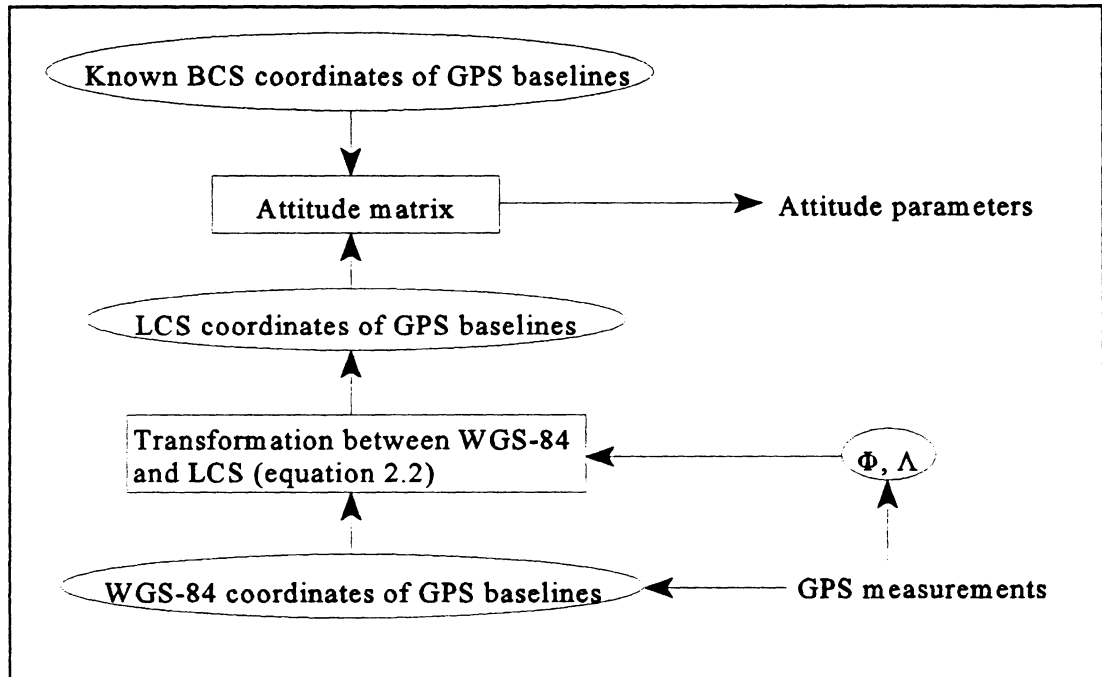


Figure 2.2 - Determination of the attitude of antenna baselines in the LCS using GPS measurements.

2.5 Attitude Determination Using the Attitude Matrix

The attitude matrix that defines the transformation between the BCS and LCS can be used to determine the attitude parameters. Using Euler angles for attitude parameterization, the transformation matrix can take twelve distinct forms. If the angle sequence is known, the three rotation angles can be determined by solving trigonometric functions of the attitude matrix. If the sequence of rotation is assumed to be heading-pitch-

roll, the attitude matrix takes the form [Wertz, 1978]:

$$Tr_{\psi-P-R} = \begin{bmatrix} c(R_E)c(\psi_E) - s(R_E)s(P_E)s(\psi_E) & c(R_E)s(\psi_E) - s(R_E)s(P_E)s(\psi_E) & -s(R_E)c(P_E) \\ -c(R_E)s(\psi_E) & c(R_E)c(\psi_E) & s(P_E) \\ s(R_E)c(\psi_E) + c(R_E)s(P_E)c(\psi_E) & s(R_E)s(\psi_E) - c(R_E)s(P_E)Sc\psi_E & c(R_E)c(P_E) \end{bmatrix} \quad (2.3)$$

where $s()$ and $c()$ stand for the sine and cosine functions, respectively.

If the attitude matrix is known and assuming a sequence of rotation heading-pitch-roll, then the three Euler angles can be determined from the following equations:

$$\begin{aligned} P_E &= \text{asin}(Tr_{23}) \\ \psi_E &= \text{acos}\left(\frac{Tr_{22}}{\cos(P_E)}\right) \\ R_E &= \text{acos}\left(\frac{Tr_{33}}{\cos(P_E)}\right) \end{aligned} \quad (2.4)$$

For pitch equal to 90° the heading and roll angles can not be recovered, however this is a very unlikely situation to occur in marine navigation. The location of the antennas onboard need only to be non-colinear, however, this technique requires the determination of the antennae BCS coordinates in a pre-survey mode.

2.5.1 Determination of the Attitude Matrix

The attitude determination technique described in this section obviously requires the determination of the attitude matrix. The problem of attitude determination using vector observations was first formulated by Wahba [1965], and was posed as follows: Find the rotation matrix (orthogonal matrix and with determinant +1) that minimizes the cost

function:

$$C(Tr) = \sum_{i=1}^{ns} (\Delta \vec{R}_{LCS}^i - Tr \cdot \Delta \vec{R}_{BCS}^i)^2 \quad (2.5)$$

where ΔR stands for the baseline vectors in LCS or BCS coordinates according to the subscripts and ns is the number of visible satellites. There are many efficient algorithms to solve this problem [Bar-Itzhack and Reiner, 1984]. The problem was first solved by Wahba et al. [1965] who derived the following matrix equation:

$$\begin{aligned} Tr &= (VU^TUV^T)^{1/2}(UV^T)^{-1} \\ U &= [\Delta \vec{R}_{BCS}^1, \dots, \Delta \vec{R}_{BCS}^{ns}] \\ V &= [\Delta \vec{R}_{LCS}^1, \dots, \Delta \vec{R}_{LCS}^{ns}] \end{aligned} \quad (2.6)$$

This equation has no solution in cases where the antennae baseline array is coplanar in the BCS and the attitude matrix is treated as a nine independent parameter matrix.

Instead of vector observations, the optimal solution for the attitude matrix can be determined from differential range measurements [Cohen, 1996]. Then, the cost defined above transforms into the following expression:

$$C(Tr) = \sum_{i=1}^{ns} (\Delta \rho_{ij} - \Delta \vec{R}_i^{BCS} \cdot Tr \cdot \vec{e}_j)^2 \quad (2.7)$$

where $\Delta \rho_{ij}$ is the differential range for baseline i and satellite j , and e_j is the pointing vector to satellite j . Given an estimate of the attitude matrix Tr_0 , the problem of finding the attitude matrix is posed as follows: Find the best value of angle γ such that the new rotation matrix defined by equation (2.8) has the minimum cost function.

$$Tr' = \begin{bmatrix} \cos\gamma & \sin\gamma & 0 \\ -\sin\gamma & \cos\gamma & 0 \\ 0 & 0 & 1 \end{bmatrix} Tr_0 \quad (2.8)$$

A description of the algorithm is given in Conway et al.[1996]. The process requires only one iteration and is executed for each rotation around the three axes.

2.6 Attitude Determination Using a Least Squares Approach

The least squares adjustment approach estimates the value of the Euler angles that best fits the measurements. As pointed out by Mowafy [1994], the basic difference between this approach and the one that estimates the Euler angles using the attitude matrix, is that the “Euler angles are treated as unknowns that should have a unique value which best fits the measurements regardless of the transformation model used”.

The attitude matrix can be defined solely by the three Euler angles. Therefore, only three elements are independent. If the BCS coordinates for each antenna are known a priori, an observation equation model is described by the following expression:

$$\vec{R}_{LCS} = Tr(\psi_{E^*} P_{E^*} R_E) \cdot \vec{R}_{BCS} \quad (2.9)$$

If, instead of the BCS coordinates for each antenna, differential range measurements have been made for each independent antenna baseline, the observation equation model is described by the following expression:

$$\Delta\rho = \Delta\vec{R}_{BCS} \cdot Tr(\psi_{E^*} P_{E^*} R_E) \cdot \vec{e}_{LCS} \quad (2.10)$$

Equation (2.9) describes an explicit relationship between the observations, LCS coordinates of the GPS antennas and the parameters (the three Euler angles). Another relationship between the observations and attitude parameters is expressed by equation (2.10), using differential range measurements. Both equations represent a model that can be used in a standard parametric least squares adjustment [Vanicek and Krakiwsky, 1986]. The solution of the least squares attitude determination problem, including linearization of the observation equations, is described in [Mowafy, 1994].

The least squares estimation gives the best estimates based on all the position information contained in a multiple GPS antenna array and the attitude solution is less affected by multipath on a single antenna since the solution is made by the best fit of all antenna positions [Lu et al., 1993].

2.7 Direct Determination of Pitch, Roll and Heading

It is possible to determine pitch, roll and heading (Euler angles) directly from the antenna vectors in the LCS. In this method one of the antenna baselines must be placed lying in the xz or yz plane of the BCS, assuming the origin of the BCS at one reference antenna. Lets assume an antenna configuration with one of the baselines lying in the yz plane as described in Figure 2.3.

The angle of inclination of this baseline with relation to plane xy of the BCS is given by the value β_1 . The inclination of the plane defined by the three antennas with relation to the x axis of the BCS is represented by β_2 . The value of these two angles are

constant (assuming a rigid antenna configuration) and are estimated after the installation of the antennas aboard.

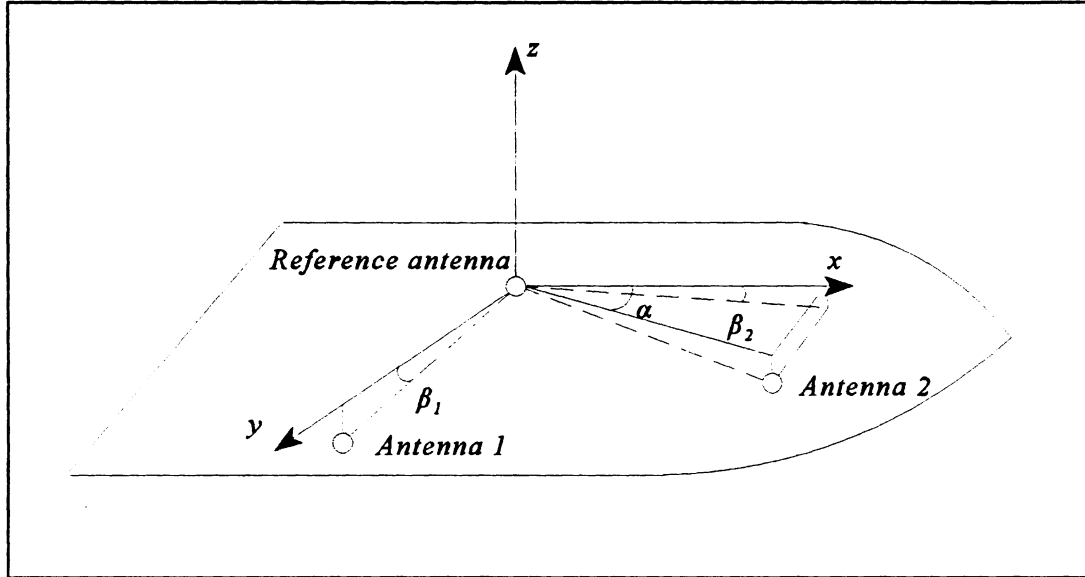


Figure 2.3 - Antenna configuration for direct determination of pitch, roll and heading.

The heading and roll components are estimated directly from the LCS coordinates of *antenna 1* relative to the reference antenna, using the equations:

$$\psi = \text{atan} \left(\frac{y_1}{x_1} \right) - 90^\circ \quad (2.11)$$

$$R = \text{atan} \left(\frac{z_1}{\sqrt{x_1^2 + y_1^2}} \right) - \beta_1 \quad (2.12)$$

Once the heading and roll are obtained, the LCS coordinates of *antenna 2* relative to the reference antenna are first rotated with respect to the U axis by the heading, and then rotated again around the rotated N axis by roll. After these two rotations the coordinates of

antenna 2 will become x_2', y_2' and z_2' :

$$\begin{bmatrix} x_2' \\ y_2' \\ z_2' \end{bmatrix} = T_x(R) \cdot T_z(\psi) \cdot \begin{bmatrix} x_2 \\ y_2 \\ z_2 \end{bmatrix} \quad (2.13)$$

where $T_x()$ and $T_z()$ represent the rotation matrices around the z axis and x axis of the BCS, respectively. After this transformation the pitch angle is given by the following equation [Lu et al., 1994]:

$$P = -\text{atan} \left(\frac{z_2'}{x_2'} \right) - \beta_2 \quad (2.14)$$

The above method uses only the coordinates of three antennas and it does not require the BCS coordinates. If more antennas are available then the method is inappropriate, since it is not designed to handle redundant baselines.

The accuracy of the computed heading, roll and pitch can be estimated by differentiating equations (2.19), (2.20) and (2.21) with respect to x , y and z and applying the error propagation law to the resulting differentiated equations. The accuracy of the estimated attitude parameters can be approximated by [Lu et al., 1994]:

$$\sigma_\psi < \frac{\sigma_{\max}(x,y)}{D_1 \cos(P)} \quad (2.15)$$

$$\sigma_R < \frac{\sigma_{\max}(x,y,z)}{D_1} \quad (2.16)$$

$$\sigma_P < \frac{\sigma_{\max}(x,z)}{D_2 \cos(\alpha)} \quad (2.17)$$

where σ stands for standard deviation, D_1 and D_2 represent the baseline length between the reference antenna and antennas 1 and 2 respectively and α is the angle in the horizontal plane between baseline 2 and the longitudinal axis of the vessel as shown in Figure 2.3.

During field data collection only three GPS antennas were available and the BCS coordinates of these antennas were unknown (see sections 6.1 and 6.2). Therefore, direct determination of pitch heading and roll was the method used to compute attitude from GPS measurements. Heading, pitch and roll estimates using this method were compared with heading, pitch and roll measurements from a commercial GPS/INS motion sensor. Results of the comparison between the two systems are shown in section 7.2.

Chapter 3

COMPENSATION OF SHIP ATTITUDE FOR MULTIBEAM SONAR SURVEYS

Multibeam echosounder systems are designed to acquire hydrographic data, allowing the production of maps with better quality than before, not because each sounding is more accurate, but because of the dense sounding pattern. This technology has the potential for efficient and economic hydrographic surveys. However, accurate attitude measurements are required in order to achieve the accuracy standards established by the International Hydrographic Organization (IHO) for depth and position of soundings.

This chapter has two main objectives. The first is to study the influence of attitude measurement errors on the depth and position determination of soundings. The second objective is to describe attitude measurement methods used for motion compensation of multibeam sonar systems. The first section introduces the multibeam sonar principles. The second section describes the various error sources in surveys with multibeam sonar systems. The third and fourth sections deal with the mapping of attitude measurement errors into depth and position errors in the bathymetric data set. The last section describes methods of attitude measurement used for motion compensation of multibeam sonar surveys.

3.1 Multibeam Sonar Principles

Multibeam echosounders (MBES) are quite different from conventional single beam echosounders, in their principle of operation and also in the way they are constructed.

A conventional echosounder measures depths by transmitting down towards the bottom. Some of the energy hitting the bottom is reflected back so that it can be detected by the echosounder. The depth under the survey vessel is calculated from the two way travel time (TWTT) and the mean speed of sound through the water column. In this way a vessel with a single beam echosounder produces a line of soundings and a map can be constructed by interpolating the depth values between several survey lines.

A MBES uses an array or multiple arrays of transducer elements to form a wide fan of narrow beams on the seafloor, in a swath that varies as a function of system type and water depth (typically with a beam-width of 90° to 150° athwartships). The transmitted pulse is narrow in the fore-aft direction and is wide in the athwartships direction. In contrast, during reception of the backscattered energy, several beams are electronically formed, which are broad in the fore-aft direction and narrow in the athwartships direction. The resulting insonified area is equivalent to the intersection between the received and transmitted beams, which can be reasonably approximated by a set of overlapping ellipses. In this manner many depth soundings are generated in the athwartships direction for each transmitted pulse.

Each received beam produces one TWTT, and this measurement is converted into a depth measurement value and a crosstrack position of the sounding by a simple calculation (see figure 3.1):

$$\begin{aligned}d &= r \cdot \cos(\theta) \\ y &= r \cdot \sin(\theta)\end{aligned}\tag{3.1}$$

where d is the measured depth with relation to the transducer, y is the crosstrack distance,

θ is the beam geometric angle with respect to the vertical, and r is the geometric range.

The determination of the geometric range and beam geometric angle requires the knowledge of the sound speed in the water. For a homogeneous water mass (constant sound speed in all directions), the geometric beam angle corresponds to the transmitted beam angle and the geometric range is equal to half the TWTT multiplied by the sound speed.

For a non homogeneous water mass, the sound speed profile has temporal and spatial variations that must be accounted for. A single beam echosounder, requires only the harmonic mean speed of sound through the water column, since the ray path is assumed to be vertical with reference to stratified water column layers. This simplification does not apply to MBES, which have beams that are inclined with relation to the vertical. Due to refraction, the beam angle inclination varies as the sound speed profile along the ray path changes. Therefore, an imperfect knowledge of sound speed profiles may introduce errors in the determination of the geometric beam angle and geometric range. This will lead to incorrect determination of depth and position of a sounding.

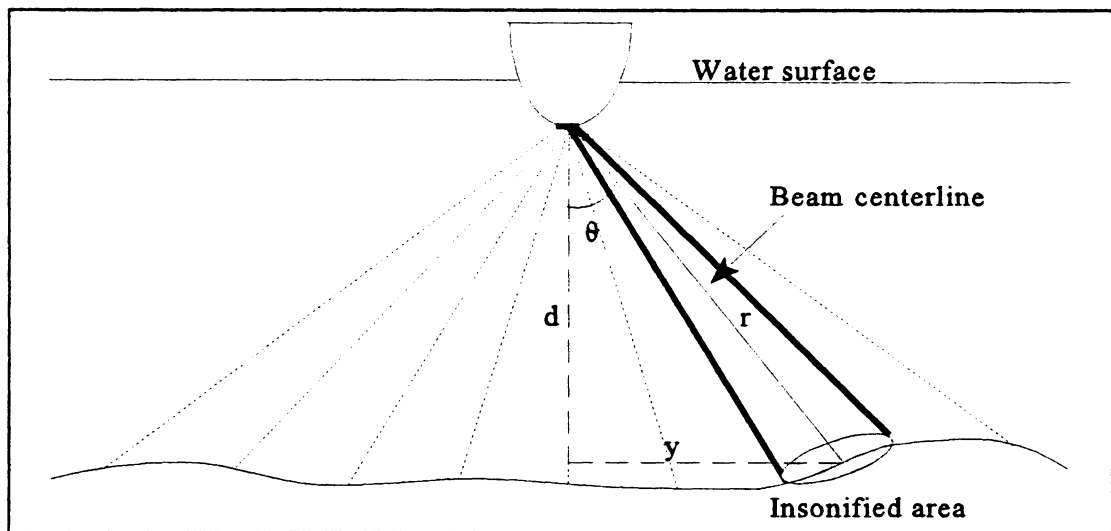


Figure 3.1- Calculation of soundings in a MBES.

A multibeam echosounder produces a dense pattern of depth soundings that covers a wide swath for each survey line. By adjusting the survey line spacing so that adjacent swaths are slightly overlapping, the whole area to be mapped is covered by the sounding pattern and virtually no interpolation between soundings is required to generate a bathymetric map. This survey practice removes all uncertainty related to interpolation, and gives more guarantee that all underwater obstacles and features are detected than surveying with single beam echosounders.

In order to arrive at a complete georeferenced sounding solution, a MBES requires the integration of external sensor information with the sonar relative bearing and TWTT. These sensors are (see figure 3.2):

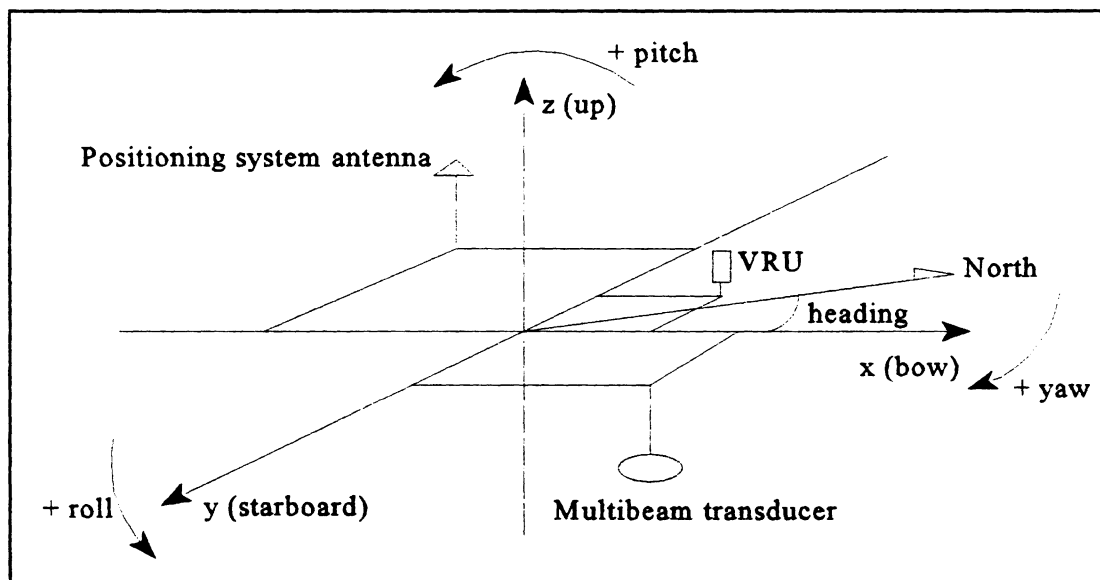


Figure 3.2 - Sensors used in a MBES system onboard. The arrows indicate positive directions following the definition of the BCS in the previous chapter.

- Positioning system: provides horizontal positioning.
- Vertical Reference Unit (VRU): provides heave, pitch and roll information.

- Gyrocompass or GPS heading system: provides heading information.
- Sound velocity profiler.
- Tide gauge or Real Time Kinematic DGPS: provides water level information.

Complete integration of all the ancillary sensors is required to obtain the full sounding solution from a MBES. This integration must account for the location, misalignment and time delays of the various instruments with respect to the BCS.

3.2 Depth and Position Errors in MBES

The errors in the multibeam data set can be divided into three types: gross errors, systematic errors and random errors. Gross errors are obvious major mistakes which are easily detected and corrected. Systematic errors tend to follow a functional relationship and can be, to some extent, predictable. Random errors have incoherent behaviour and are assumed to follow a Normal distribution.

There are more possible sources of measurement errors (systematic and random) for a MBES than for a conventional survey with a single beam echosounder. Common contributions for both instrument types are:

- echosounder instrument error.
- errors in tide and heave measurement.
- positioning errors.
- mean sound velocity error.

With the MBES, there are additional error sources:

- attitude measurement errors. Attitude determination is not required for single beam echosounders since the beam angle is wide enough (beamwidths as large as 30° are common) to ensure that some energy has been radiated toward the seabottom in the direction of the transducer nadir.
- sound velocity profile errors.

The errors resulting from these sources can be divided into two main categories: depth errors and position errors. Each category is further divided into the sub-component contributors [Hare, 1995]. The total error budget in depth measurement is made up of the following components:

- sounder system error (includes TWTT and beam angle measurement errors and uncertainty due to beam width resolution).
- roll error (includes roll measurement and misalignment errors).
- pitch error (includes pitch measurement, misalignment and mechanical stabilization errors).
- heave error (includes errors due to heave measurement and induced heave due to errors in the measurement of pitch and roll as well as errors in the measuring of the coordinate offset between transducer and motion sensor).
- refraction error (includes effect of sound speed profiles on ray-traced range determination and beam angle)
- The reduced depth error should include the errors due to water level and dynamic draught measurement.

The total error budget for positioning a sounding on the seafloor is made up of the

following components:

- Positioning system error.
- Errors in the knowledge of the positioning system latency.
- Relative transducer-sounding positioning error (due to range and beam angle measurement, roll, pitch and transducer misalignment errors).
- Heading error.
- Relative antenna-transducer position error (due to offset and pitch and roll measurement errors).

Hare et al.[1995] estimated the accuracy of Canadian MBES systems SIMRAD EM-1000 and EM-100 onboard the hydrographic vessels NCS *F.G. Creed* and CSS *Matthew*. Different scenarios were assumed and from the analysis of results it is clear that the depth accuracy degrades as a function of swath width and that IHO accuracy standard specifications cannot be met for the full swath width of the system mainly due to errors in roll measurements and refraction.

For the sounding position error budget, the positioning system dominates all the error sources for the inner beams but heading errors in the outer beams cause the position error to more than double [Hare et al.,1995].

3.3 Influence of Attitude Errors in Depth Determination

In this section attitude errors will be examined separately from the other error sources to study their effects on depth. The error equations are derived in Hare [1995]. The

effect of roll error on depth is given by the following equation:

$$\sigma_{d_\theta} = r \sin(\theta) \cos(P) \sigma_\theta \quad (3.2)$$

Figure 3.3 shows that errors in the outer beams grow rapidly with increasing roll measurement error. If not corrected, roll measurement errors can dominate all the error sources for the outer beams. Even an error of 0.5° can contribute more than one percent of depth error for beam angles greater than 45° . For a beam width of 75° , the maximum allowable error in roll is 0.05° , in order to accomplish the IHO accuracy standards [Loncarevic and Scherzinger, 1994].

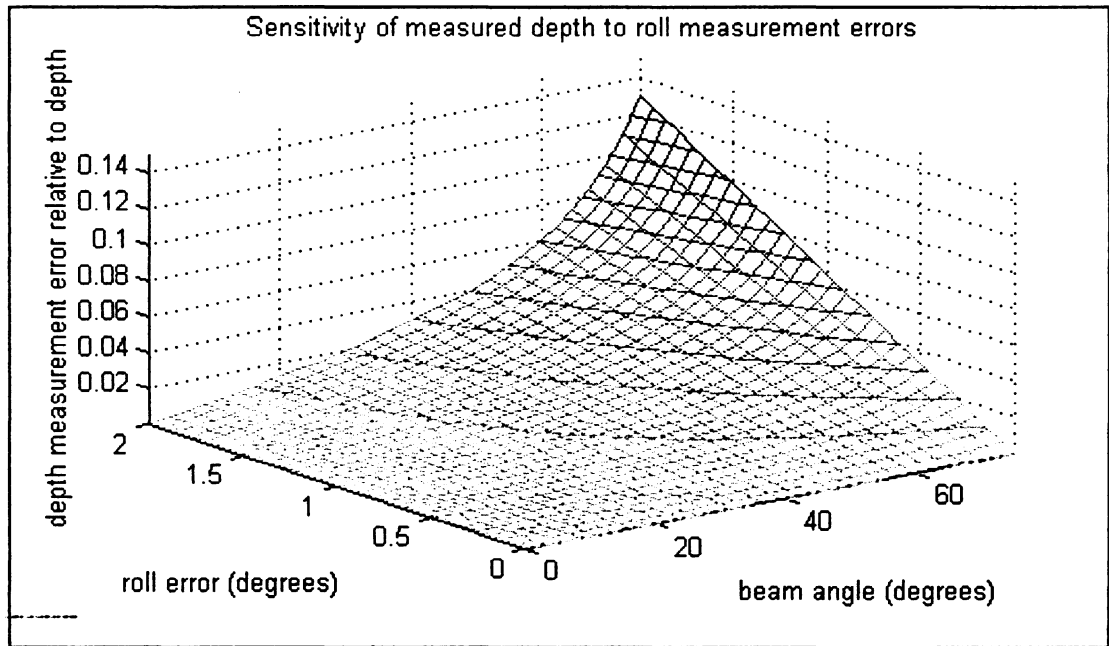


Figure 3.3 - Sensitivity of depth to roll measurement errors (after Hare et al. [1995]).

The mapping for pitch error into depth is given by the following expression:

$$\sigma_{d_p} = r \cos(\theta) \sin(P) \sigma_p \quad (3.3)$$

With a calm sea state or when using pitch stabilization, the pitch angle is restricted to small amplitudes. Therefore, the error in depth due to pitch measurement error is negligible.

An error in heading has no influence in depth measurements since this angle is defined in the horizontal plane.

3.4 Influence of Attitude Errors in Position Determination

In this section attitude errors are examined separately from other error sources to study their effect on sounding position determination. The error propagation equations were derived by Hare [1995]. The mapping of heading measurement error into position error is given by the following expression:

$$\sigma_{Pos_{\psi}}^2 = r^2(1 - (\cos\theta \cdot \cos P)^2)\sigma_{\psi}^2 \quad (3.4)$$

Figure 3.4 shows that sounding position error of the outer beams can be more effectively controlled if heading could be measured within 0.5° of accuracy.

The influence of roll measurement error on sounding position is given by the following equation:

$$\sigma_{Pos_{\theta}}^2 = r^2(1 - (\sin\theta \cdot \cos P)^2)\sigma_{\theta}^2 \quad (3.5)$$

For small pitch angles ($\cos P = 1$) we get the following expression:

$$\sigma_{Pos_{\theta}} = d \cdot \sigma_{\theta} \quad (3.6)$$

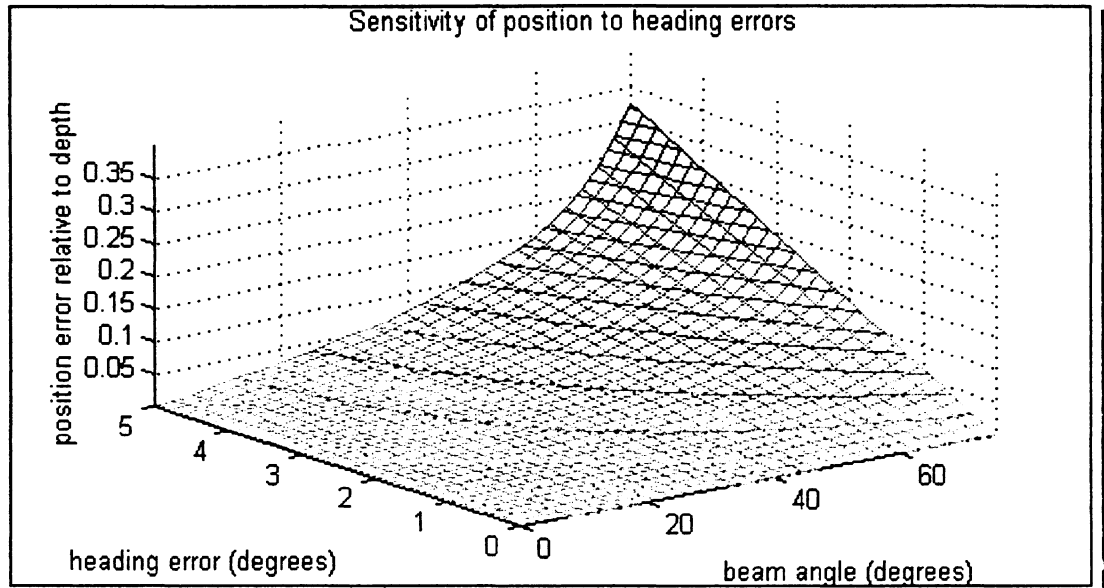


Figure 3.4 - Sensitivity of sounding position to heading errors (after Hare et al.[1995]).

This means that errors in sounding position due to roll errors do not depend on the beam angle. For a 30 m depth sounding, a roll error of 1° will contribute 0.5 m to the position error. Sounding position determination does not require very accurate roll measurements. Considering only roll measurement errors, if depth accuracy requirements are achieved they are also achieved for sounding position determination.

The effect of pitch measurement errors on sounding position is given by the following equation:

$$\sigma_{Pos_p}^2 = (r \cdot \cos\theta \cdot \cos P)^2 \cdot \sigma_p^2 \quad (3.7)$$

For small pitch angles equation (3.7) simplifies to:

$$\sigma_{Pos_p} = d \cdot \sigma_p \quad (3.8)$$

This expression is similar to equation (3.6). The mapping of pitch and roll measurement errors into position errors does not depend on the beam angle. Heading errors are the main cause of the position uncertainty of the outer beams.

3.5 Attitude Measurement

Attitude measurements are usually separated into those dealing with the vessel heading, which can have any angular value, and vessel roll and pitch, which are assumed to be relatively small amplitude oscillations about a level orientation [Wells, 1996].

Traditionally, heading measurements in marine navigation are usually made by a magnetic compass or a gyrocompass. Heading determination using two GPS antennas was already described in chapter 2.

Pitch and roll measurements require the use of a triad of accelerometers and angular rate sensors. Two algorithms can be used to derive pitch and roll measurements from accelerometers and angular rate sensors: the vertical gyro algorithm and the inertial navigation algorithm [Wells, 1996].

Inertial motion measurement by itself has error sources which limit its application in a marine environment. These error sources and their influence in multibeam sonar surveys are described in subsection 3.5.3. The integration of external data, namely position, velocity and heading from GPS receivers, allows the correction of most of the errors common to inertial sensors and provide a complete navigation solution.

3.5.1 Heading Determination

Chapter 2 already mentioned how GPS measurements can be used to derive heading. This subsection describes the instruments commonly used by the mariner to measure heading, which are the magnetic compass and the gyro compass.

3.5.1.1 The Magnetic Compass

The magnetic compass tends to align itself with the magnetic lines of force of the earth. Horizontal stabilization is made with a gimbaled platform or by floating the sensor at the interface of two liquids (Wells, [1996]).

Such a device is subject to limitations which include (Bowditch, [1984]):

- Deviation of the local magnetic field as a result of the presence of the vessel.
- Variation of the local magnetic field from the geographic north direction.
- Non level axis of the compass platform during long period accelerations (cornering) causing the heading vector to be measured with relation to an inclined plane rather than a local level one.
- Time response lag of the sensed magnetic north with relation to the actual magnetic north under large yaw conditions.

Despite these limitations, such devices are still in common use for marine navigation, since they do not require a power supply or depend on any other device. Even assuming that the variation correction is well known, and the deviation is well calibrated, few magnetic compasses can be relied on to better than two degrees, because of remaining

uncertainty in the deviation correction (Wells, [1996]).

3.5.1.2 The Gyrocompass

The gyrocompass is a navigational instrument which depends on the inherent properties of the gyroscope (gyroscope inertia and gyroscope precession) and accurately seeks the direction of the true north under the combined effect of the gravity and earth's daily rotation (Bowditch, [1984]).

A conventional gyroscope consists of a massive wheel like rotor balanced in gimbals which permits rotation about three mutually perpendicular axes through the centre of gravity of the device. Through the application of damping (either pendulous or a system of reservoirs and tubes filled with mercury), the spin axis of the gyroscope is forced to seek and maintain true north (Bowditch, [1984]).

Gyrocompasses are subject to several systematic errors such as speed error, tangent latitude error, ballistic damping error, quadrantal error, and gimbaling error. Furthermore, gyrocompasses are subject to errors common to directional instruments, such as the inaccurate graduation of the compass rose and incorrectly located lubber's line (Bowditch, [1984]), however this is not a problem if the gyro has a digital output. The gyro error of modern compasses is generally small, however, several errors can be introduced in various ways and it is good practice to check the accuracy of a gyrocompass by celestial observations (azimuth to the sun at sunset and sunrise) or observations to landmarks.

The gyrocompass is not subject to magnetic compass errors and if an error is present

it is the same for all heading angles. However, such an instrument is an intricate mechanism of many parts which requires maintenance and a suitable electric power. The correction of some of the systematic errors requires the input of speed and latitude from external sensors. Gyroscope accuracies are stated to be in the range 0.5° to 1.0° (Wells, [1996]).

3.5.2 Inertial Sensors

Inertial sensors are devices that mechanize Newton's laws of motion. Since these laws are expressed relative to the inertial space, the term inertial is used to describe these sensors. There are two types of inertial sensors: accelerometers and angular rate sensors.

Accelerometers:

Accelerometers sense linear accelerations as a result of change in linear velocity. In its simplest form, an accelerometer consists of a proof mass constrained to measure accelerations in a particular direction (the sensitive axis). If the accelerometer frame is accelerated in the direction of its sensitive axis, then the proof mass is deflected in the opposite direction and the readout gives an indication of the acceleration value.

Since accelerometers are sensitive to all accelerations in space their output includes other accelerations which are not due to travel over earth's surface. The most important of these accelerations is due to the force of gravity. If the quantity of interest is the acceleration with respect to the earth then the acceleration due to gravity must be compensated for in the accelerometer readout. Other accelerations due to polar motion, and Coriolis's law will affect accelerometer response but are small and are disregarded [Vanicek

and Krakiwsky, 1986].

Angular rate sensors:

Angular rate sensors are designed as gyroscopes. These sensors measure the angular velocity about a single axis and are insensitive to linear movements in any direction. Conventional technologies use the concept of a spinning mass, based on the principle of conservation of angular momentum which states that a system will maintain a constant angular momentum about its spin axis if no external forces are applied [Bowditch, 1984]. The spin axis, therefore, tends to maintain the same direction in inertial space.

Modern technologies use the principle of the Sagnac effect in devices designed as ring laser gyros and fibre optic gyros. These devices are based on the inertial properties of electromagnetic radiation [Bose, 1996a]. Other devices designated as Vibrating Structure Gyroscopes measure the vibration pattern of high frequency oscillations of a piezo-electric crystal [TSS, 1996].

The rotations affecting angular rate sensors are the vessel's rotation with respect to the earth (pitch, roll and yaw), earth's rotation and changes in latitude and longitude. If the quantity of interest is rotation with respect to the earth, the effect of other inertial rotations should be compensated at the angular rate sensor readout.

3.5.3 Combining Inertial Sensors in Orthogonal Triads

An orthogonal triad of motion sensors is made by three accelerometers and three gyros (see figure 3.5). This array of inertial sensors is referred to as the Inertial

Measurement Unit (IMU).

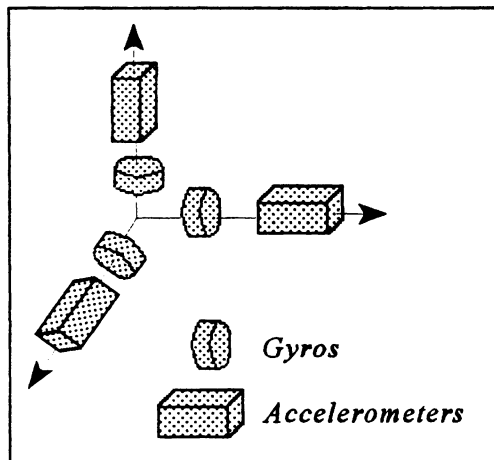


Figure 3.5 - Triad of inertial sensors.

There are several strategies for specifying the orientation of such an array. The three main designs are “space stable” (platform remains stable in an inertial coordinate system); “local level” (platform remains stable in the LCS); and “strapdown” (platform remains stable in the BCS).

“Space stable” and “Local level” systems are “gimbaled”. These systems have the IMU isolated from the vessel’s attitude motions by a mechanical assembly of concentric rings called gimbals.

In a “strapdown” system the IMU experiences the same angular motions as the vessel. These systems are less expensive and require less hardware than “gimbaled” systems, however, they are usually less accurate and require greater computational effort [Wells, 1996]. When mounted correctly, the three arms of the “strapdown” orthogonal array is aligned with the BCS axes of the vessel.

In a static environment the attitude of a platform can be measured using a pendulum made from a single weighted line. At rest, the line will provide a vertical reference against which attitude measurements can be made. The orthogonal array formed by the three accelerometers is equivalent to a pendulum. Thus, in static conditions, the array of three accelerometers can be used to measure attitude.

Problems arise when using this form of attitude measurement in dynamic

conditions. In a marine environment the principal source of error in inertial attitude sensors are caused by short term acceleration transients due to sea action (waves and swell) and long-term horizontal acceleration when the vessel executes a prolonged turn [TSS, 1996].

For vessels undergoing short period accelerations, the low pass filtered output of the accelerometer triad provides a good estimate of the gravity vector. This allows the output from the accelerometers to provide a stable vertical reference, from which short term departures can be sensed, using the triad of angular rate sensors. Measurements from the array of angular rate sensors continue to respond throughout very high rates of pitch and roll. A high-pass filter is used to reject the drift errors in the gyros. The estimate of the gravity vector combined with angular rate measurements from the orthogonal array of gyros has the potential to measure attitude under dynamic conditions. This combination has been designated the vertical gyro algorithm [Wells, 1996].

When the vessel undergoes any systematic acceleration whose duration exceeds the time constant of the low pass filter applied to the accelerometers, such as a prolonged turn, the centripetal acceleration is perceived by the accelerometer triad as a prolonged horizontal acceleration. This long term component can not be filtered out by the low pass filter, and causes the apparent vertical to be deflected from the true vertical, which eventually, causes errors to appear on the output. The amount of the apparent vertical deflection is controlled by the cut-off frequency of the low pass filter. The lower the cut-off frequency of the accelerometers, the longer is the settling time of the apparent vertical. The design of the low pass and high pass filters is a trade off between rejections of deflections in the apparent vertical and rejection of drift errors in the gyros [Applied Analytics, 1996a].

The vertical gyro implementation can be replaced by a fully-functional inertial navigation implementation, which is not limited by the low pass and high pass filters used by the vertical gyro. However the component quality must be higher, and such full inertial navigation implementation is more expensive.

Tests made on accelerometer based attitude sensors for multibeam sonar surveys indicate errors that place some limitations on ship maneuvering and efficient mapping [Dinn and Loncarevic., 1994]. If these sensors are to be used, it is necessary to make turns outside the survey zone and allow sufficient time for the sensors to settle down before data collection begins.

3.5.3.1 GPS Input

The centripetal acceleration that exists when a vessel turns, is sensed by the motion sensor as a horizontal acceleration in the direction defined by the projection of the pitch axis in the horizontal plane. The value of this acceleration can be calculated simply as the product of the vertical rate of turn by the vessel horizontal speed.

The velocity and rate of turn information provided by a GPS receiver and the angular rate sensors can be used to compute the magnitude of the centripetal acceleration. Vessel turns, however, show differences between the instantaneous heading and track of the vessel. This could arise from the lateral force exerted by the rudder or from the effects of winds or currents. This situation causes the pitch axis of the vessel to be misaligned with respect to the vector that defines the true centripetal acceleration and only a portion of its

value will be sensed by the roll axis accelerometer [TSS, 1996].

In the situation illustrated in Figure 3.6 the accelerometer aligned with the roll axis will measure only some part, a_r , of the full centripetal acceleration a_c . The relation between the two accelerations depends on the angle between the instantaneous heading and the track of the vessel γ :

$$a_r = a_c \cdot \cos \gamma \quad (3.9)$$

Full compensation for the effects of centripetal acceleration requires the knowledge of velocity and heading. True vessel speed information can be input from a GPS receiver and vessel's heading information can be provided by a gyrocompass or a two-antenna GPS system.

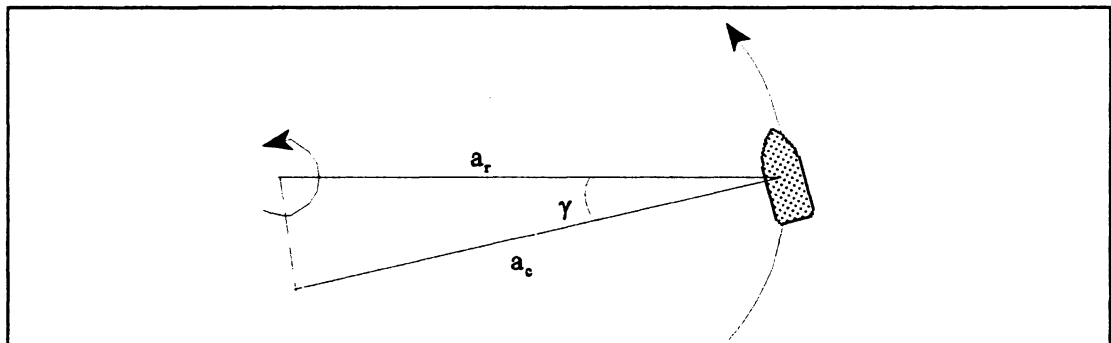


Figure 3.6 - Accelerometer roll axis misaligned with centripetal acceleration.

The simplified block diagram shown in Figure 3.7 shows how the motion sensor combines inertial data with aiding data from GPS or other aiding sources.

The symbols of the components of the block diagram follows the control systems terminology, where the arrows represent the direction of the signal flow, a rectangle describes a system component where some mathematical operations are performed, the

circle represents a summing point and the symbol \int represents the integration operator [Distefano et al, 1990].

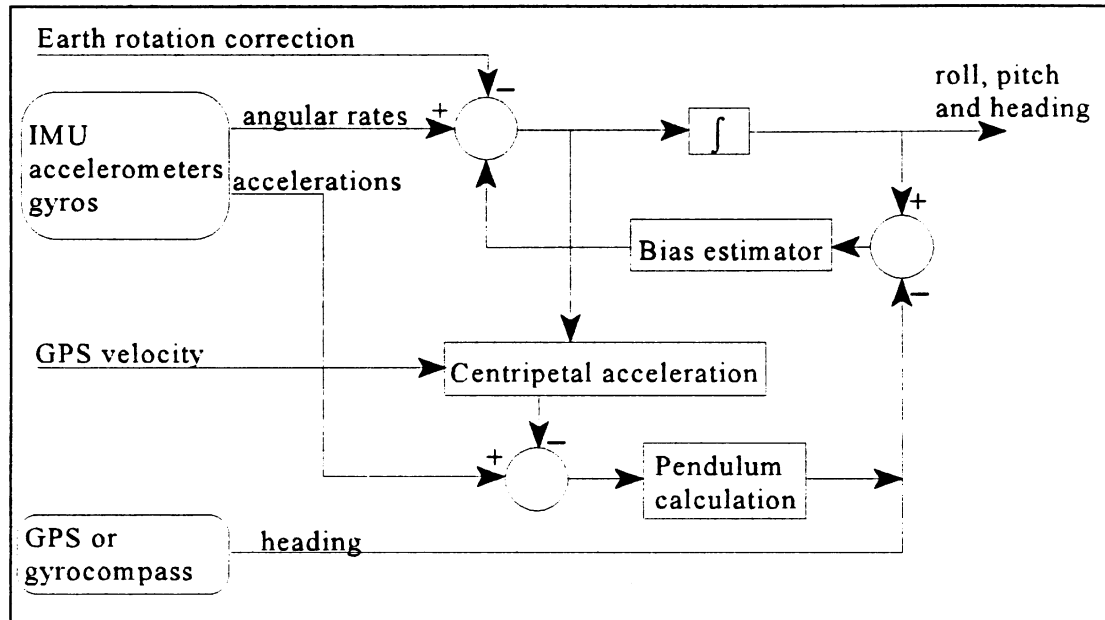


Figure 3.7 - Block diagram of a motion sensor (after TSS [1996, p.A-12]).

The summarized operations of a motion sensor can be described as follows [TSS, 1996]:

- The accelerometer signals are converted to pitch and roll information through a pendulum calculation.
- At the same time, angular rate information from the gyros is applied to the input of an integrator after corrected for the earth rotation rate. The determination of the earth rotation rate requires information of the vessel's heading and latitude, which can be provided by a GPS and/or a gyrocompass.
- The integrator derives the angle of turn for the rotation axis of each gyro. Therefore, the integrator output provides angles of roll, pitch and yaw occurring during the

integration time.

- The attitude angles resulting from the integrator output are compared with pitch and roll angles derived from measurements made by the accelerometers. The difference between the two independent attitude measurements is used to estimate the magnitude of offset for each of the gyros.
- Velocity measurements made by a GPS receiver are used in conjunction with the rate of turn information to derive the centripetal acceleration.
- Heading information from a gyrocompass or a two antenna GPS heading system provides a reference for the yaw axis of the accelerometers.

3.5.4 Inertial Navigation Systems

Inertial Navigation Systems (INS) are autonomous devices that provide a complete navigation solution (position, velocity and attitude) based on measurements from inertial sensors. The inertial navigation starts with known initial conditions and iteratively estimates changes in position, velocity and attitude through the integration of the outputs of inertial sensors. Since observations from inertial sensors are available at a very high rate (100 Hz), INS provide virtually continuous measurements. Unlike the vertical gyro algorithm, the inertial navigation algorithm does not need to estimate the apparent vertical.

Strapdown systems are the dominant installation type for marine applications due to their mechanical simplicity, smaller volume and weight, and lower costs. Figure 3.8 is a simplified block diagram of a strapdown INS. Vessel accelerations and angular rates with

respect to the inertial space are obtained from the IMU. The navigator computer utilizes the body frame inertial increments in conjunction with angular rates due to earth rotation and vessel's translational motion to maintain an estimate of the vessel's attitude that is used to convert the accelerometer outputs to a LCS reference frame. Subsequent to compensation for gravitation, earth rotation, and centripetal acceleration effects, the navigator computer accumulates changes in velocity to obtain north, east and vertical velocities, with a following accumulation to obtain LCS coordinates.

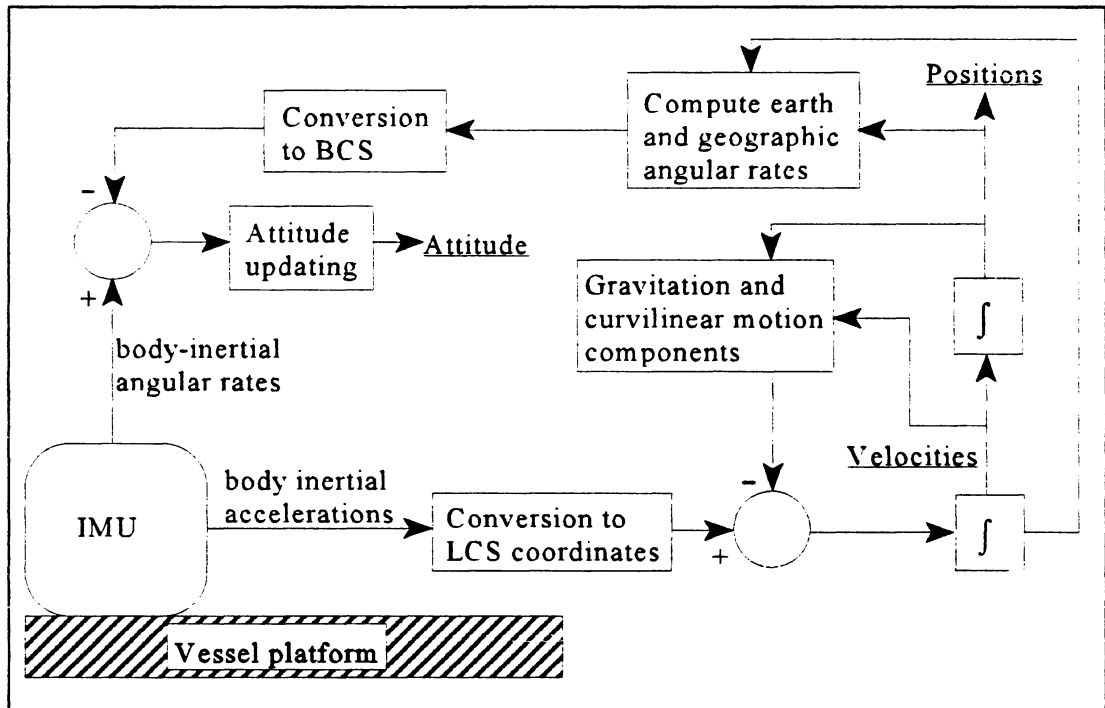


Figure 3.8 - Simplified block diagram of a strapdown INS (after May [1993, p.60]).

Errors in INS arise from the iteration of vehicle motion with instrument noise, instrument and platform misalignments, gravitational disturbances and initial condition errors. Since INS solutions are based on the iterative estimates, errors from one epoch

propagate to the next. To use an inertial sensor for a period of an hour or more requires a good knowledge of the gravitational force and remarkable quality inertial sensors. Good quality inertial sensors are expensive, thus one of the major limitations on the use of INS is the cost of the instrument [Wells, 1996].

3.5.5 GPS Integrated with Inertial Navigation Systems

Over a period of time the INS accumulates errors, therefore the accuracy of its solution decays. Data from external navigation sensors, allows the inertial sensor to estimate the errors in its solution and therefore to improve the quality of its measurements.

Practically since the beginning of existence of the GPS, it was apparent that its integration with INS will supersede the utilization of other aiding sources (Omega, Transit, Loran-C, speed sensors and Doppler radar) due to its superior performance [May, 1993]. Although errors in INS are significantly larger than those of GPS, they have much higher frequency than GPS errors. In integrated GPS/INS the long term accuracy of GPS measurements is combined with the short term accuracy and fast update rate of INS in order to achieve a resulting performance (not accuracy) that is better than any of the systems alone.

The requirement for the data processing of GPS and inertial data is to combine all the measurements in order to yield a best estimate of position, velocity and attitude. Here, “best” means to satisfy the criterion of minimization of the sum of squares of the weighted residuals (least squares approach). The most common algorithm for processing GPS with

inertial data is the Kalman filter. The Kalman filter is essentially a sequential least squares approach to the estimation of parameters that change with time [Gelb, 1974]. Two generic Kalman filter mechanizations for integration of GPS data with inertial measurements are used: Open loop and closed loop Kalman filters [Bose, 1996b].

In an open loop mechanization the INS is corrected using the GPS solution. There is no feedback to the INS to correct inertial sensor errors. The errors therefore will propagate. INS positions and velocities can be sent to the GPS receiver where they are used for code aiding acquisition. Open loop is the simplest mechanization, can use any GPS receiver with any INS and bad GPS measurements do not affect INS operation, however, error dynamics must be accurately modeled which is difficult to do with strapdown INS [Bose, 1996b].

In the closed loop approach, corrections are fed back to the INS, thereby avoiding the necessity for error propagation in the Kalman filter. Since INS data is continuously updated while GPS data is available, better performance is ensured in the event of a GPS outage. Care must be taken, however, to monitor GPS measurements and guarantee that erroneous GPS data do not contaminate INS parameters [Bose, 1996b].

Two separate filters for the GPS and INS, as shown in Figure 3.9, provides redundancy. In case of INS failure the GPS navigation solution may still be obtained. The use of separate Kalman filters, however, leads to several compromises in terms of design flexibility and performance in favor of redundancy [Tzartas and Mark, 1988]. An integrated Kalman filter that processes both GPS and INS yields maximum performance. In this situation the GPS and INS are limited to their sensor functions. This is designed as a tightly coupled integration and is usually used when a GPS receiver is physically and

electrically integrated with an INS.

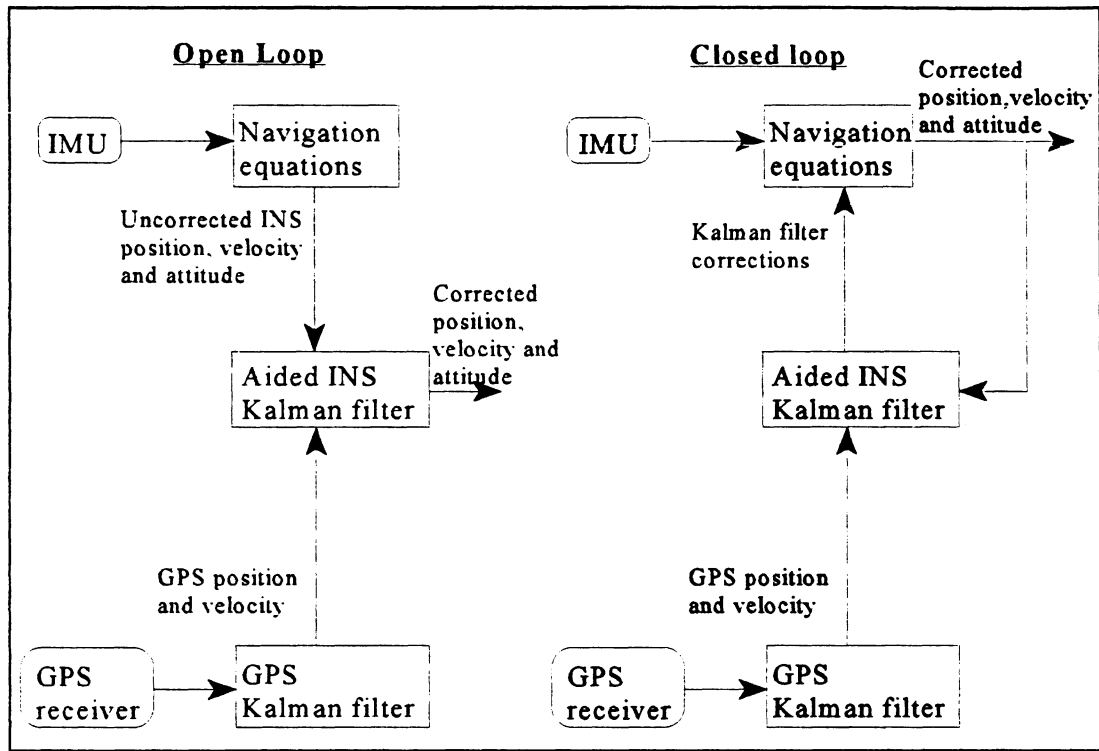


Figure 3.9 - GPS/INS open loop and closed loop mechanization (after Bose, [1996b]).

Chapter 4

GPS CARRIER PHASE AMBIGUITY RESOLUTION

A prerequisite to obtain accurate attitude determination is that the carrier phase ambiguities are resolved. Different techniques have been developed to estimate the carrier phase ambiguities in differential GPS positioning. All the techniques have in common the need of an approximate initial position in order to define a search space where trial sets of possible solutions are included. In attitude determination it is possible to significantly aid integer ambiguity resolution by exploiting redundant information such as baseline length and elevation angle. The baseline length must be surveyed beforehand, while for the elevation angle, maximum limits can be set or data from a motion sensor may be used.

Since attitude determination is needed in real time for hydrographic applications, ambiguity resolution using data from a single epoch (instantaneous) is very important to avoid initialization periods, when starting out or when a signal loss and a cycle slip occurs. Therefore, this chapter is focused on instantaneous ambiguity resolution using a least squares search technique. The first section introduces the GPS carrier phase observable and its observation equations, and addresses the question of simultaneity of observations made by two receivers tracking the same satellites. The second section describes the least squares ambiguity resolution technique and an efficient method of determining the search space on a spherical layer defined by the known baseline length between two antennas, plus or minus an estimated baseline length error [Lu and Cannon, 1994]. The problems of satellite selection, and of validation of the estimated solution are also addressed.

4.1 Carrier Phase Observation Equations

GPS signals are modulated on carrier waves defined on the L1 and L2 bands. The phase observable is the difference between the satellite carrier phase (as sensed by the receiver's antenna and tracking loops) and the phase of the internal receiver oscillator [Leick, 1995]. The measurement process does not account for the number of whole cycles of carrier waves between the receiver and satellite. However, the fractional part of the carrier wave can be measured with a precision that is about 1/100 of a cycle, which equals two or three millimetres in linear distance [Leick, 1995].

Through this section, a superscript identifies the satellite, and a subscript identifies the receiver. The carrier phase observation equations described in the next sub-sections were taken from Leick [1995], with small modifications justified in the text.

4.1.1 Undifferenced Carrier Phase

The measured carrier phase at nominal time t for station k and satellite p in units of cycles is described by the following observation equation:

$$\begin{aligned} \Phi_k^p(t) = & \frac{f}{c} \rho_k^p(t) + f \left[1 - \frac{\dot{\rho}_k^p(t)}{c} \right] dt_k - f dt^p + N_k^p + \frac{a^p}{c} \rho_k^p(t) \\ & - I_k^p(t) + T_k^p(t) + M_k^p(t) + h_k(t) + h^p(t) + \varepsilon \end{aligned} \quad (4.1)$$

where f is the carrier frequency, c is the speed of light in the vacuum, ρ is the geometric range, $\dot{\rho}$ is the range rate, dt is the clock error, N is the carrier phase ambiguity, a is the satellite frequency offset, I and T denote the ionospheric phase advance and tropospheric

delay on the carrier signal, M is the multipath effect, the terms h^p and h_r refer to the satellite hardware delay and receiver hardware delay respectively, and ε is the random carrier phase measurement noise.

The clock error and ionospheric terms in equation (4.1) have different signs when compared with the expression derived by Leick [1995]. The cause for the difference in the sign of the clock error terms lies in the equation that relates nominal times with true times via the clock errors. To find the true time of transmission or reception of a signal, one needs to subtract the clock error from the nominal time of transmission or reception. Following this approach, to compute the geometric range from carrier phase measurements the receiver clock error term must be subtracted and the satellite clock error term must be added, which is in accordance with expression (4.1) and with the derivation described by Teunissen and Kleusberg [1996]. Since the ionosphere causes an advance in the carrier phase propagation [Teunissen and Kleusberg, 1996], it is necessary to add the ionospheric term to the measured carrier phase in order to compute the geometric range, thus the minus sign in equation (4.1).

The receiver clock error has a large component due to the product $f dt_r$ and a smaller term which is a function of the topocentric range rate. The range rate, can be computed using the measured doppler frequency, f_D , through the following expression [Leick, 1995]:

$$\dot{\rho}_k^p = \frac{f_D}{f} c \quad (4.2)$$

Satellite clock errors affect the phase observable through the large term $f dt^p$ and the small satellite frequency offset term which depends on the tropocentric range.

4.1.2 Carrier Phase Single Differences Between Receivers

If two receivers observe the same satellite at the same nominal receiver time, it is possible to eliminate some common mode errors. The single difference between receivers k and m that observe satellite p is defined by the following expression:

$$\begin{aligned}\varphi_{km}^p(t) &\equiv \varphi_k^p(t) - \varphi_m^p(t) \\ &= \frac{f}{c}[\rho_k^p(t) - \rho_m^p(t)] + \frac{a^p}{c}[\dot{\rho}_k^p(t) - \dot{\rho}_m^p(t)] - \frac{f}{c}[\dot{\rho}_k^p(t)dt_k - \dot{\rho}_m^p(t)dt_m] + f[dt_k - dt_m] + N_{km}^p \\ &\quad + I_{km}^p(t) + T_{km}^p(t) + M_{km}^p(t) + h_{km}(t) + \varepsilon_{km}^p\end{aligned}\quad (4.3)$$

In the above expression, the subscript km is used to identify the difference operation in accordance with the following convention, where x is any variable except multipath and random measurement noise:

$$x_{km}^p = x_k^p - x_m^p \quad (4.4)$$

The single difference of random measurement noise is given by the quadratic mean:

$$(\varepsilon_{km}^p)^2 = (\varepsilon_k^p)^2 + (\varepsilon_m^p)^2 \quad (4.5)$$

Multipath can be divided into a coherent part and another incoherent (see subsection 5.1.3). The single difference of the coherent component follows equation (4.4), while the single difference of the incoherent part is in accordance with (4.5).

The main advantage of the single difference observation is that most of the errors common to the satellite cancel. The satellite clock error and the satellite hardware delay

also have canceled. The small term of the satellite frequency offset converges toward zero as the separation of the receivers decreases. All these errors cancel as long as they remain constant between satellite emissions. If the nominal reception time is the same for both receivers, the emission times differ slightly because of different distances between the satellite and the two stations [Leick, 1995]. In attitude determination, the distance between antennas is limited to a few metres, and the changes in the clock error between emission times are negligible. Also for small baselines, the tropospheric and ionospheric errors cancel out. However, the noise term is increased by a factor of $\sqrt{2}$ if we assume the same random measurement noise for the two receivers.

The mathematical model that relates a small baseline vector ΔR , to the differential range measurement $\Delta\rho$ (obtained via carrier phase techniques, for example) is given by the following equation [Vanicek et al.,1984], after made some simplifications, assuming a small distance between receivers:

$$\vec{e}^p \cdot \Delta \vec{R} = \Delta \rho^p \quad (4.6)$$

Where e^p is the unit pointing vector (direction cosine vector) to satellite p .

4.1.3 Carrier Phase Double Differences

If two receivers k and m observe two satellites p and q at the same nominal time, the double difference observable is given by the following expression:

$$\begin{aligned}
\varphi_{km}^{pq}(t) &\equiv \varphi_{km}^p(t) - \varphi_{km}^q(t) & (4.7) \\
&= \frac{f}{c}([\rho_k^p(t) - \rho_m^p(t)] - [\rho_k^q(t) - \rho_m^q(t)]) - \frac{f}{c}([\dot{\rho}_k^p(t) - \dot{\rho}_m^p(t)] + [\dot{\rho}_k^q(t) - \dot{\rho}_m^q(t)]) \\
&\quad + \frac{f}{c}([\rho_k^p(t) - \rho_m^p(t)] - [\rho_k^q(t) - \rho_m^q(t)]) + N_{km}^{pq} + I_{km}^{pq}(t) + T_{km}^{pq}(t) + M_{km}^{pq}(t) + \varepsilon_{km}^{pq}
\end{aligned}$$

In the above expression, the superscript pq and the subscript km are used to identify the difference operation in accordance with the following convention, where x is any variable except random measurement noise and multipath:

$$x_{km}^{pq} = [x_k^p - x_m^p] - [x_k^q - x_m^q] = \nabla \Delta x \quad (4.8)$$

Double difference of multipath and random measurement noise can not be defined by equation (4.8) due to their random component, as mentioned in section 4.1.2.

In addition to the cancellation of the satellite clock errors, the most important feature of the double difference observation is the cancellation of the receiver clock errors. These errors cancel completely as long as the observations to the satellites are made at the same time or the receiver clock drifts between epochs are negligible [Leick, 1995]. The small clock term which is a function of the topocentric range rate remains. The terms due to the satellite frequency offset, ionospheric effect and tropospheric effect are negligible for small baselines.

The mathematical model that relates the double difference range measurement, $\nabla \Delta \rho$, with the baseline vector is given by the following equation, after simplifying the general expression given in Vanicek et al.[1984] for a small distance between stations:

$$(\bar{e}^p - \bar{e}^q) \Delta \vec{R} = \nabla \Delta \rho \quad (4.9)$$

After double differencing the noise level is 2 times larger than the undifferenced observable and $\sqrt{2}$ times larger than that after single differencing, if the measurement noise is the same for measurements from two satellites and two receivers. Double differencing is usually the preferred technique for attitude determination for the following reasons [Mowafy, 1994]:

- Double differencing eliminates the large receiver and satellite clock errors.
- Even with a common oscillator, hardware delays between satellites and receivers may exist, and double differencing is required to eliminate this error.

If a common oscillator is used for both receivers, any local time error affects both carrier phase measurements identically. These variations cancel in the single differencing process between receivers. If the problem due to receiver hardware delay is overcome, then it is preferable to use single differences instead of double differences, because they are less noisy.

4.1.4 The Question of Simultaneity

Because of differing distances between a receiver and different satellites the propagation delay will also differ. Therefore, signals that are received at the same time were emitted at different times, and signals that are emitted at the same time will be received at different times. Due to satellite motion, signals emitted at different times were emitted from different satellite positions.

Assuming the signals are received at the same nominal time, the problem is to find

the magnitude of the error due to lack of simultaneity at transmission.

Let us assume the signals are received at the same nominal time, t_r , and that the receiver antennas are separated by less than 10 m. As sketched in figure 4.1, the signal would have been emitted earlier Δt_e units of time, for the receiver further away from the satellite. If the time for which the satellite position is computed is t_{e2} then the measured range ρ_1 should be corrected to account for the different time of emission. For a 10 m baseline the value of Δt_e is always less than $3.3 \cdot 10^{-8}$ seconds and assuming a range rate less than 1000 m/s, the correction to the range will be less than 0.033 mm. Under this condition, which is appropriate for attitude determination on a marine vessel, the error introduced by lack of simultaneity of emission times is negligible.

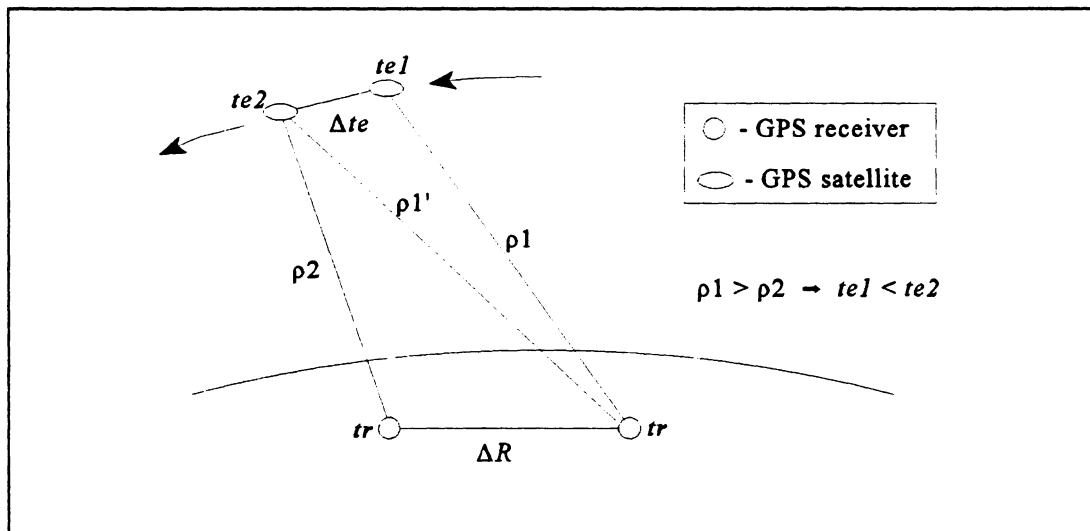


Figure 4.1 - The problem of no simultaneity at transmission.

4.2 Least Squares Ambiguity Search

Least squares search techniques are the most suitable for instantaneous ambiguity resolution. These techniques have proven to be successful in differential GPS positioning. The main alternative, motion based methods, which make use of the information provided by vessel or GPS satellite motion, are not suitable for instantaneous ambiguity resolution [Mowafy, 1994].

The least squares search technique is described in Hatch [1990]. The technique is based on the least squares adjustment and uses the least squares residuals of the observations to measure the disagreement between the phase measurements corresponding to different ambiguity sets being tested. A flow chart of the least squares ambiguity search technique is represented in Figure 4.2.

At least four satellites are needed to generate an entire set of potential ambiguity solutions within a pre-defined search space. Four satellites are designated as the primary satellites and the remaining visible satellites are designated as secondary. The larger the search space, the greater is the number of possible integer ambiguity solutions which must be calculated and tested, and the longer the computation time required. In differential GPS the search space is usually centered at an approximate pseudorange-derived position, and its size is typically taken to be three times the estimated standard deviations of these approximate coordinates [Lachapelle et al., 1992]. In attitude determination, the size of the search space can be reduced by using redundant information from an external sensor, or incorporating the known baseline length as a constraint.

The observation equation that relates the measured carrier phase double differences to the baseline vector is given in matrix form as:

$$\begin{aligned} A\Delta\vec{R} + \vec{w} &= 0 \\ \vec{w} &= \lambda(\nabla\Delta N_1 - \nabla\Delta\phi_1, \dots, \nabla\Delta N_{ns-1} - \nabla\Delta\phi_{ns-1}) \end{aligned} \quad (4.10)$$

where λ is the carrier phase wavelength, ns is the number of visible satellites, A is a design matrix that results from the difference of the pointing vectors defined in equation (4.9), w is the misclosure vector and $\nabla\Delta$ is the double difference operator with the same meaning as the operator defined by equation (4.8). In equation (4.10) it is assumed that the carrier phase double difference observable has been corrected from all the possible error sources described in equation (4.7), or these errors are negligible.

Based on the potential solution for the ambiguities coming from the primary satellites to be tested, a potential solution for the coordinates can be calculated with:

$$\Delta\vec{R}_p = -A_p^{-1}\vec{w}_p \quad (4.11)$$

where p designates the group of primary satellites.

The double difference range for each pair of secondary satellites, $\nabla\Delta\rho_s$, can be computed using equation (4.9), for each of the potential solutions. The double differenced integer ambiguities for each pair of secondary satellites can be calculated by the formula:

$$\nabla\Delta N_s = \text{rint} \left[\nabla\Delta\phi_s - \frac{\nabla\Delta\rho_s}{\lambda} \right] \quad (4.12)$$

where subscript s refers to the secondary satellites, λ is the carrier phase wavelength and

nint is the “nearest integer” operator.

Once the integer ambiguities have been determined, the measurement residuals for each potential solution can be computed through a linear least squares adjustment:

$$\Delta\vec{R} = -(A^T C^{-1} A)^{-1} A^T C^{-1} \vec{w} \quad (4.13)$$

where *C* is the covariance matrix of the double differenced observations. The measurement residuals computed through the least squares adjustment are:

$$\vec{v} = A \cdot \Delta\vec{R} + \vec{w} \quad (4.14)$$

These residuals provide the basis for testing each potential solution. For the correct solution the computed observations for the secondary satellites should be very close to the corresponding measured observations. The measure of disagreement is given by the estimated variance factor, formulated as:

$$\hat{\sigma}_0^2 = \frac{\vec{v}^T \cdot C^{-1} \cdot \vec{v}}{ns - 4} \quad (4.15)$$

The variance-covariance matrix of the estimated coordinates is given as:

$$C_R = \hat{\sigma}_0^2 (A^T \cdot C^{-1} \cdot A)^{-1} \quad (4.16)$$

At the correct solution the estimated variance factor should be a minimum, thus the potential solution that corresponds to the smallest variance factor is the solution selected for validation.

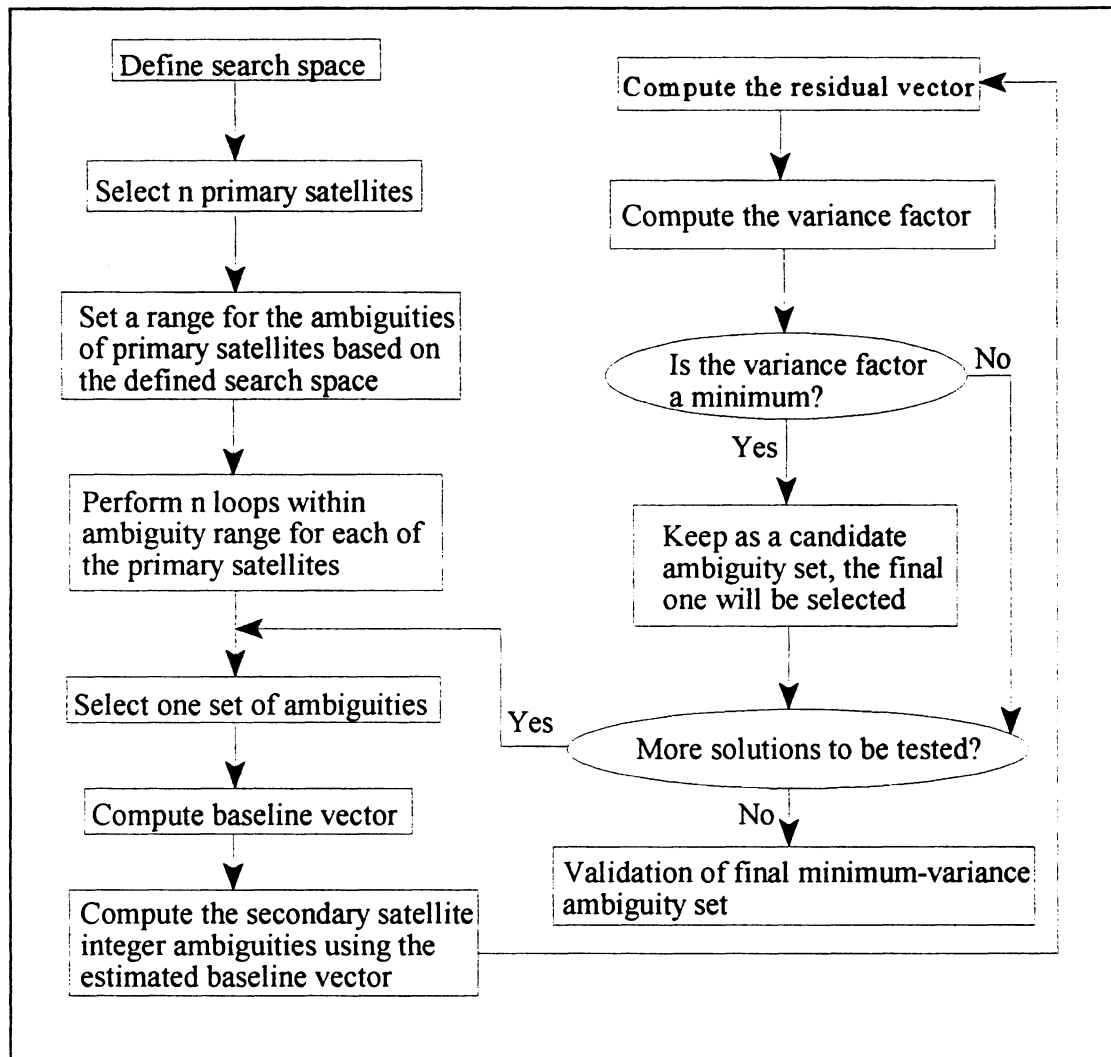


Figure 4.2 - Flowchart of the least squares ambiguity searching technique.

4.2.1 Ambiguity Search with a Fixed Baseline Length

Ambiguity search spaces are usually based upon the uncertainty associated with a differential pseudorange solution for the baseline between two GPS antennas. This uncertainty depends upon the pseudorange measurement noise level, which is typically a few metres for wide-correlator receivers and a few centimetres for narrow-correlator receivers [Van Diederendonck et al., 1992].

The technique for determining the ambiguity search space described in this section is based on a method described by Lu and Cannon [1994] which utilizes the Cholesky decomposition and the known baseline length between GPS antennas as a constraint to construct the potential ambiguity sets on a sphere.

Squaring equation (4.11) we obtain:

$$D^2 = \Delta\vec{R}^T \cdot \Delta\vec{R} = \vec{w}^T (AA^T)^{-1} \vec{w} \quad (4.17)$$

where D is the baseline length and AA^T is a 3 by 3 positive definite matrix that can be Cholesky decomposed into the product LL^T of a lower triangle matrix L times its transpose. With this substitution equation (4.17) can be rewritten as:

$$D^2 = (L^{-1}\vec{w})^T (L^{-1}\vec{w}) \quad (4.18)$$

For a short baseline (less than the accuracy of the pseudorange solution) the search space is centered at one antenna, designated as the reference antenna, and the ambiguities of the primary satellites can be sequentially constrained using equation (4.18). The search range for the first ambiguity parameter is given by:

$$\text{rint} \left[-\frac{(D+\delta D)}{l_{11}\lambda} + \nabla\Delta\phi_1 \right] \leq \nabla\Delta N_1 \leq \text{rint} \left[\frac{(D+\delta D)}{l_{11}\lambda} + \nabla\Delta\phi_1 \right] \quad (4.19)$$

where δD is the baseline length error and l_{ij} is the element in row i and column j of the matrix L^{-1} . For a given value of the first ambiguity parameter, the search range of the second ambiguity parameter is given by the following expression:

$$\text{nint}\left[\frac{-\sqrt{(D+\delta D)^2-(l_{11}w_1)^2}-l_{21}w_1}{l_{22}\lambda}\nabla\Delta\varphi_2\right]\leq\nabla\Delta N_2\leq\text{nint}\left[\frac{\sqrt{(D+\delta D)^2-(l_{11}w_1)^2}-l_{21}w_1}{l_{22}\lambda}+\nabla\Delta\varphi_2\right] \quad (4.20)$$

where w_i is the i^{th} element of the misclosure vector. Finally the range of the third ambiguity parameter is given by the following expressions:

$$\begin{aligned} \text{nint}\left[\frac{-\sqrt{(D+\delta D)^2-C_1-C_2-C_3}}{l_{33}\lambda}+\nabla\Delta\varphi_3\right]\leq\nabla\Delta N_3\leq\text{nint}\left[\frac{-\sqrt{(D-\delta D)^2-C_1-C_2-C_3}}{l_{33}\lambda}+\nabla\Delta\varphi_3\right] \\ \text{nint}\left[\frac{\sqrt{(D-\delta D)^2-C_1-C_2-C_3}}{l_{33}\lambda}+\nabla\Delta\varphi_3\right]\leq\nabla\Delta N_3\leq\text{nint}\left[\frac{\sqrt{(D+\delta D)^2-C_1-C_2-C_3}}{l_{33}\lambda}+\nabla\Delta\varphi_3\right] \\ C_1=(l_{11}w_1)^2 \\ C_2=(l_{21}w_1+l_{22}w_2)^2 \\ C_3=l_{31}w_1+l_{32}w_2 \end{aligned} \quad (4.21)$$

If the baseline length error is very small ($\delta D=0$) the third ambiguity parameter is restricted to two possible values. Assuming the ambiguity search ranges for the first and second ambiguity parameters are ± 10 cycles, the total potential ambiguities to be tested are $21 \times 21 \times 2 = 882$, as opposed to $21^3=9261$ with a cubic search space where the known baseline length is not considered. Therefore, the number of ambiguities is reduced by an order 10.

The Cholesky decomposition must only be performed once per epoch, and only the misclosure vector needs to be computed for each potential solution. This greatly speeds up the computation and enhances the reliability of the ambiguity search process.

4.2.2 Selection of the Primary Satellites

The selection of the primary satellites is very important to successfully resolve the carrier phase ambiguities. If the trial position computed from the corrected set of ambiguities for the primary satellites has a significant error, then the ambiguities for the secondary satellites as computed from this trial position may differ from the correct ones and the correct solution will not be found. Therefore, when more than four satellites are being tracked simultaneously by two GPS receivers, the primary satellites should be chosen such that the error in the estimated parameters (in this case the relative position vector) is the minimum for all the possible combinations of four visible satellites.

The variance-covariance matrix of the estimated parameters is given by equation (4.16). In this equation the factor that depends on satellite geometry is formed by the cofactor matrix: $(A^T \cdot C^{-1} \cdot A)^{-1}$. The cofactor matrix is the matrix of multipliers of the double difference range variance to give position variance.

A figure of merit is formed by the trace of the cofactor matrix. This figure of merit is similar to the Geometric Dilution of Precision (GDOP), both in form and in dependency on satellite geometry. However, the figure of merit depends on the covariance matrix of the observations, which varies with the observation differencing strategy. The primary satellites are chosen such that the trace of the cofactor matrix for that particular set of satellites is less than for any other possible combination of four satellites.

4.2.3 Validation of the Estimated Solution

In instantaneous ambiguity resolution only measurements from a single epoch are used. Since no more than ten satellites are tracked simultaneously the sample size is limited to 10 or fewer observations for single frequency and 20 or fewer observations for dual frequency receivers. When the number of secondary satellites is small, it can happen that the element of the set of trial positions giving minimum variance is not necessarily the correct one. This will lead to wrong ambiguity resolution and incorrect estimation of the antenna vector. Among the strategies implemented to address this problem are the comparison of the current ambiguity solution with previous ones, and statistical tests.

If continuous tracking of the signal is maintained from epoch to epoch, the estimated ambiguities should be constant. Thus, one validation test is to compare the current solution with the previous one. If the solution differs from one epoch to the next, this may indicate a bad solution and/or a lost of signal. If the solution does not differ from one epoch to the next, it means that it is correct or that the same wrong solution was estimated for at least two consecutive epochs. This method may work for a majority of situations but it is not completely reliable.

A more reliable validation parameter, using the same principle, is the moving average technique [Mowafy and Schwarz, 1994]. A moving average for each double difference ambiguity is computed at each epoch, starting from a reset point, as follows:

$$avr_n = \frac{(n-1) avr_{n-1} + amb}{n} \quad (4.22)$$

where avr is the ambiguity average, n is the epoch index starting from the reset and amb is the current computed ambiguity. Before considering the current ambiguity in the computation of the moving average, a test is performed to detect the occurrence of cycle slips above a selected ambiguity window (plus or minus four cycles, for example). If the difference between the computed ambiguity and the moving average is less than the specified ambiguity window, no cycle slip is assumed. If the difference is larger than the specified limit, it is assumed that a cycle slip occurred, and the moving average is reset. Without cycle slips and when ambiguities are correctly solved, the moving average should be an integer number. Without cycle slips and when an incorrect solution is selected, the moving average, as computed from equation (4.22), is a real number. Once the moving average has been computed, the computed ambiguity is compared to it. If they agree, the computed ambiguity is considered as correct. Otherwise, the moving average is taken as the correct ambiguity. Before comparing the estimated ambiguities with the moving average a certain number of epochs should elapse after the reset, in order to allow reliable computation of the moving average. This period depends on the expected noise of the observations.

Other tests commonly used to identify the correct ambiguity are statistical tests on the estimated variance factor, namely the chi-square test and the F-test. In the chi-square test the a posteriori variance factor is checked for compatibility with the a priori variance factor and the acceptance criterion is given as follows [Lachapelle et al., 1992]:

$$\hat{\sigma}_0^2 < \left(\frac{\sigma_0^2}{df} \right) \chi_{df, 1-\alpha}^2 \quad (4.23)$$

where σ_0^2 is the a priori variance factor and $\chi_{df, 1-\alpha}^2$ is the chi-square percentile for degrees of freedom df and confidence level $1-\alpha$.

The F-test uses the ratio between the smallest variance and the second smallest variance to ensure their statistical independence. The smallest variance comes from the ambiguity set selected as described in Figure 4.2. The second smallest variance comes from the “next best” ambiguity set, which would be selected by modifying Figure 4.2 to maintain both the best ambiguity sets having smallest and next smallest variance. This comparison is given as [Erickson, 1992]:

$$\frac{\hat{\sigma}_0^2(2)}{\hat{\sigma}_0^2(1)} \geq F_{df1, df2, \alpha} \quad (4.24)$$

where the numbers under parenthesis stand for the smallest and second smallest variance factor, and F is the Fisher distribution for $df1$ degrees of freedom (for the solution with smallest variance), $df2$ degrees of freedom (for the solution with second smallest variance) and significance level α . If the ratio is greater than a specified value, the ambiguities are considered solved, otherwise the result is considered incorrect. A reliable acceptance limit for this ratio was taken to be greater than or equal to 2 by Landau and Euler [1992], and greater than or equal to 3 by Cannon and Haverland [1993], based on empirical results.

Both the chi-square test and the F-test are based on the assumption that the residuals are normally distributed. When solving for the ambiguities instantaneously, the number of measurements is not large enough to give a good description of the residual distribution. Therefore statistical testing may not be reliable in rejecting wrong solutions, particularly

when single frequency observations are used.

Due to this considerations, the validation strategy used in later chapters of this reports is based on the moving average and statistical tests, both the chi-square test and the F-test. An assessment of the performance of each validation strategy is made in Chapter 7.

Chapter 5

FACTORS AFFECTING THE ACCURACY OF ATTITUDE DETERMINATION WITH GPS

In this chapter the main factors affecting accuracy of attitude determination from a multi-antenna GPS are described. These factors can be divided in two categories [Mowafy, 1994]. The first category comprises errors in GPS carrier phase measurements. These errors are due to receiver-specific errors, antenna phase centre variation and multipath propagation. The second category addresses operational factors such as baseline length, structural flexing, satellite geometry and antenna configuration.

5.1 Measurement Errors

Due to the short lengths of baselines used in attitude determination, some of the measurement errors cancel out (or become negligible) when a double difference observable is used (see section 4.1.3). The main errors left are receiver specific errors, antenna phase centre variation and multipath. These errors will be briefly described and quantified.

5.1.1 Receiver Specific Errors

The measurement of GPS observables can not be made with infinite precision. There is always some level of noise contaminating the observations. The most basic kind of noise is due to the electrical current generated by the electrical motion of the electrons

and is known as thermal noise or Johnson noise (after J.B. Johnson who first observed the effect in 1927) [Looney, 1993]. The thermal noise power, P_t , is proportional to the effective noise temperature of the device in which the noise current flows, T_e , as expressed by the following relationship [Langley, 1996]:

$$P_t = k \cdot T_e \cdot B \quad (5.1)$$

where k is the Boltzmann's constant and B is the bandwidth in Hertz.

The minimum received GPS signal power, including minimum transmitted signal power, free-space loss and atmospheric attenuation is 10^{-16} Watts [Braasch and Graas, 1991]. The signal to noise ratio S/N can be derived from:

$$S/N = \frac{10^{-16}}{k \cdot T_e \cdot B} \quad (5.2)$$

The r.m.s. error on the reconstructed carrier, σ_c , which dictates the measurement accuracy, is given by the following equation [Cohen, 1996]:

$$\sigma_c = \sqrt{\frac{B}{C/N_0} \cdot \frac{\lambda}{2 \cdot \pi}} \quad (5.3)$$

where C/N_0 is the carrier signal to noise ratio, and λ is the carrier wavelength in metres.

The equation of C/N_0 can be written as follows:

$$\begin{aligned} C/N_0 &= S/N \cdot B && \text{Hz} \\ &= 10 \cdot \log_{10}(S/N \cdot B) && \text{dB-Hz} \end{aligned} \quad (5.4)$$

The antenna gain has a direct effect on the estimated value of the carrier signal to noise ratio [Jurgens et al., 1992]. Higher antenna gain increases system performance by increasing the carrier signal to noise ratio, and consequently lowering receiver measurement error. In most GPS antennas the gain is small for low elevation angles; thus measurements of low elevation angles are noisier.

The carrier tracking loop bandwidth (B) should be tuned to accommodate changes in the receiver-satellite relative motion. For most geodetic applications the receiver is stationary, therefore bandwidths of 2 Hz or less can be used. A tracking loop with such a narrow bandwidth might have problems due to rapid variations in phase caused by the ionosphere [Langley, 1996]. For dynamic applications up to 4g the bandwidth is typically 20 Hz. The magnitude of the receiver noise in static applications can be less than 0.5 mm, while in dynamic situations can increase to 1-5 mm [Braasch and Graas, 1991].

The choice of the tracking loop bandwidth should be wide enough to avoid loss-of-lock during motion and to allow a high data renewal rate. The bandwidth should be narrow enough, however, to achieve a small probability of occurrence of cycle slips [Braasch and Graas, 1991].

Other receiver specific errors include local oscillator instability, crosstalk, inter-channel biases, drifts and quantization noise [Langley, 1996]. The error due to local oscillator instability can be solved or differenced out if measurements on all visible satellites are made at the same instant.

Crosstalk is the interference between Radio Frequency (RF) paths that causes signal energy from one path to couple into another. A high level of isolation between paths is

required to keep crosstalk to a level of 0.5 mm or lower.

Inter-channel bias results from using different hardware channels to measure the carrier phase for each satellite. In modern receivers these errors are calibrated at the level of 0.1 mm or better [Hofmann-Wellenhof et al., 1994].

Drifts are a nearly constant offset from one channel to another, due to different antenna cable length and temperature changes inside the receiver. Since such drifts are the same for simultaneous observations, they are removed in the double-differencing process.

Finally, quantization noise results from imprecision of analogue to digital conversion in the digital receiver. This error can usually be neglected in a digital receiver [Langley, 1996].

In summary, receiver specific errors in carrier phase measurements are within 1 mm level for low dynamic applications such as hydrographic surveying.

5.1.2 Antenna Phase Centre Variation and Imaging

The antenna phase centre is the apparent electrical centre of the antenna, or the point at which the radio signal measurements are received. The antenna phase centre of GPS antennas is dependent on the direction of the signal and does not generally coincide with the physical centre of the antenna [Schupler et al., 1994]. A mean phase centre is computed during a calibration process and its location is a function of antenna type and design.

In real applications the antenna receives signals from different directions. Each

signal is received at an actual phase centre. The difference between the mean of the actual phase centres and the nominal mean phase centre is defined as the antenna phase centre variation. For modern geodetic GPS receivers, this variation is of the order of a fraction of a millimetre to a few millimetres depending on satellite geometry and antenna design [Mowafy, 1994].

Since a differencing technique is employed in GPS measurements for attitude determination, it is very important to ensure repeatability of phase centre variations between antennas. In this case, the variations will be minimized in the differencing process. The repeatability between antennas can be reinforced by using the same type of antennas and orienting them towards north in the same way.

Imaging occurs when another conducting body in the immediate vicinity of the antenna, such as a large reflector or a ground plane, changes the radiation pattern of the isolated antenna. The total pattern will be in general more complicated than the original antenna pattern which contributes to an increase in the phase centre variation. Although this phenomenon seems similar to multipath, one distinction, as mentioned by Tranquilla [1986, p.561], is “the ability to more easily model the effect as an array phase centre movement and to visualize the interference pattern as a function of observation angle.” In shipborne applications, for example, the metal superstructure may contribute to imaging problems.

During field data collection (see Chapter 6) three microstrip geodetic GPS antennas were used. These antennas were all aligned to the same direction in order to minimize the error due to phase center variations. The vessel where the antennas were mounted was made of fiber glass (a bad conductor of electrical energy) and no other metallic structures

were located in the vicinity of the antennas. In this case, errors due to imaging effects are assumed to be negligible.

5.1.3 Carrier Signal Multipath

The term multipath denotes the possibility of radio signal propagation along various paths from the transmitter to the receiver. In multipath propagation two or more paths exist: a direct path and other paths via diffractions and refractions from surfaces that are not part of the antenna itself. Reflections from parts of the antenna are most conveniently described as antenna phase centre variations [Georgiadou and Kleusberg, 1988].

The reflected and diffracted component can be separated in two parts: one specular (coherent) and the other diffuse (incoherent). The specular component is well defined in terms of amplitude, phase and incident direction. Its main characteristic is its conformance to Snell's law. The diffuse component arises from the random nature of the scattering surface and is non-deterministic [Sadiku, 1993].

The effect of the coherent part is the main source of multipath error. Its maximum possible error on carrier phase measurements was estimated to be 90 degrees or 4.8 cm in range of the L1 carrier. It can be demonstrated [Georgiadou and Kleusberg, 1988] that the following factors influence the carrier phase multipath error frequency:

- it is inversely proportional to the carrier wavelength.
- it is proportional to the perpendicular distance of the antenna phase center from a flat reflector.

- proportional to the cosine of the elevation of the satellite above the reflector plane.
- proportional to the rate of change of the elevation of the satellite above the reflector plane.

Multipath errors are a function of the specific antenna environment, materials, antenna gain pattern, geometry and receiver design. An approximate rule of thumb for a differential ranging error between a pair of closely spaced microstrip antennas, due to multipath is about 5 mm standard deviation [Cohen, 1996].

In small-launch hydrographic applications multipath interference for pseudorange can be expected mainly from specular reflections of objects in the vicinity on the antenna (with period of 5 to 10 minutes depending on satellite elevation) and very low frequency (25 to 60 minutes period) reflections from the water surface [Tranquilla and J.P. Carr, 1991]. It has been shown [Fu, 1992] that, at a static site, carrier phase multipath error from water surface observed on GPS carrier phase measurements can be modeled as a coherent reflected signal superimposed with a small random component. The periodicity of the coherent signal lies between 20 to 50 minutes period. This result is in accordance with multipath error models derived for the code tracking loop and carrier tracking loop. Simulated results using these models predicted code and carrier phase multipath with the same periodicity, however, the pseudorange error peak occurs when the carrier phase error are zero and vice-versa [Braasch, 1996].

The rolling and pitching motion of a hydrographic launch rapidly changes the satellite-reflector-antenna geometry and this randomizes the effects of multipath, so that it becomes more noise-like, and does not have a systematic effect. As the motion dynamics

decrease, however, multipath effects become more significant [Lachapelle, 1989]. Thus, under calm water conditions, multipath effects are more significant than under rough water conditions.

5.1.3.1 Carrier Signal Multipath Detection and Minimization Techniques

The topic of multipath mitigation in GPS carrier phase measurements has received considerable attention in the literature, thus, it is not possible to describe all the methods in one small subsection. Instead, a brief overview is presented of some of these techniques.

The simplest method to reduce multipath is by placing the antenna where it is less likely to receive reflected signals. One example that eliminates ground bounce reflection is by placing the receiver GPS antenna on the ground instead of a tripod [Weill, 1997].

Some multipath mitigation techniques attempt to take advantage of signal propagation geometry through the use of special antennas. Such techniques include the use of ground planes, choke rings, absorbing material, and polarization discrimination. The groundplane is a metallic circular disk in the horizontal plane and centered at the GPS antenna's base. The disk should provide a shield against signals coming from below the horizon. The groundplane does not perform as well as expected because signals from below may induce edge-currents which produce significant diffracted components [Tranquilla, 1986]. For this reason an electrically lossy material may be incorporated into the groundplane or the groundplane can be replaced by a choke ring which is essentially a groundplane containing a series of concentric circular troughs one-quarter wavelength deep.

The use of groundplanes or choke rings is not recommended in marine applications where the ship's motion may raise the antenna groundplane horizon well above the earth horizon.

Additional multipath attenuation by the antenna results from polarization discrimination. The direct GPS signal is right-hand circularly polarized. Upon reflection from a planar surface the signal will be left polarized. An ideal antenna will completely reject all signals that are left polarized. In practice this does not happen but some level of attenuation can be achieved. Reflections from very rough surfaces have random polarization characteristics and thus are less attenuated [Braasch, 1996].

Other methods for reducing multipath effects, considered the most promising [Weill, 1997], use real-time signal processing within the receiver tracking loop. These include the use of narrow correlator spacing [Braasch, 1996] and the Multipath Estimating Delay Lock Loop (MEDLL) [Townsend et al., 1995] to improve the carrier phase tracking performance.

The use of special antennas and signal processing within the receiver tracking loop attempt to reduce the effect of multipath on the carrier observable. Other methods, which can be used in conjunction with the above two, attempt to reduce multipath through special processing of the measurements. One technique that can be used to accurately determine multipath at a fixed site, such as a differential GPS station, is to observe the same satellites from one day to the next and to analyze the correlation between carrier phase measurements, advanced by about four minutes per day due to the half-a-sidereal-day period of the satellites. Since the satellite-reflector-antenna repeats from satellite pass to pass, multipath effects should also repeat, and will show up as correlation peaks. Another

technique is temporal averaging, which removes short period multipath signatures but does not work very well for low frequency multipath variations and does not eliminate multipath bias [Meehan and Young, 1992]. Obviously, these techniques require batch processing.

Other methods use measurements by multiple receivers to reduce carrier phase multipath. Using the geometrical aspects of reflection in combination with special arrangement of GPS antennas it is possible to detect multipath [Becker et al., 1994]. Another approach is described by Raquet [1996] which uses observations from multiple receivers, with well known positions, to estimate the code or carrier phase multipath by performing a least squares condition adjustment using all the available measurements from all the reference receivers. This method was tested in a kinematic field test involving one mobile receiver and an improvement was observed of 28 to 35% in the positioning accuracy of the mobile receiver [Raquet and Lachapelle, 1996]. Further development of this method will be the use of another constraint (such as antenna baseline length), instead of the relative positioning vector between antennas. This development will have application in instantaneous ambiguity resolution, since the method estimates the multipath error using measurements from a single epoch.

The Signal-to-Noise Ratio (S/N) measured by the receiver depends on the amplitude of the direct signal, the antenna gain pattern and multipath. One multipath mitigation technique [Axelrad et al., 1994] uses the SNR to estimate the spectral parameters of the multipath and then constructs a profile of the multipath in the carrier phase which is used to correct the original measurements.

For short baselines the differential ionospheric delay will be very small and

variations in the dual frequency ionospheric free solution will be an indicator of multipath contamination [Georgiadou and Kleusberg, 1988]. This is based on the idea that multipath effects vary with wavelength, and are unlikely to occur on both L1 and L2 frequencies simultaneously. The carrier phase ionospheric free solution, in units of length, is given by:

$$\Delta_f = \lambda_2\phi_2 - \lambda_1\phi_1 + C \quad (5.5)$$

where the subscript stands for the carrier frequency (L1 or L2) and C is a linear combination of the carrier phase ambiguities. For short baselines, the carrier phase ionospheric delay computed from dual frequency carrier phase observations can be used to indicate the presence of multipath.

During field data collection (see Chapter 6), antennas were mounted free from any reflecting structure of the vessel, and this was the best way to avoid multipath. These antennas have a built-in ground plane which, we believe, avoided multipath signals reflected by the water surface. Note that the pitching and rolling motion of the vessel were less than ten degrees (see Appendix B) which was the selected satellite mask angle. If the amplitudes of these motions were greater, then use of ground planes would have been avoided since the groundplanes may raise above the satellite elevation angle mask.

5.2 Operational Factors

In addition to measurement errors, operational factors may affect the accuracy of attitude determination with GPS. These factors are structural distortion, baseline length,

satellite number and geometry, and antenna configuration. The influence of these factors is briefly discussed in the following sub-sections.

5.2.1 Structural Flexing

For determination of the attitude of a moving platform using GPS, the antennas must be mounted at stable points. In practice, the body of ships and other large vehicles may experience torsion, vibration and bending. These changes may result in significant attitude errors.

Antenna mounting is another factor that must be considered to ensure the stability of the antennas. In shipborne applications, for example, the antennas usually can not be mounted on the surface and requires elevating the antennas above the surface. When elevating the antennas, care must be taken to minimize vibrations in the antenna supporting structure.

5.2.2 Baseline Length

The attitude pointing error depends directly on the differential range error and baseline length, according to equations (2.22) to (2.24). The most basic strategy for diminishing GPS attitude error is to increase antennae baseline length. As the baseline length increases, however, multipath effect becomes less correlated and differential multipath error may increase. Furthermore, the flexibility and bending of the surface carrying the antennas becomes more likely as the baseline length increases. In dynamic

applications, the accuracy achieved by a GPS attitude system is not linearly dependent on baseline length mainly due to the increase in differential multipath and structural flexing.

5.2.3 Satellite Number and Geometry

The minimum requirement for attitude determination using GPS is measurements from four satellites. If a common time reference is used then only signals from three satellites are required to compute the relative positioning vector between antennas. Given additional radial and geometrical constraints between antennas, a minimum of two GPS satellites is required for an attitude fix [Knight and Hatch, 1990]. This does not apply for instantaneous ambiguity resolution using the least squares search method. This method relies upon the existence of redundant satellites, therefore, more satellites than the minimum number are required.

The number of visible satellites affects measurement redundancy. Increasing the number of visible satellites improves attitude reliability [Mowafy, 1994]. Measurement redundancy also has an important effect in ambiguity resolution using the least squares search method. If only the minimum number of measurements are made, then it will be impossible to solve the ambiguities. Increasing the degree of freedom of the observed carrier phase double differences will improve the accuracy of the final solution.

Satellite geometry has an important effect in carrier phase ambiguity resolution. In the ambiguity least squares search approach a set of four primary satellites is selected to generate a set of potential solutions. The four satellites should have a good geometry to

generate the correct ambiguities. The Geometric Dilution of Precision (GDOP) algorithm is used to select the best satellites [Parkinson, 1996] for receiver position and clock error determination. The GDOP matrix results from the position and time solution covariance matrix divided by the variance of the ranging errors to the satellites. The GDOP value is defined to be the square root of the trace of the GDOP matrix:

$$GDOP = \sqrt{EDOP^2 + NDOP^2 + VDOP^2 + TDOP^2} \quad (5.6)$$

where EDOP (East DOP), NDOP (North DOP), VDOP (Vertical DOP) and TDOP (Time DOP) are the successive diagonal elements of the GDOP matrix. The lower the GDOP value the better position and clock error determination will be.

Based on the GDOP concept, Brown and Evans [1990] introduced other figures of merit such as the Az-DOP and El-DOP (stand for Azimuth and Elevation Dilution of Precision respectively) as given by the following formulas:

$$Az-DOP = \frac{\sqrt{\cos^2(Az) \cdot NDOP^2 + \sin^2(Az) \cdot EDOP^2}}{D} \quad (5.7)$$

$$El-DOP = \frac{VDOP}{D} \quad (5.8)$$

These figures of merit indicate the influence of the baseline length and satellite geometry for a given baseline orientation.

5.2.4 Antenna Configuration

The minimum number of antennas required for attitude determination is three, with the condition that not all the antennas are collinear. Factors such as multipath minimization and baseline length are of major concern when choosing the best antennae location.

Another factor is the antenna configuration. This factor depends on the method used for attitude determination. Using the direct method described in section 2.6, at least one of the baselines must be parallel to one of the BCS axis. The method that uses the attitude transformation matrix and the least squares approach do not impose any restriction on antenna locations, hence, some configurations may be more advantageous than others.

The effect of antenna configuration has been analyzed when using three and four antennas in planar and three dimensional configuration [Serrano et al., 1995]. For a three antenna system the best configuration consists of two orthogonal baselines. For a four antenna system the orthogonal triad gives the best results. However, the results for a planar distribution of the four antennas in a square shape do not differ significantly from the orthogonal triad.

In this study the number of available antennas was limited to three. There existed some constraints concerning the possible locations of the antennas aboard the vessel. Within these constraints, the triangular configuration, used in the experiment described in Chapter 6, was selected due to the following reasons:

- The angle between two baselines was almost orthogonal (about 76°).
- Using existing frames and poles the antennas could be well fixed to the vessel in

order to avoid possible vibrations and displacements due to vessel motion and sea action.

- At these locations the antennas were free from any metallic structure or obstruction in their vicinity.

Chapter 6

FIELD DATA

This chapter deals with the collection of field data. This occurred on 23 January 1997 aboard the Canadian Hydrographic Service survey launch *Plover* [Bedford Institute of Oceanography, 1996] at Bedford Basin, Halifax. This data was used to compare GPS attitude results with data from a GPS/INS system used for motion compensation of multibeam sonar surveys, and to gain experience with some of the conditions and problems encountered when processing GPS carrier phase measurements. The chapter describes the equipment used, its installation aboard and data collection methodology. The last section deals with time tagging of data from both sensors, gaps in the data set and interpolation.

6.1 Equipment Used

The survey launch “Plover” is a 10 metre hydrographic survey launch used to carry out port surveys and near-shore mapping.

Table 6.1 - Hydrographic launch characteristics [After Dinn and Crutchlow, 1996].

Length overall	9.5 m
Beam	3 m
Draft	0.7 m
Displacement	6 Ton
Typical survey speed	6 to 10 kts

This launch is made by fiberglass-reinforced-plastic and is equipped with a SIMRAD EM 3000 MBES capable of 120° swath survey [Dinn and Crutchlow, 1996]. The

system uses a keel mounted transducer and a POS-MV model 320 motion sensor [Applied Analytics, 1996a] for position and attitude determination.

The GPS attitude determination system was composed of three Ashtech Z12 GPS receivers. Two of these sensors were provided by the University of New Brunswick, Department of Geodesy and Geomatics Engineering. The third was provided by the Canadian Hydrographic Service, Atlantic division at the Bedford Institute of Oceanography.

A fourth Ashtech Z12 GPS receiver was used as a base station onshore to provide real time positioning of the survey launch with centimeter level accuracy, using Carrier Phase Differential GPS (CPD) [Ashtech, 1995]. RFM96 radio modems from Pacific Crest Corporation [Pacific Crest, 1995] were used for wireless communication between the GPS base station and one of the receivers aboard.

6.1.1 Ashtech Z-12™ GPS Receiver

The Ashtech Z12 is a 12 channel, dual frequency GPS receiver that provides code and carrier phase measurements on both the L1 and L2 bands in the Z-tracking mode or in the P-code mode. The Z-tracking is a technique developed by Ashtech, used to neutralize the effect of Anti-Spoofing (AS) [Leick, 1995].

A standard Ashtech Z12 with the RTZ option installed, can be used for CPD. The navigation solution is processed in the rover receiver using the raw data transmitted via radio modem from one Ashtech Z12 at the base station. After some initialization time, centimetre level kinematic positioning accuracies can be achieved.

These receivers have the capability to internally record raw data which can be downloaded to a computer in real time or after the survey is completed. Raw data files (pseudorange, carrier phase and ephemeris data) can be post-processed using Ashtech's PNAV (stands for Precision Navigation), which is a software trajectory package that provides positioning solutions using CPD.

Standard accessories of each of the GPS receivers used for data collection were a precision geodetic antenna with groundplane.

6.1.2 POS/MV 320

POS/MV stands for Position and Orientation System for Marine Vessels and designates a group of inertial navigation system products that deliver position and orientation solution for marine vessels. This system has been developed in conjunction with the CHS in order to provide dynamically accurate and reliable position and attitude information for modern swath sonars (150 degrees or greater swath width)[Scherzinger et al., 1996].

POS/MV 320 is a GPS aided inertial navigation system which combines an IMU, and two GPS receivers in a single integrated package. The two GPS receivers are NovAtel GPSCard, both equipped with NovAtel antennas. One of the receivers, designed as master, is a model 3151R Performance Series Card, capable of receiving and processing differential corrections and the other, designed as slave, is a model 3151 Performance Series Card.

The aided inertial navigation algorithm of the POS/MV 320 comprises a strapdown

inertial navigator, a GPS Azimuth Measurement Subsystem (GAMS) and an error regulation component. The strapdown navigator computes the navigation solution with reference to an ellipsoidal rotating earth using inertial data of the IMU. These computations occur at the IMU sampling rate of 100 Hz. The GAMS computes heading aiding data using the carrier phase observable from the two GPS receivers. The GAMS azimuth measurements are combined with the inertial sensor data in order to obtain heading measurements. The error regulation component comprises the Kalman filter and a closed-loop error controller.

The POS/MV accuracy specification (with GAMS), given by the manufacturer, is equal to 0.05 degrees r.m.s. error for roll, pitch and heading. This error level is maintained under all vessel dynamics [Applied Analytics, 1996b].

6.2 Equipment Installation

The sensors used for data collection were six GPS receivers and one IMU. As mentioned in section 6.1 the GPS antennas were four Ashtech microstrip model (one as a base station) and two Novatel models as part of the POS/MV 320.

6.2.1 GPS Antennas

Within the constraints imposed by the survey launch structure, three Ashtech antennas were mounted in a triangular pattern with two antennas parallel to the pitch axis in a symmetric position and the other antenna mounted above the IMU, on the roll axis of

the vessel. The two NovAtel antennas were mounted parallel to the pitch axis in the baseline defined by two Ashtech antennas as depicted in Figure 6.1.

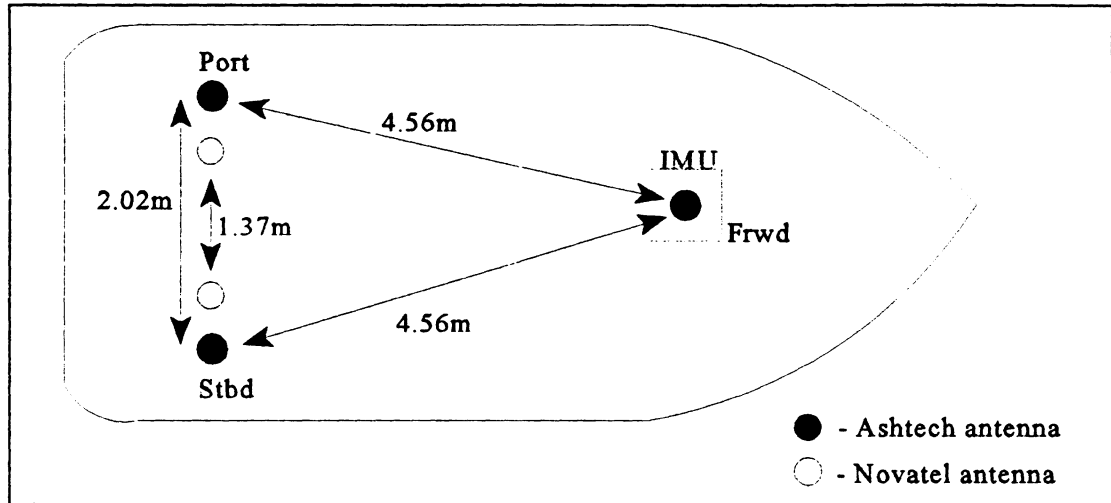


Figure 6.1 - Antenna Layout onboard.

The distance between Ashtech antennas were evaluated after processing raw GPS data using PNAV, with a standard deviation less than 0.5 cm for all baselines. The distance between NovAtel antennas was based on BCS coordinates previously measured [Bedford Institute of Oceanography, 1996].

The Ashtech antennas *Stbd* and *Port* as well as the two NovAtel antennas were mounted on a solid metal frame and the Ashtech antenna *Frwd* was mounted on the top of a pole. All antennas were well fastened to the vessel's structure in order to minimize remaining vibrations due to motion and sea action. All Ashtech and Novatel antennas were oriented the same way to minimize the error due to phase center variations.

Some of the attitude determination methods described in Chapter 2 require the knowledge of antennas BCS coordinates. However, BCS coordinates of the location of Ashtech antennas were unknown and was not possible to measure this coordinates in static

GPS survey due to the following reasons:

- The launch was never in a static position even when anchored in the harbour.
- Even when the launch was strongly tied to the pier, and could be considered “almost” in a static position, satellite visibility and multipath were limiting factors caused by the ships anchored beside the launch.

It was very important to have at least one of the Ashtech antenna baselines parallel to pitch or roll axis. Since the BCS of those antennas are unknown, the only way to compute the vessel’s attitude parameters is through the direct determination method (see section 2.6) which requires one antenna baseline parallel to the roll or pitch axis.

The Ashtech antenna designed as *frwd* was connected to one Ashtech Z12 receiver that was working as a rover in CPD mode. The base station was mounted on the top of the Bedford Institute of Oceanography and radio link communications were established using the Pacific Crest RFM96 radio modem.

6.2.2 Inertial Measurement Unit

The IMU was part of the POS/MV 320 already installed aboard. Its position was right above the echosounder transducer. During POS/MV installation it was necessary to perform measurements on the mounting of the IMU with respect to the echosounder, the ship and the GPS NovAtel antennae. For attitude determination it is important to determine the ship to IMU misalignment angles, which in this case were:

- pitch offset: +2.30°

- roll offset: 0°

These angles were determined after an underway assessment of the physical alignment during installation. This assessment is designed as patch test and is used to identify systematic errors in MBES [Hughes Clarke, 1996]. The accuracy of the measured misalignment angles is within 0.05°, which is the same accuracy as expected from the POS/MV attitude measurements. These parameters are loaded into the POS/MV controller program after each new installation.

6.3 Data Logging

GPS raw data from the Ashtech receivers installed aboard were logged in the receivers at a 1Hz output rate and downloaded to a computer after the experiment was completed. The Ashtech receiver identified as *frwd* (see Figure 6.1) was connected to a computer for real time recording of NMEA GGA messages [NMEA, 1995] resulting from CPD positioning mode. This data was used to generate the vessel trajectory plots in Appendix C.

The POS/MV 320 was operated by a Windows controller program installed on a computer supplied as part of the POS/MV system. Data logging operations were performed through this program and the files were stored in the computer hard drive. There are many output data groups available from the POS/MV system [Applied Analytics, 1996c]. For this experiment data group 4 was selected, which includes echosounder pitch, roll, heading, yaw and heave. A 10 Hz output rate was selected.

Eighty three minutes of data were collected, starting at 408440 seconds (aprox. 17:27 UTC) and finishing at 413472 (aprox. 18:50 UTC) on 23 January 1997, as shown in Figure 6.2.

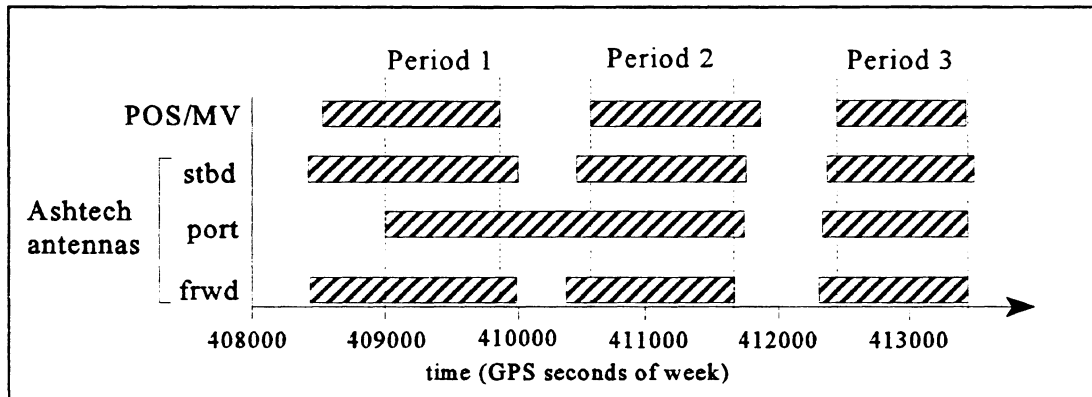


Figure 6.2 - Data collection periods for the POS/MV and GPS Ashtech antennae.

In order to transfer POS/MV data into 1.44 Mbytes diskettes data collection had to be interrupted after approximately 20 minutes of internal Z-12 data logging, due to limitations in the data storage capacity of the Ashtech receivers installed aboard. The data collection gaps are shown in Figure 6.2. There are three periods with data from all sensors, each lasting between 13 and 18 minutes (see Table 6.2), with a total of 47 minutes of simultaneous data.

Table 6.2 - Periods of observation with data from all sensors.

	Start (GPS time)	End (GPS time)	Duration
Period 1	409016.0	409849.0	833 sec. or 13.9 minutes
Period 2	410573.0	411613.0	1040 sec. or 17.3 minutes
Period 3	412463.0	413413.0	950 sec. or 15.8 minutes

During data collection the water surface was flat and the wind was calm. The vessel performed several maneuvers and changed speed from 0 to 8 m/s. Although sudden changes

of course and speed are not usual in hydrographic surveys, testing a motion sensor under such dynamic conditions, will enable us to evaluate its real performance under linear and rotational accelerations. The trajectory plots are shown in Appendix C.

The satellite configuration during the test is described in Appendix D. The satellite elevation mask angle was set for 10 degrees in order to avoid the multipath effect from satellites near the horizon. With this elevation mask angle there were always six or more satellites visible (see Figure D4). The satellite geometry during all the periods of data collection was good, as shown by the satellite configuration plots (see Figures D1, D2 and D3) and confirmed by the PDOP value being always less than 2.0 (see Figure D4).

6.4 Problems and Solutions

The quality of the data set collected was dependent on a number of factors. Since data from different sensors is going to be compared the first problem was related with time tagging the data. The second problem was the identification of gaps in the data set. Finally, there was the problem due to interpolation of the POS/MV 320 data set to Ashtech Z12 epochs, since these sensors are not synchronized. The next subsections describe these problems and the solutions used to correct them.

6.4.1 Time Tagging the Data

Data from the Ashtech Z12 receivers was time tagged with GPS time and data from the POS/MV 320 was time tagged with UTC (Coordinated Universal Time). These two

time systems are related by an integer number of seconds. For the date of the experiment GPS time was ahead of UTC by eleven seconds [U.S. Naval Observatory, 1995]. All POS/MV observation epochs were corrected for GPS time. Thus all the data sets were referred to GPS time. That does not mean that observations occurred simultaneously. The problem of mismatching observation epochs is dealt with in section 6.4.3.

6.4.2 Data Gaps

All the raw data files were examined for the occurrence of missing epochs. Data files from the Ashtech receivers are evenly spaced at one second epoch interval, with no gaps in the data set. The POS/MV 320 raw data files have a total of 22 isolated single epochs with no data, considering a data rate collection of 10 Hz. These data gaps on POS/MV files occurred during Period 2 between GPS time epochs 411310 to 411330 seconds, and during Period 3 between GPS time epochs 413130 to 413150 seconds. The number of epochs with data gaps in the POS/MV files is 0.07% of the number of epochs with data.

6.4.3 Interpolation

Attitude measurements made by the POS/MV 320 at a 10 Hz data rate, need to be interpolated for the Ashtech GPS receiver epochs. The interpolation method had to be chosen such that the error introduced was within the estimated error for POS/MV 320 attitude measurements (0.05 degrees r.m.s. error).

In order to test the errors induced by interpolation, two data sets were formed from each POS/MV file. The first set was formed by the odd elements and the second set was formed by the even elements of the original POS/MV data file. The first set contains measurements at 5 Hz data rate and was interpolated for the epochs of the second set. The difference between the interpolated parameters (using the file with even elements) and the observations (file with odd elements) is due to interpolation and measurement errors. The interpolation of the original data set, at a 10 Hz data rate, will induce an error smaller than the one evaluated by the process described above.

Due to its simplicity and fast computational speed, linear interpolation was the first method to be tested. The difference between linearly interpolated attitude angles and measurements is shown in Figure 6.3.

The difference between interpolated values and measurements is related with sudden changes of course (for heading and roll differences) and sudden variations of velocity (for pitch differences). From Figure 6.3, maximum errors due to linear interpolation for heading pitch and roll are, respectively, 0.08, 0.4 and 0.18 degrees. Therefore, errors due to linear interpolation exceed the POS/MV 320 error given by the manufacturer, which is 0.05 degrees. Thus another interpolation method had to be used.

The second method tested was cubic spline interpolation [Press et al.,1992]. Using the procedure described above, with the same data sets, the difference between cubic spline interpolated values and measurements is shown in Figure 6.4. From this figure, maximum errors due to cubic spline interpolation for heading pitch and roll are, respectively, 0.02, 0.07 and 0.03 degrees. Now, the difference between interpolated values and measurements

is within the POS/MV 320 error except for pitch. The error in interpolating pitch using cubic splines exceeds 0.05 degrees only in four epochs and the increment is not significant. Furthermore, these error limits are reduced when interpolating for a 10 Hz data rate. This is a significant improvement when compared to linear interpolation, which satisfies the initial requirement of an interpolation error less than 0.05 degrees. Therefore, cubic spline interpolation was the method used to compute the POS/MV attitude values for the Ashtech GPS receiver epochs. The plots shown in Figures 6.3 and 6.4 use the POS/MV data set collected during period 1. Similar results were achieved for the other two files.

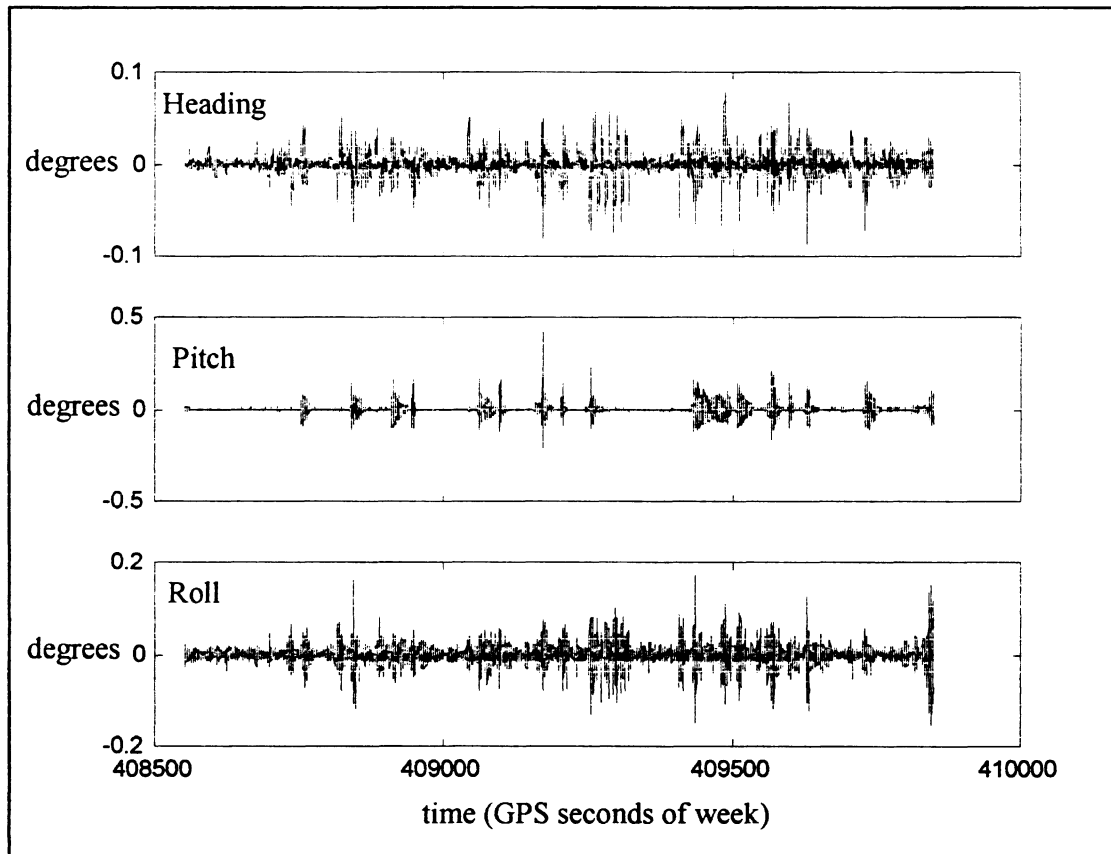


Figure 6.3 - Error due to linear interpolation of heading, pitch and roll.

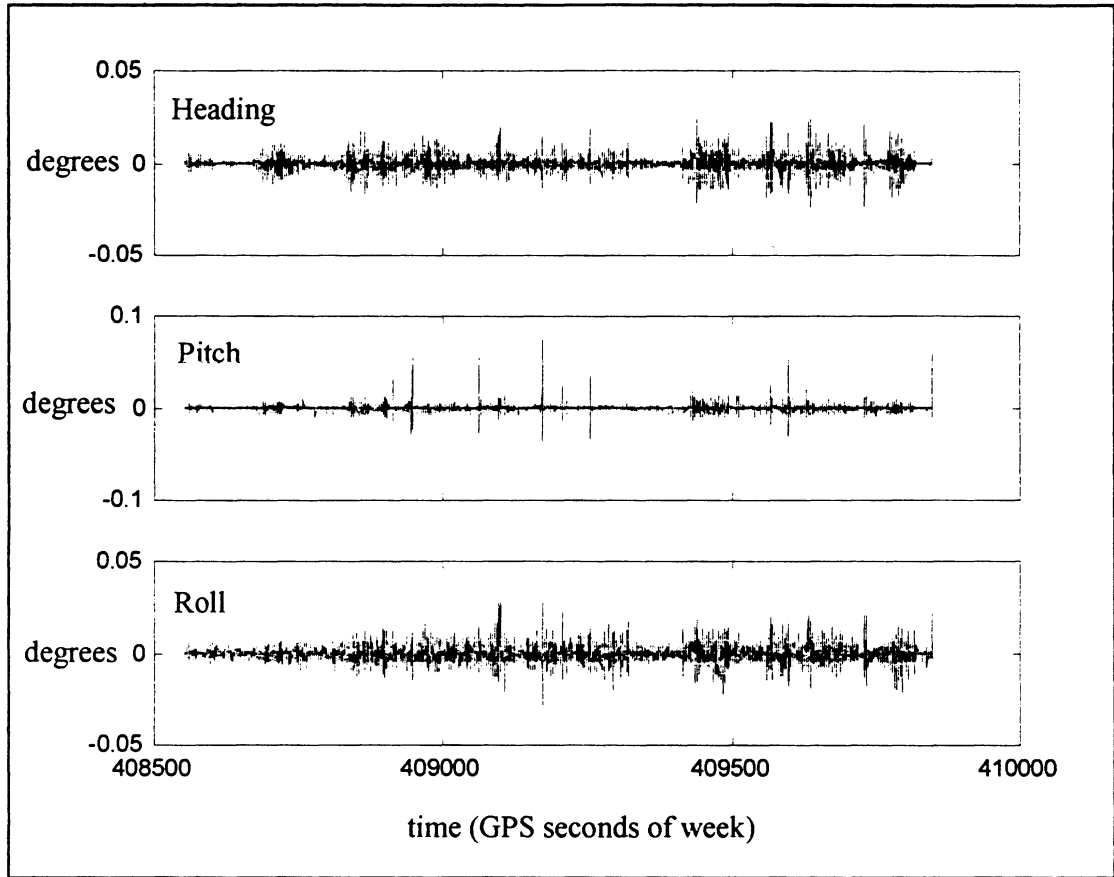


Figure 6.4 - Error due to cubic spline interpolation of heading, pitch and roll.

Chapter 7

DATA PROCESSING AND RESULTS

The final stage of this investigation was the processing of the data collected in the field. The processing was done in two steps. First, GPS derived relative LCS coordinates between antennas were estimated. Second, GPS attitude measurements were derived from the antennas LCS relative coordinates and compared with interpolated POS/MV 320 attitude measurements. The first section describes the processing of GPS measurements to derive LCS coordinates between antennas. In this section results achieved using the techniques described in section 4.2 are compared with PNAV solutions. The second section deals with determination of attitude using previously computed LCS coordinates from GPS measurements and shows results of the comparison between GPS and POS/MV 320 attitude measurements.

7.1 Processing GPS Carrier Phase Measurements

This section contains the bulk of the data processing effort. Without fixing the GPS carrier phase ambiguities it would not have been possible to derive attitude measurements. Raw GPS data collected on the field was first processed using PNAV, and independently processed using the technique of least squares instantaneous ambiguity resolution as described in section 4.2. Results from PNAV were used only to derive the vessel trajectory, and to evaluate the performance of the ambiguity resolution method described in this report.

7.1.1 Using PNAV

Ashtech's PNAV software trajectory package was used to provide LCS coordinates between antennas with centimeter level accuracy provided by CPD positioning mode. PNAV derived relative positions between the shore base station and the vessel *frwd* antenna were used to generate the trajectory plots in Appendix C. PNAV was also used to compute the relative coordinates of the three antennas installed aboard.

The setup parameters chosen to process the data correspond to the ship motion dynamics. The setup parameters comprise the Kalman filter system parameters, Kalman filter measurement noise parameters and run time parameters, all set by the default PNAV dynamic model. The quality of the PNAV solution is measured by the averaged post-fit carrier-phase residual of the measurements and a goodness of fit criteria given by the Chi^2 value. The maximum allowed averaged carrier phase residual was set to 0.02 m, and the maximum allowed Chi^2 value was set to 1.0, in accordance with the PNAV manual instructions [Ashtech, 1993]. The carrier phase ambiguities were considered fixed if the mentioned quality assurance parameters are less than the defined threshold. It is good practice to check the time history of the quality assurance parameters, by examining their plots. A sudden increase in the quality assurance parameters may indicate that the integer ambiguities are not fixed correctly.

In the processing of the GPS observation files for the three vessel-fixed antennas, antenna *port* was considered the reference. Analysis of the PNAV output files reveals that the ambiguities are considered fixed after a period of initialization that varies between 35

and 50 seconds. After initialization, no cycle slips or wrong results were found, based on the analysis of the ASCII message log file containing a time-history of what occurred while the receiver was collecting data, or while the receiver was processing data. To overcome the loss of accurate results during the initialization period, observation files were processed forward and backward. This procedure would not be possible if PNAV were to be used to process data in real time. The quality of the PNAV solution was also confirmed by the comparison of GPS and POS/MV 320 attitude measurements described in section 7.2.

7.1.2 Instantaneous Ambiguity Resolution

A computer program was written using the algorithm described in section 4.2 for the least squares ambiguity resolution technique. The C programming language was used with a Borland Turbo C++ 3.0 compiler in an IBM compatible computer with a Pentium 90 MHz microprocessor.

The input data is formed by pseudorange and carrier phase measurement files and ephemeris files downloaded from the Ashtech Z12 GPS receivers. The known baseline lengths and their uncertainties are used to form the search space. The program allows the user to define elevation angle limits or to define an estimate of the elevation angle and its error to speed up ambiguity resolution by rejecting the potential solutions that do not fall within the elevation angle limits.

Instantaneous ambiguity resolution was tested for single frequency data and dual frequency data. The processing time and number of possible solutions were recorded for

different baseline lengths and baseline length errors as well as when elevation angle limits are considered. The influence of the selection of primary satellites was also evaluated. Instantaneous ambiguity resolution results are given in the following.

7.1.2.1 Using Single Frequency Data

Results for instantaneous ambiguity resolution using single frequency data indicate a low success rate, as shown in Table 7.1:

Table 7.1 - Single frequency instantaneous ambiguity resolution results.

	Carrier frequency	Good results	% of success
Period 1 (987 epochs)	L1	667	67
	L2	689	70
Period 2 (1242 epochs)	L1	1018	82
	L2	1005	81
Period 3 (1029 epochs)	L1	356	35
	L2	440	43

The final result of instantaneous ambiguity resolution were considered a good result when the distance to the PNAV solution did not exceed 2 cm. The best results were achieved during period 2, when more satellites were continuously tracked. The worst performance occurred during period 3 when the number of satellites being tracked was the smallest for all the collected data.

Statistical testing to validate the final solution did not perform well since the degrees of freedom, defined by the total number of satellites minus four, was too low. It was not possible to distinguish bad from good solutions using statistical methods. No

improvement was observed when using the moving average, due to a high percentage of bad results, which did not allow a reliable computation of the moving average.

Although not impossible, instantaneous ambiguity resolution with single frequency data is not sufficiently reliable for operational use. This was expected since one epoch of single frequency data does not contain enough information to efficiently compute the correct ambiguity set based on a statistical criterion such as the variance factor.

7.1.2.2 Using Dual Frequency Data

Instantaneous ambiguity resolution using dual frequency data indicated 100% good results. This was based on the processing of all the data for the three periods of observation which includes more than 3000 epochs. The results of the comparison with PNAV results for two different baseline lengths are given in the Table 7.2. The numbers refer to the distance between the PNAV position and the instantaneous solution in metres and the criterion used to classify a result as good was based on a distance from the PNAV solution smaller than 2 cm.

Table 7.2 - Dual frequency instantaneous ambiguity resolution results.

Baseline	Period	Mean	St. dev.	Max	No. Obs.	% of success
2.028 m	1	0.0018	0.0010	0.0130	987	100
	2	0.0015	0.0007	0.0041	1243	100
	3	0.0025	0.0012	0.0062	1030	100
4.498 m	1	0.0023	0.0010	0.0050	991	100
	2	0.0013	0.0006	0.0041	1194	100
	3	0.0020	0.0011	0.0064	1023	100

Results show that the adopted epoch-by-epoch ambiguity resolution approach is efficient and has an overall success rate of 100%, based on the collected data. Even with a number of satellites as small as six, the correct ambiguities have been determined. This means that the trial solution with smallest variance factor corresponds to the correct solution.

Both the moving average technique and statistical tests validated the final solution, which is a good indication of its ability to accept correct solutions. To test the performance of statistical validation tests in rejecting erroneous results, instantaneous ambiguity resolution was executed using a search space which did not contain the correct solution. This was done by defining a baseline length smaller than the true distance between antennas.

Figure 7.1 contains two histograms which describe the frequency of occurrence of the variance factor for a specific bin, whose center is represented on the horizontal axis. The upper histogram represents the situation when correct results were achieved, while the lower histogram represents the situation where wrong results were “intentionally” produced by changing the search space.

From the above histograms, the value of 0.001 m^2 seems to be a good threshold for the variance factor since all correct results have a variance factor smaller than this threshold and all the erroneous results have a variance factor greater than this threshold.

The same approach was used to plot the frequency of occurrence of the ratio between the two smallest variances. The histograms are plotted in Figure 7.2, with the same organization as in Figure 7.1.

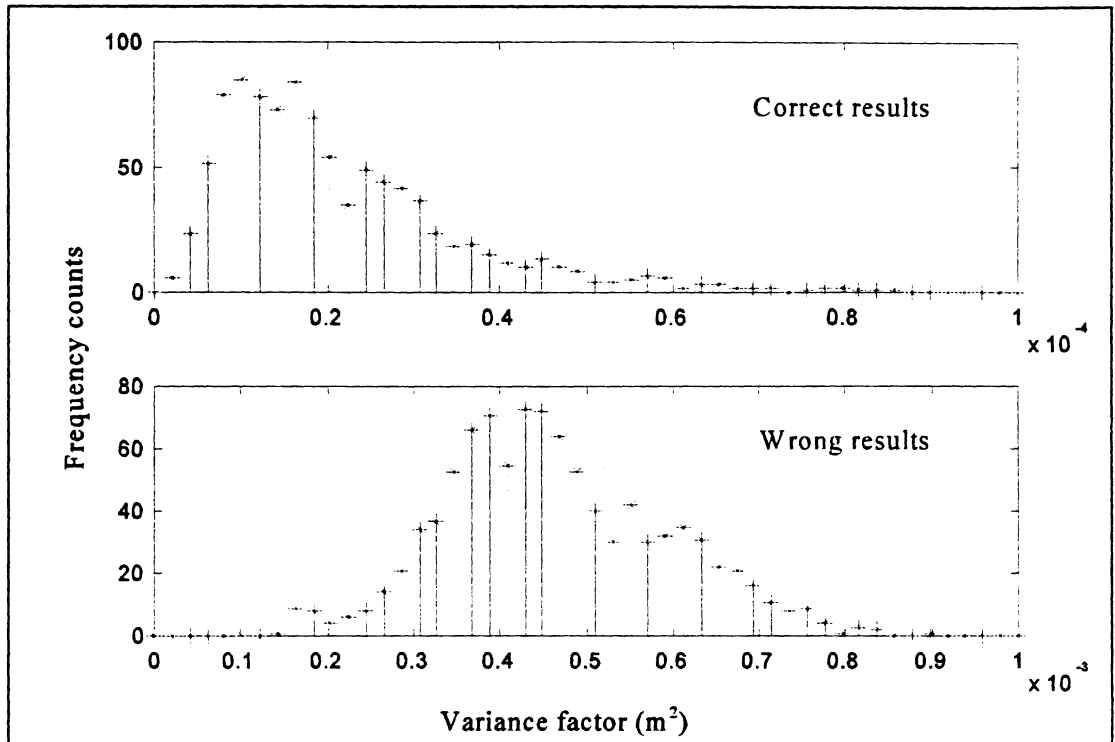


Figure 7.1 - Frequency distribution of the variance factor.

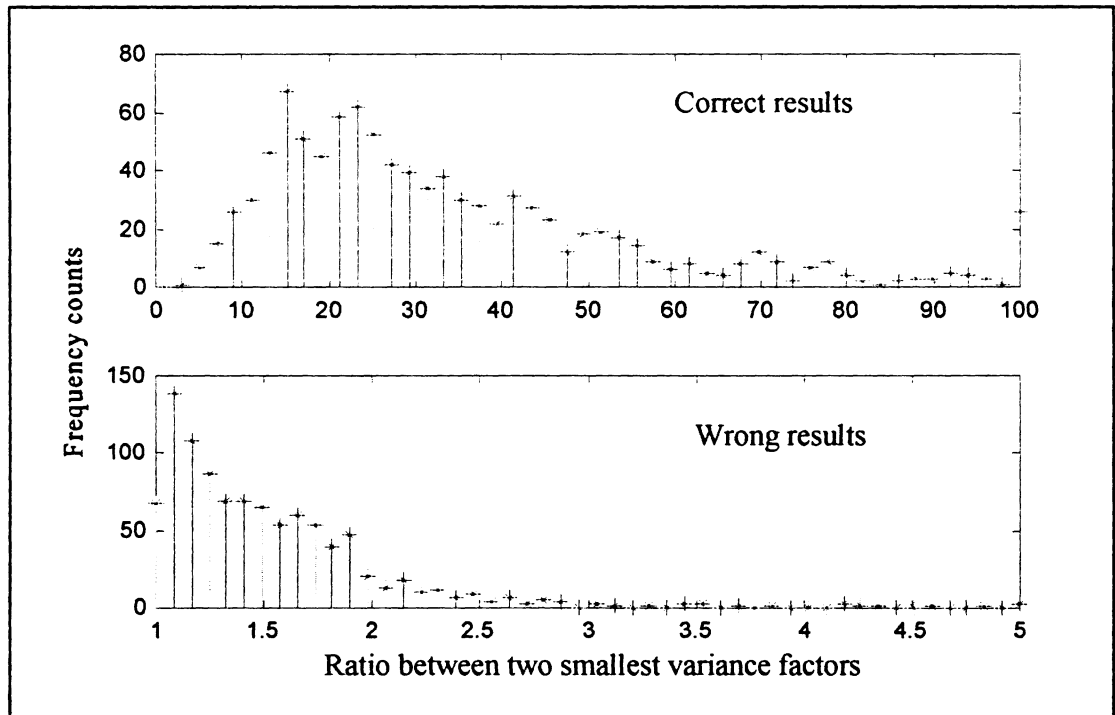


Figure 7.2 - Frequency distribution of the ratio between the two smallest variances.

The frequency distribution plots for the ratio between the two smallest variances indicate a clear separation between correct results and erroneous results. The ratio can fluctuate widely from epoch to epoch. It seems, however, that when the ratio is higher than three the ambiguities are correctly solved. This result is in accordance with experimental results by Cannon and Haverland [1993]. However, a ratio equal to two [Landau and Euler, 1992] may be efficient in accepting correct solutions but may fail in rejecting bad solutions.

Instantaneous ambiguity resolution was tested for two different baseline lengths, different baseline length errors and for the use of elevation angle errors. The use of elevation angle requires ancillary pitch and roll data from another sensor. If pitch and roll amplitudes of the vessel are restricted, then elevation angle limits can be set. The results are summarized in Table 7.3, where the values are the processing time in seconds and the number of possible solutions. The elevation angle used to process the data in the fourth column was given by the POS/MV 320 after interpolation for the GPS epochs.

Table 7.3 - Processing time and number of epochs versus baseline length error.

Baseline length error (cm)	- Length = 2.028 m. - No elevation angle limits.	- Length = 4.498 m. - No elevation angle limits.	- Length = 2.028 m. - Elevation angle error = +/- 10 degrees.
1.0	0.43 / 750	2.14 / 3620	0.38 / 125
2.0	0.49 / 870	2.41 / 4140	0.43 / 140
5.0	0.66 / 1185	3.29 / 5656	0.54 / 200
10.0	0.93 / 1700	4.67 / 8170	0.77 / 275
50.0	3.40 / 6100	15.43 / 28585	2.47 / 960
100.0	6.48 / 12190	30.14 / 54580	4.83 / 1720

The results in Table 7.3 may vary from epoch to epoch, although not significantly, as the satellite geometry or the set of primary satellites change. Since the search space depends on the baseline length, the bigger the baseline length, the more possible solutions there are to be processed and the longer the processing time. If the update rate is one second, for a two meter baseline length and a baseline length error less than 10 seconds, the ambiguities could be solved instantaneously, with the Pentium 90 processor used in this experiment.

For the 4.5 m baseline the processing time exceeds the update rate even for a baseline length error of one centimetre. This can be enhanced by using the information provided by the differential position from pseudorange measurements. The algorithm described in section 4.2 can be used to compute the ambiguity search space in a spherical volume centered at the differential position with radius equal to three times its standard deviation. The final search space will result from the intersection of the spherical volume centered at an approximate differential position with a spherical layer centered at the reference antenna.

The processing time is not significantly reduced by using elevation angle limits because the algorithm does not use the elevation angle in the definition of the ambiguity search space. Instead, the search space is formed only by using the baseline length and its error. Then, the potential solutions, in the position domain, that fall over the elevation angle limits are disregarded. The elevation angle acts more like a validation test for the potential solutions, therefore the number of potential solutions is greatly reduced but not the processing time.

To take full advantage of elevation angle information, the ambiguity search space should be formed using this constraint. This will greatly reduce the number of possible solutions and the processing time. One method that uses baseline length and elevation angle to form the search space is described by Li [1996]. Li's method demonstrates that it is mathematically possible using the baseline length as well as the elevation angle to form the ambiguity search space. However, it is not clear, from his derivation [Li, 1996], how to incorporate the error bounds associated with baseline length and elevation angle determination. For this reason, Li's method, did not perform well when tested with field data, and the author of this report is not aware of another experimental result.

Whenever the baseline length is used to define the search space an error bound must be assumed. This error must account for the uncertainty associated with baseline length determination, possible vibration and distortion, and GPS measurements errors. GPS measurement errors may cause the correct set of primary satellite ambiguities to fall outside the search space if the baseline length error bound is set too small. Therefore, the correct solution is not achieved. For example, although baseline *port-stbd* was well fixed and determined with an accuracy of few millimetres, a baseline length error bound of one centimetre may cause instantaneous ambiguity to fail at certain epochs. From Figure 7.3, we can see that baseline length as determined from GPS measurements has variations greater than one centimetre. Due to these variations when a one centimetre baseline length error bound was assumed some bad results were found.

The same thought can be applied when the elevation angle is used as a constraint. In this case the elevation angle error bound must be wide enough to incorporate the

uncertainty associated with its measurement, and GPS measurement errors. The effects of vibration and distortion do not apply since the elevation angle is measured for each epoch by an ancillary sensor, such as an IMU. With baseline length and/or elevation angle as constraints, the ambiguity search space must be wide enough to account for GPS measurement errors.

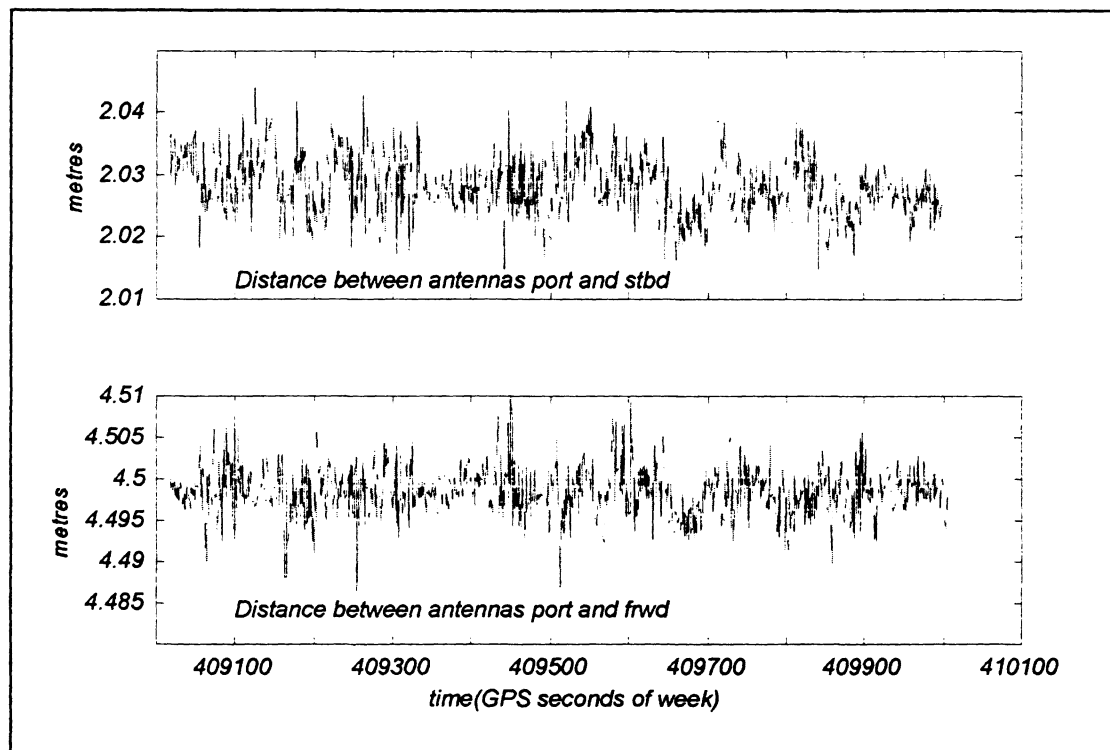


Figure 7.3 - Baseline length derived from GPS measurements.

To test the influence of the selection of primary satellites, a simple test was carried out. First, instantaneous ambiguity resolution was executed without selecting the primary satellites and 0.5% bad results were found over the whole data span. Then, instantaneous ambiguity resolution was executed using the satellite selection algorithm described in section 4.2 and zero bad results were found over the whole data span.

7.2 Comparison between POS/MV 320 and GPS attitude measurements

The three GPS antennas installed aboard *Plover* allow for the determination of attitude. The method used to derive attitude was through direct determination, as described in section 2.6, since the BCS coordinates are unknown and one of the baselines was parallel to the transverse axis of the vessel.

The echosounder transducer pitch and roll angles measured by the POS/MV 320 during the experiment are represented by the figures of Appendix B. The bias in the pitch plot is due to the POS/MV pitch offset angle at installation. The magnitude of pitch and roll motions do not exceed 5 and 10 degrees respectively.

GPS derived pitch, roll and heading were compared with POS/MV 320 interpolated attitude measurements in order to evaluate the performance of GPS attitude determination. Using equations (2.15), (2.16) and (2.17), the predicted accuracy (standard deviation) for GPS estimated attitude parameters, with the antenna configuration shown in Figure 6.1, is approximated by:

- heading: 0.07 degrees (Port-Frwd baseline) and 0.14 degrees (Port-Stbd baseline).
- pitch: 0.07 degrees.
- roll: 0.14 degrees.

To derive the above values a total differential GPS ranging error of 5 mm (standard deviation) was assumed, excluding antennae baseline distortion (vessel flexing).

Figure 7.4 shows the results of the comparison between POS/MV 320 and GPS attitude measurements over the whole data span. Detailed plots for each of the three data

periods, with velocity and rate of change of heading, are represented in Appendix E.

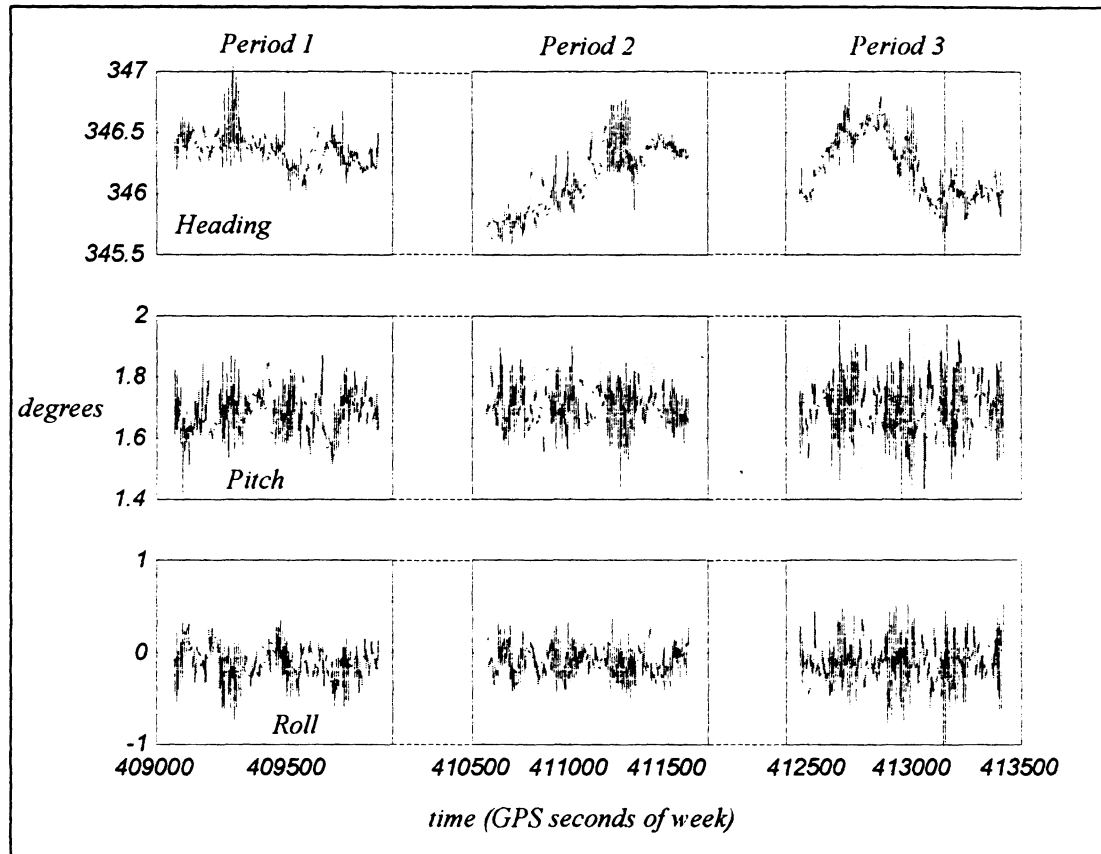


Figure 7.4 - Heading, pitch and roll differences between POS/MV 320 and GPS attitude measurements.

The statistical analysis of the attitude differences is summarized in Table 7.4. The standard deviation for pitch and roll differences agree with the expected accuracy of GPS pitch and roll measurements. Heading differences, however, have a standard deviation three times bigger than the expected accuracy for the difference between the two systems. Some of the spikes represented in the plots of Figure 7.4 are caused by data gaps in the POS/MV data set and, therefore, they have been neglected in the statistical analysis. These data gaps occur in period 2 between GPS epochs 411310 to 411330 seconds and in period 3 between

GPS epochs 413130 to 413150 seconds. The mean value for heading and pitch differences are caused by a misalignment of GPS antennas with respect to the POS/MV reference frame.

		mean	std. dev.	minimum	maximum	range
Period 1	Heading	346.3518	0.1277	345.9659	347.0515	1.0856
	Pitch	1.6805	0.0709	1.4148	1.9437	0.5289
	Roll	-0.1145	0.1862	-0.7362	0.4617	1.1979
Period 2	Heading	346.1149	0.2638	345.5846	346.7715	1.1869
	Pitch	1.7024	0.0613	1.4357	1.9251	0.4894
	Roll	0.0927	0.1547	-0.4973	0.3829	0.8802
Period 3	Heading	346.2207	0.2581	345.6684	347.0584	1.3900
	Pitch	1.7067	0.1362	1.3856	1.9898	0.6042
	Roll	-0.0882	0.3931	-1.0257	0.5544	1.5801
Total	Heading	346.2185	0.2499	345.5846	347.0515	1.4669
	Pitch	1.6958	0.0750	1.3856	1.9898	0.6042
	Roll	-0.1020	0.1911	-1.0257	0.5544	1.5801

Table 7.4 - Comparison between POS/MV 320 and GPS (units are in degrees).

Heading differences are related with sudden variations of heading as shown in figure E.4 to E.8. When the launch turns to one side and, suddenly, changes course to the other side, as a zigzag type manoeuvre, the heading difference plots show spikes of 0.5 degrees. These spikes are not due to interpolation errors or mismatching time tags. If this was the cause, then a constant heading difference offset value would be visible while the launch was changing course. It is unlikely that the spikes are caused by structural distortion of the GPS antenna baseline. If this was the cause, then simultaneous spikes would be

visible in the pitch difference plots.

When the vessel is turning a centripetal acceleration exists that is sensed by the IMU, as mentioned in section 3.5.3. The POS/MV 320 uses measurements from two GPS antennas to compensate for the effect of the centripetal acceleration in the motion sensors readout. Although, POS/MV 320 heading measurements integrate heading measurements from two GPS antennas, the update rate is limited to 10 Hz. Between each GPS heading update, POS/MV heading measurements are made using only high frequency IMU measurements. During a turn, when the launch suddenly changes course to the opposite side the IMU requires compensation for the new centripetal acceleration in the opposite direction from which it was previously using. Thus, POS/MV attitude measurements increase in error until updated by GPS measurements. This effect is more visible in the heading differences plot than in the pitch and roll difference plots because the magnitude of the latter two motions is much smaller than for heading.

Pitch and roll differences show variations within the noise level predicted for the comparison of the two attitude determination systems. The standard deviation of the observed heading differences is three times bigger than the estimated standard deviation as computed from the POS/MV manufacturer accuracy specifications and from the error of the standalone three-antenna GPS attitude. This may be due to the relatively small baseline length between POS/MV 320 GPS antennas (1.37 metres). To confirm this hypothesis, however, further testing will be required using a wider antenna spacing between POS/MV 320 GPS antennas.

CHAPTER 8

CONCLUSION

The emphasis of this research was on real time instantaneous attitude determination using GPS carrier phase measurements in a marine kinematic experiment. This chapter starts with a summary and discussion of the issues that were raised during the investigation. Next, the main conclusions drawn from experimental results of using GPS for attitude determination are presented. The chapter ends with suggestions for future research in this field.

8.1 Summary and Discussion

During the investigation of this topic several methods of attitude determination from GPS measurements were described. Only the direct determination of attitude parameters was used to process the data. Since this method uses only the minimum number of antennas, other procedures which accept redundant measurements from more than three antennas may, eventually, yield more reliable results.

Hydrographic surveying with MBES requires accurate attitude measurements in order to compensate the bottom reflected echo for the vessel's motion. The trend in marine motion compensation is the integration of a dual antenna GPS system with an INS. Such integration will overcome the limitations of each of these sensors alone, with some additional advantages.

Attitude determination with GPS uses carrier phase measurements which require

extreme care in its numerical processing. Complete observation equations with all possible error sources were described and implemented in a computer program to determine the baseline vector between two antennas. The question of simultaneity of observations between two receivers was also discussed.

GPS data was first processed with Ashtech's PNAV software in order to determine relative positions between antennas with sub-centimetre level accuracy. After a period of initialization that varied between 30 and 40 seconds, the ambiguities were successfully determined without any bad solutions, according with the quality assurance parameters of the PNAV. The quality of the PNAV solution was also confirmed by the comparison between GPS attitude results with POS/MV 320 attitude measurements. PNAV derived positions were used to test results from instantaneous ambiguity resolution using the algorithm described in this report.

The algorithm presented in this report to solve the carrier phase integer ambiguity, is a modification of the least square search technique. This modification uses the known baseline length to reduce the search space to a sphere. Some additional modifications were introduced in order to consider the error associated with the baseline length measurement. The algorithm was implemented in a computer program and some aspects of instantaneous carrier phase resolution were tested. This includes influence of satellite geometry, processing time and the number of possible solutions versus baseline length and baseline length error, and validation of the final solution using statistical methods and the moving average technique.

The coordinates computed with the above algorithm were used to determine the

attitude angles: pitch, heading and roll. These results were compared with measurements from the dual antenna GPS/INS POS/MV 320, after interpolation of the POS/MV data for the GPS three antenna system observation epochs. Care was taken to minimize the error due to interpolation. It was found that cubic spline interpolation yields an interpolation error which does not significantly influence the results of the comparison between the two systems.

8.2 Conclusions

Several conclusions may be drawn from the results of this investigation regarding GPS carrier phase instantaneous ambiguity resolution the use of GPS to determine the attitude of an hydrographic survey launch:

Ambiguity resolution using the known baseline length appears to be an efficient technique with a high reliability of determining the correct ambiguities when using dual frequency data from a single epoch, for short baselines.

The processing time required to compute each epoch solution depends on the baseline length and its error. For a two metre baseline length with less than 10 cm error, the ambiguities are solved in less than one second. This indicates that instantaneous ambiguity resolution is possible, although dependent on the software structure, microprocessor speed and update rate.

When forming the search space using the baseline as a constraint, an error bound must be assumed. This error bound must be wide enough to incorporate the uncertainty

associated with baseline length determination, the effects due to vibration and distortion, and GPS measurement errors. Therefore, if the baselines are well fixed and determined with millimetre level accuracy, an error bound of at least two centimetres must be considered to account for GPS measurement errors.

Ambiguity resolution results were reliably validated by statistical testing, namely the chi-square test and the ratio test, whenever dual frequency data is used and more than six satellites are being tracked.

Hydrographic survey launch tests show clearly the feasibility and high reliability of GPS attitude determination. With the three antenna configuration used, the accuracy of the results were mainly dependent on the baseline length as shown by the standard deviations of the roll differences (dependent on the small baseline) and pitch differences (mainly dependent on the longest baseline).

GPS only, and POS/MV 320 pitch and roll, were statistically compatible. That is, the difference between these results show a standard deviation for pitch and roll uncertainty which is within the accuracy limits as estimated from POS/MV manufacturer specifications and predicted GPS attitude error.

The standard deviation for the heading differences between GPS and POS/MV 320 shows a standard deviation three times bigger than the expected value. When a sudden variation of heading rate of change occurs, the heading differences can reach 0.5 degrees for a single epoch. The explanation for this unexpected result may be related with the small baseline length between the two GPS antennas of the POS/MV 320 (about 1.4 metres) and/or with the integration of the GPS and INS measurements. Further testing (using a wide

POS/MV 320 antenna spacing) and investigation will be necessary to more fully explain this behavior.

8.3 Suggestions for Future Research

Based on the results of this research, further investigations are warranted in the following aspects:

Additional tests are required to assess the performance of POS/MV 320 heading determination with a baseline length up to five metres between GPS antennas of the POS/MV.

A method should be developed and tested which uses baseline length and elevation angle information with respective error bounds, to form the GPS carrier phase ambiguity search space.

Additional tests are required to assess the performance of instantaneous ambiguity resolution with longer baselines (up from tens of metres to tens of kilometres), using the differential pseudorange estimate of the relative position and its error to form the search space.

Reliability improvements in ambiguity resolution and attitude determination should be investigated, when redundant baselines (4 or more antennas) are used.

REFERENCES

- Applied Analytics (1996a) *POS MV Description and Theory of Operation*. Equipment brochure, Applied Analytics Corporation, Markham, Ontario, Canada.
- Applied Analytics (1996b) *POS MV 320, Installation and operation manual*. Version 1, revision 1.0, Applied Analytics Corporation, Markham, Ontario, Canada.
- Applied Analytics (1996c) *POS MV 320, Ethernet Interface Control Document*. Version 1, revision 2.0, Applied Analytics Corporation, Markham, Ontario, Canada.
- Ashtech (1993). *Precise Differential GPS Navigation and Surveying (PNAV) Software User's Manual*. Ashtech Inc., Sunnyvale, California.
- Ashtech (1995). *Supplement to Z-12 Receiver Operating Manual Covering RTZ Functions*. Document number 600292, Revision A, Ashtech Inc., Sunnyvale, California.
- Axelrad, P., C. Comp and P. MacDoran (1994) "Use of Signal-to-Noise Ratio for Multipath Error Correction in GPS Differential Phase Measurements: Methodology and Experimental Results." *Proceedings of the ION GPS-94*, Salt lake City, Utah, September 1994, pp. 655-666.
- Bar-Itzhack, I.Y. and Reiner, J. (1984) "Recursive Attitude from Vector Observations: Direction Cosine Matrix Identification." *Journal of Guidance Control and Dynamics*, vol. 7, No. 1, Jan.-Feb. 1984, pp. 51-56.
- Becker, D., K.H. Thiel and P. Hartl (1994) "A Special Method of Managing Multipath Effects". *Proceedings of the ION GPS-94*, Salt lake City, Utah, September 1994, pp. 157-163.
- Bedford Institute of Oceanography (1996) "Drawing of the 31' survey launch Plover." Engineering and technical services, Bedford Institute of Oceanography, Department of Fisheries and Oceans, May 16, 1996.
- Bose, S.C. (1996a) "Optical Gyros" *Lecture Notes of the GPS/INS integrated Navigation Systems Course*, Technalytics inc., Destin, Florida, USA.
- Bose, S.C. (1996b) "GPS/INS Kalman Mechanizations" *Lecture Notes of the GPS/INS integrated Navigation Systems Course*, Technalytics inc., Destin, Florida, USA.
- Bowditch, N. (1984) *American Practical Navigator*. Vol. 1, Defence Mapping Agency, Hydrographic/Topographic Centre, U.S.A.

- Braasch, M. (1996) "Multipath Effects." Chapter 14 of *Global Positioning System: Theory and Applications, Volume 1*, Progress in Astronautics and Aeronautics vol. 164, Edited by B.W. Parkinson and J.J Spilker Jr., Published by the American Institute of Aeronautics and Astronautics, pp. 547-568.
- Braasch, M. and F. Van Graas (1991). "Guidance Accuracy Considerations for Real-Time GPS Interferometry." *Proceedings of the ION GPS-91*, Albuquerque, New Mexico, September, pp.373-385.
- Brown, R.A. and A.G. Evans (1990). "GPS Pointing System Performance." *Proceedings of the ION GPS-90*, September, Colorado Springs, Colorado, pp. 645-654.
- Cannon M.E. and M. Haverland (1993). "Experiences of GPS Attitude Determination within a Helicopter Pod." *Proceedings of the ION GPS-93*, Salt Lake City, Utah, September, pp. 633-641.
- Cohen, C.E. (1996). "Attitude Determination." Chapter 19 of *Global Positioning System: Theory and Applications, Volume 2*, Progress in Astronautics and Aeronautics vol. 164, Edited by B.W. Parkinson and J.J Spilker Jr., Published by the American Institute of Aeronautics and Astronautics, pp. 519-538.
- Conway, A., P. Montgomery, S. Rock, R. Cannon and B. Parkinson (1996)" A new motion-based algorithm for GPS attitude integer resolution" *Navigation: Journal of the Institute of Navigation*, Vol. 43, No. 2, Summer, pp. 179-190.
- Dinn, D.F. and M. Crutchlow (1996) "A First Look at the EM3000 Multibeam Sonar." *Proceedings of the Canadian Hydrographic Conference*, Halifax, Nova Scotia, June 1996, pp.89-97.
- Dinn, D.F. and B.D. Loncarevic (1994) "An Evaluation of Ship Motion Sensors." *Proceedings of the Kinematics Systems Conference*, Department of Geomatics, University of Calgary, Aug.-Sept., Banff, Alberta, pp. 47-55.
- DiStefano, J.J., A.R. Stubberud and I.J. Williams (1990) *Feedback and Control Systems*. 2nd edition, Schaum's Outline Series, MacGraw-Hill.
- Erickson, C. (1992). "An Analysis of Ambiguity Resolution Techniques for Rapid Static GPS Surveys Using Single Frequency Data." *Proceedings of the ION GPS-92*, Albuquerque, New Mexico, September, pp. 453-462.
- Fu, Xiaolu (1992). "Investigation of Multipath Carrier Phase Effects in GPS Hydrographic Applications." *Proceedings of the ION GPS-92*. Albuquerque, New Mexico, September, pp. 491-499.

- Graas, V.G. and M. Braasch (1992). "GPS Interferometric Attitude and Heading Determination: Initial Flight Test Results." *Navigation: Journal of the Institute of Navigation*, Vol. 38, No. 4, Winter, pp 297-316.
- Gelb, A. (Ed.)(1974). *Applied Optimal Estimation*. M.I.T. Press, Cambridge, Mass..
- Georgiadou, Y., and A. Kleusberg (1988). "On Carrier Signal Multipath Effects in Relative GPS Positioning." *Manuscripta Geodaetica*, Vol. 13, pp. 172-179.
- Goldstein, H. (1950). *Classical Mechanics*. Addison-Wesley Publishing Company, Reading, Massachusetts, USA.
- Hare, R. (1995). "Depth and Position Error Budgets for Multibeam Echosounding." *International Hydrographic Review*, Monaco, LXXII(2), September, pp. 37-69.
- Hare, R., A. Godin and L. Mayer (1995). *Accuracy Estimation of Canadian Swath (multibeam) and Sweep (multi-transducer) Sounding Systems*. Canadian Hydrographic Service Internal report, 248 pp.
- Hatch, R. (1990). "Instantaneous ambiguity resolution." *Proceedings of International Association of Geodesy Symposia No. 107 Kinematic Systems in Geodesy, Surveying and Remote Sensing*, Banff, Canada, 10-13 September, Springer Verlag, New York, pp. 299-308.
- Hofmann-Wellenhof, B., H. Lichtenegger and J. Collins (1994). *Global Positioning System: Theory and Practice*. 3rd edition, Springer-Verlag, Vienna, 355 pp.
- Hughes Clark, J. (1996) "Field Adjustments." *Lecture 23 from 1996 Coastal Multibeam Sonar Training Course*. United States / Canada Hydrographic Commission, St. Andrews, New Brunswick, Canada.
- Jurgens, R., L. Fan, D. Diefes and C. Rodgers (1992). "Measurement of Errors in GPS Attitude Determination Systems." *Proceedings of the ION GPS 92*, Albuquerque, New Mexico, September, pp. 793-799.
- Knight J. and R. Hatch (1990). "Attitude Determination with GPS." *Kinematic Systems in Geodesy, Surveying and Remote Sensing, Symposium No. 107*, Banff, Alberta, Canada, pp. 168-177.
- Lachapelle, G., M.E. Cannon and G. Lu (1992) "High-Precision GPS Navigation with Emphasis on Carrier-Phase Ambiguity Resolution." *Marine Geodesy*, Vol. 15, pp. 253-269.

- Lachapelle, G., W. Falkenberg and D. Neufelt (1989) "Marine DGPS Using Code and Carrier in a Multipath Environment." *Proceedings of the ION GPS 89*, Colorado Springs, Colorado, September, pp. 343-347.
- Landau, H. and H.J. Euler (1992). "On-The-Fly Ambiguity Resolution for Precise Differential Positioning." *Proceedings of the ION GPS-92*, Albuquerque, New Mexico, September, pp.607-613.
- Langley, R.B. (1996). "GPS Receivers and the Observables." Chapter 4 of *GPS for Geodesy*. Lecture Notes in Earth Sciences No. 60, Edited by A. Kleusberg and P.J.G. Teunissen, Springer.
- Leick, A. (1995). *GPS Satellite Surveying*. Wiley Interscience Publication, John Wiley and Sons, N.Y.
- Li, R. (1996). "A Super-Fast Integer Ambiguity Resolution Approach to GPS Interferometric Heading Determination for the Application in a Low Cost Integrated GPS/Inertial Navigation System." *Proceedings of the National Technical Meeting*, The Institute of Navigation, Santa Monica, CA, January, pp. 83-88.
- Loncarevic, B.D. and B.M. Scherzinger (1994) "Compensation of Ship Attitude for Multibeam Sonar Surveys." *Sea Technology*, pp.10-15.
- Looney C.G. (1993). "Noise." Section 2 of Chapter 67 "Information Theory" of *The Electrical Engineering Handbook*. CRC Press, Editor-in-Chief: R.C.Dorf, pp. 1488-1499.
- Lu, G., G. Lachapelle, M. E. Cannon and P. Kielland (1993). "Attitude Determination in a Survey Launch Using Multi-antenna GPS Technology." *Proceedings of the ION National Technical Meeting*, The Institute of Navigation, San Francisco, California, January, pp. 251-260.
- Lu, G., G. Lachapelle, M.E. Cannon and B. Vogel (1994). "Performance Analysis of a Shipborne Gyrocompass with a Multi-Antenna GPS system", *Proceedings of the 1994 IEEE Position Location and Navigation Symposium*, pp 337-343.
- Lu G. and M.E. Cannon (1994). "Attitude Determination Using a Multi-Antenna GPS System for Hydrographic Applications." *Marine Geodesy*, Vol. 17, pp 237-250.
- May, B.M. (1993) "Inertial Navigation and GPS." *GPS World*, September, pp. 56-66.
- Meehan, T.K. and E.Y. Young (1992). "On-Receiver Signal Processing for GPS Multipath Reduction." *Proceedings of the 6th International Geodetic Symposium on Satellite*

Positioning, March, pp. 200-208.

- Mowafy, A. (1994). *Kinematic Attitude Determination From GPS*. Ph.D dissertation, Department of Geomatics Engineering, University of Calgary, Calgary, Alberta, Canada, 215 pp.
- Mowafy, A. and K. P. Schwarz (1994) “ Epoch by Epoch Attitude Determination Using a GPS Multi-Antenna System in Kinematic Mode.” *Proceedings of the KIS-94*, Banff, Canada, August-September, pp. 331-340.
- NMEA (1995). *NMEA 0183 - Standard For Interfacing Marine Electronic Devices*. Version 2.1, National Marine Electronics Association, October.
- Pacific Crest (1995). *RFM96 Radio Modem*. User’s guide, Revision 1.3, November 1995, Pacific Crest Corporation, California, USA.
- Parkinson, B.W. (1996). “GPS Error Analysis.” Chapter 11 of *Global Positioning System: Theory and Applications, Volume 1*, Progress in Astronautics and Aeronautics vol. 164, Edited by B.W. Parkinson and J.J Spilker Jr., Published by the American Institute of Aeronautics and Astronautics, pp. 469-483.
- Pøhner, F., E. Hammerstad, K. Nilsen and E. Grong (1996). “A New Generation of Instrumentation for Hydrographic Launches.” *Proceedings of the Canadian Hydrographic Conference '96*, Halifax, N.S., Canada, pp. 80-88.
- Press, W.H., S.A. Teulosky, W.T. Vetterling, B.P. Flannery (1992). *Numerical Recipes in C*. 2nd ed., Cambridge University Press.
- Raquet, J.F. (1996). “Multiple Reference GPS Receiver Multipath Mitigation Technique.” *Proceedings of the 52nd Annual Meeting*, Cambridge, Massachusetts, June, pp. 681-690.
- Raquet, J. and G. Lachapelle (1996) “Determination and Reduction of GPS Reference Station Multipath using Multiple Receivers.” *Proceedings of the ION GPS-96*, September, Kansas City, Missouri, pp.673-681.
- Roth, B.D. and P.R. Singh (1986). “Applications of NAVSTAR GPS to Precision Attitude Determination.” *Proceedings of the Fourth International Geodetic Symposium on Satellite Positioning*. Austin, Texas, pp 1345-1359.
- Sadiku, M.N.O. (1993). “Space Propagation”. Section 1 of Chapter 35 “Wave Propagation” of *The Electrical Engineering Handbook*. CRC Press, Editor-in-Chief: R.C.Dorf, pp. 837-849.

Seatex (1996) *Seapath 200*. Equipment brochure, Seatex AS, Trondheim, Norway.

Scherzinger, B., S. Woolven, B. Reid and R. Ballok (1996). "Dual Antenna GPS/Inertial Integration Provides Precision Attitude, True Heading and Position for Multibeam Systems." *Proceedings of the Tenth Biennial International Symposium of The Hydrographic Society, HIDRO 96*, Rotterdam, The Netherlands, 24-26 September, pp. 204-210.

Schupler, B.R., R.L. Allshouse and T.A. Clark (1994). "Signal Characteristics of GPS User Antennas." *Navigation: Journal of the Institute of Navigation*. Vol. 41, No. 3, Fall 1994.

Serrano, J., P. Bernedo and P. Gonzalez (1995). "A GNSS-based Attitude Determination System for Low-Earth Observation Satellites." *Proceedings of the ION GPS-95*, September, Palm Springs, California, pp. 1775-1784.

Tazartes, D.A. and J.G. Mark (1988). "Integration of GPS Receivers into Existing Inertial Navigation Systems." *Navigation: Journal of the Institute of Navigation*, vol. 35, No.1, Spring 1988.

Teunissen P.J.G. and A. Kleusberg (1996). "GPS Observation Equations and Positioning Concepts." Chapter 5 of *GPS for Geodesy*. Lecture Notes in Earth Sciences No. 60, Edited by A. Kleusberg and P.J.G. Teunissen, Springer 1996.

Townsend, B., P. Fenton, K. Van Dienrendonck and R. van Nee (1996). "L1 Carrier Phase Multipath Error Reduction Using MEDLL Technology." *Proceedings of the ION GPS-95*, Palm Springs, California, 12-15 September, pp. 1539-1544.

Tranquilla, J.M. (1986). "Multipath and Imaging Problems in GPS Receiver Antennas." *Proceedings of the Fourth International Geodetic Symposium on Satellite Positioning*. Austin, Texas, pp. 557-571.

Tranquilla, J.M. and J.P. Carr (1991). "GPS Multipath Field Observations at Land and Water Sites." *Navigation: Journal of the Institute of Navigation*. Vol. 37, No. 4, Winter, pp. 393-414.

TSS (1996) *Dynamic Motion Sensor DMS-05/-10 System Manual*. TSS UK Ltd.

U.S. Naval Observatory (1995). "Leap second alert!" *Time Service Announcement Series 14*, <http://tycho.usno.navy.mil/leap.html>, 2 August.

Van Dierendonck, A.J., P. Fenton and T. Ford (1992). "Theory and Performance of Narrow Correlator Spacing in a GPS Receiver." *Navigation: Journal of the Institute of*

Navigation. Vol. 39, No. 3, Fall, pp. 265-283.

Vanicek, P., R.B. Langley, D.E. Wells and D. Delikaraoglou (1984). "Geometrical Aspects of Differential GPS Positioning." *Bulletin Geodesique*. Vol. 58, pp. 37-52.

Vanicek, P. and E.J. Krakiwsky (1986). *Geodesy: The Concepts*. 2nd ed., Elsevier Science B.V., Amsterdam.

Wahba, G. (1965) "Problem 65-1, A least squares estimate of satellite attitude", *SIAM Review*, vol. 7, pp 409.

Wahba, G., J.L. Farrel and J.C. Stuelpnagel. (1965) "Problem 65-1 (solution)" *SIAM Review*. Vol. 8, pp 384-386.

Weill, L.R. (1997). "Conquering the Multipath: The GPS Accuracy Battle." *GPS World*, April, pp. 59-66.

Wells, D. (1996) "Attitude and Orientation Requirement and Methods" *Lecture 17 from 1996 Coastal Multibeam Sonar Training Course*. United States / Canada Hydrographic Commission, St. Andrews, New Brunswick, Canada.

Wertz, J.R. (1978) *Spacecraft Attitude Determination and Control*. D. Reidel Publishing Company, Dordrecht, Holland.

Appendix A

TRANSFORMATION BETWEEN EULER ANGLES AND PITCH, ROLL AND HEADING

Euler angles determined from the attitude matrix must be compatible with heading, pitch and roll as defined in section 2.2. A method for correcting Euler angles for a sequence of rotation heading-pitch-roll is given below. Similar corrections will be needed if other sequences are adopted.

Assuming a sequence of rotation heading-pitch-roll, the first rotation is around the z axis of the BCS by heading. In this case the Euler heading is the same as defined in section 2.2. This rotation does not affect the next two rotations, pitch and roll, since the z axis of the BCS remains in the same position.

Figure A.1 represents the sequence of rotations required to align the BCS with the LCS after a first rotation by heading. This can be achieved by the rotation sequence pitch-roll or roll-pitch. Although, we are interested only on the pitch-roll sequence, the other sequence will be used in the derivation of the transformation between Euler angles and heading, pitch and roll as defined in section 2.2.

For a pitch-roll sequence of rotation, the Euler pitch angle is the same as defined in section 2.2. However, the z axis of the BCS is rotated from position 1 to position 2. This means that the Euler roll angle will be different from the one defined in section 2.2. For a roll pitch sequence of rotation, the Euler roll angle is the same as defined in section 2.2. However, the z axis of the BCS is rotated from position 1 to position 4. This means that the

Euler pitch angle will be different from the one defined in section 2.2

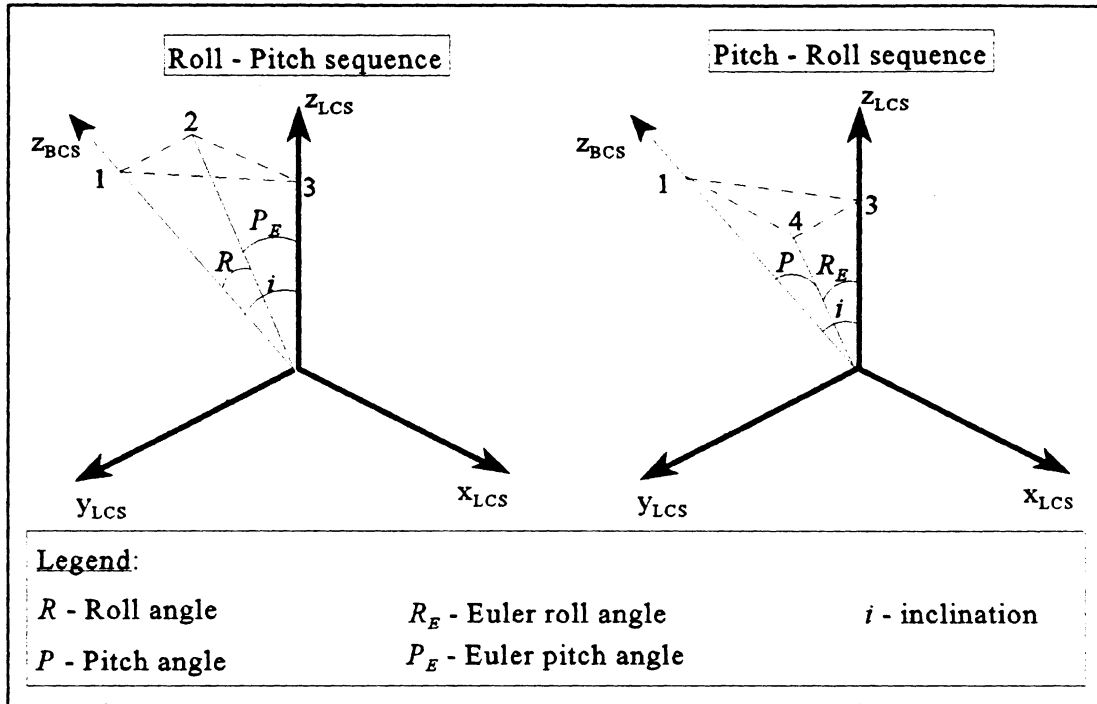


Figure A.1 - Rotations of the BCS to coincide with the LCS.

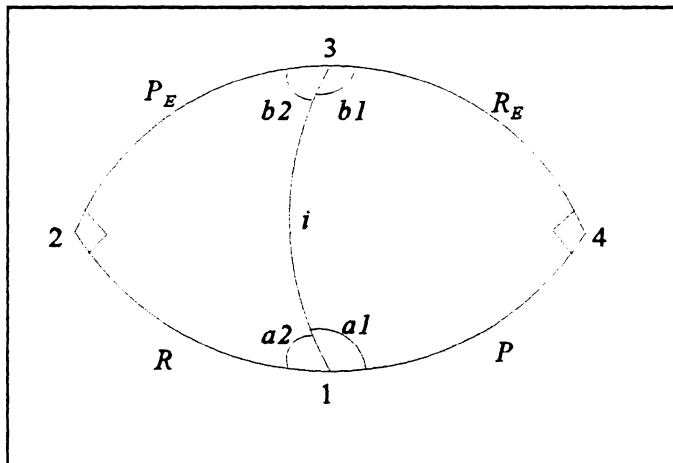


Figure A.2 - Spherical triangles of rotations.

The spherical triangles represented in Figure A.2, which are based in Figure A.1, represent the two sequence of rotations. From Figure A.1, angles $\angle 234$ and $\angle 214$ are equal to 90 degrees. Therefore angles $a1+a2$ and $b1+b2$ are equal to 90 degrees. The following equations were derived using the spherical triangles represented in Figure A.2.

The following equations were derived using the spherical triangles represented in Figure A.2.

From the law of sines for spherical triangles we get the following equation:

$$\sin(R_E) = \frac{\sin(a1)}{\sin(a2)} \sin(P_E) \quad (\text{A.1})$$

Since $a1+a2$ is equal to 90 degrees $\sin(a1)=\cos(a2)$, therefore equation (A.1) transforms to:

$$\sin(R_E) = \frac{1}{\tan(a2)} \sin(P_E) \quad (\text{A.2})$$

Again, from the law of sines, we get the following equation:

$$\sin(a2) = \frac{\sin(P_E)}{\sin(i)} \quad (\text{A.3})$$

Using law of cosines (for the angles of spherical triangles) we get the following equation:

$$\cos(a2) = \sin(b2) \cos(P_E) \quad (\text{A.4})$$

Using the law of sines, we get the following equation:

$$\sin(b2) = \frac{\sin(R)}{\sin(i)} \quad (\text{A.5})$$

Combining equations (A.4) and (A.5) we get the following relation:

$$\cos(a2) = \frac{\sin(R)}{\sin(i)} \cos(P_E) \quad (\text{A.6})$$

Combining equations (A.2), (A.3) and (A.6), we get the following equation:

$$\sin(R_E) = \sin(R) \cos(P_E) \quad (\text{A.7})$$

Using the law of cosines (for the sides of spherical triangles) we get the following equations:

$$\cos(P_E) = \frac{\cos(i)}{\cos(R)} \quad (\text{A.8})$$

$$\cos(i) = \cos(R_E)\cos(P) \quad (\text{A.9})$$

The final relation is obtained by combining equations (A.7), (A.8) and (A.9):

$$\tan(R_E) = \tan(R)\cos(P) \quad (\text{A.10})$$

For a heading-pitch-roll sequence of rotation, only the roll angle is different from the equivalent Euler angle. The relation between the two angles is given by equation (A.10)

APPENDIX B

Vessel Attitude Plots

This appendix contains the plots of heading, pitch and roll measured by the POS/MV 320 referred to the vessel's echosounder.

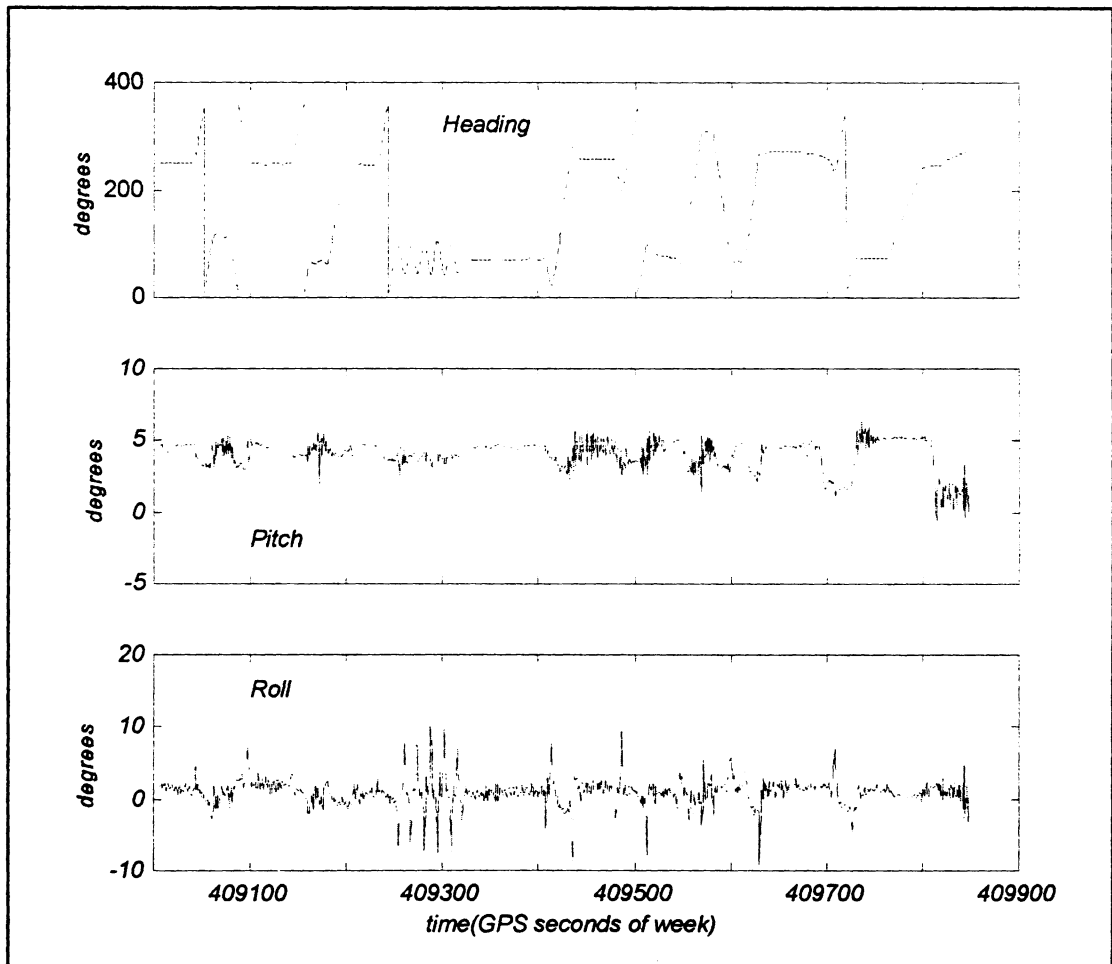


Figure B.1 - Heading, pitch and roll measured by the POS/MV 320 during period 1.

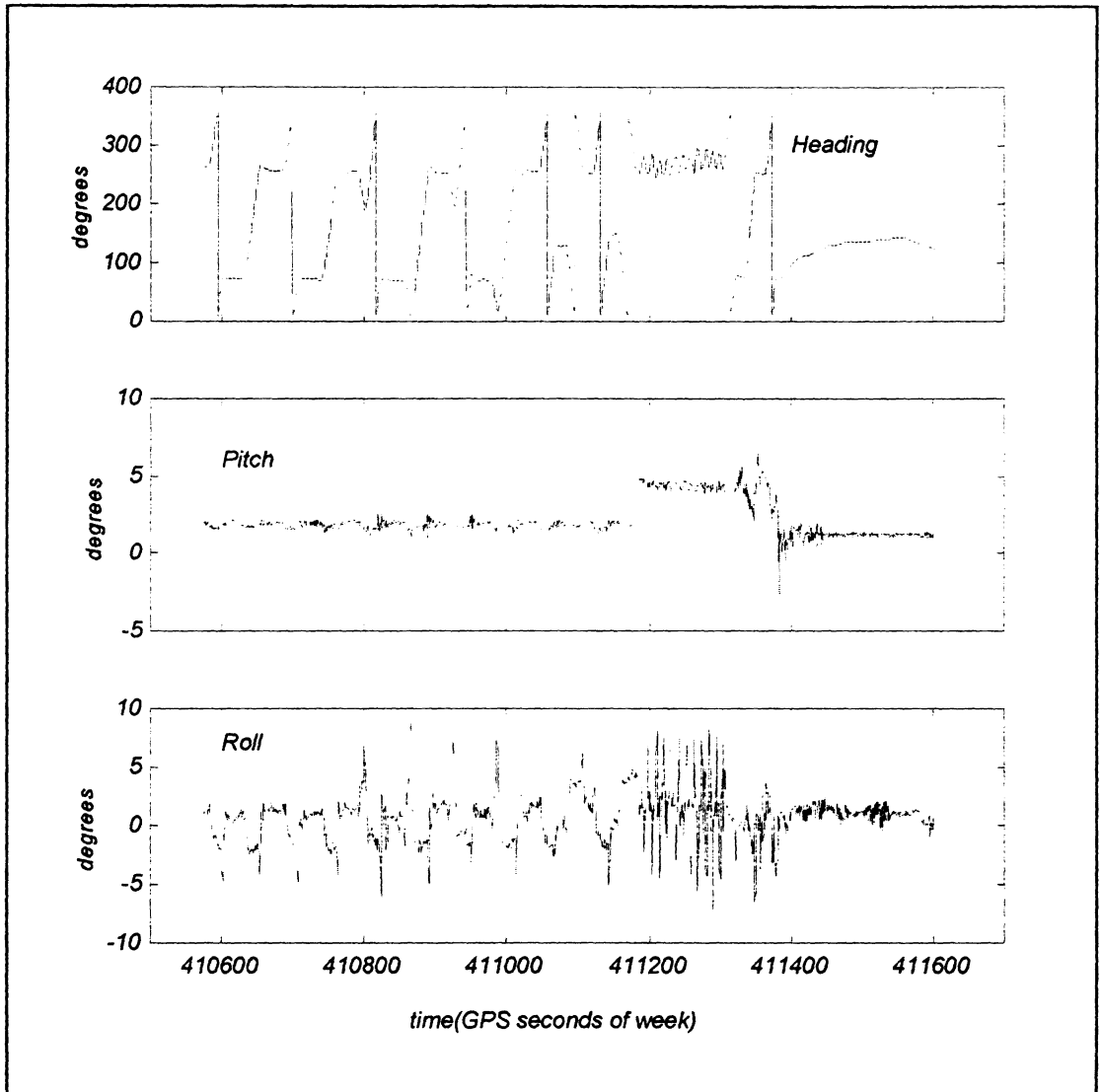


Figure B.2 - Heading, pitch and roll measured by the POS/MV 320 during period 2.

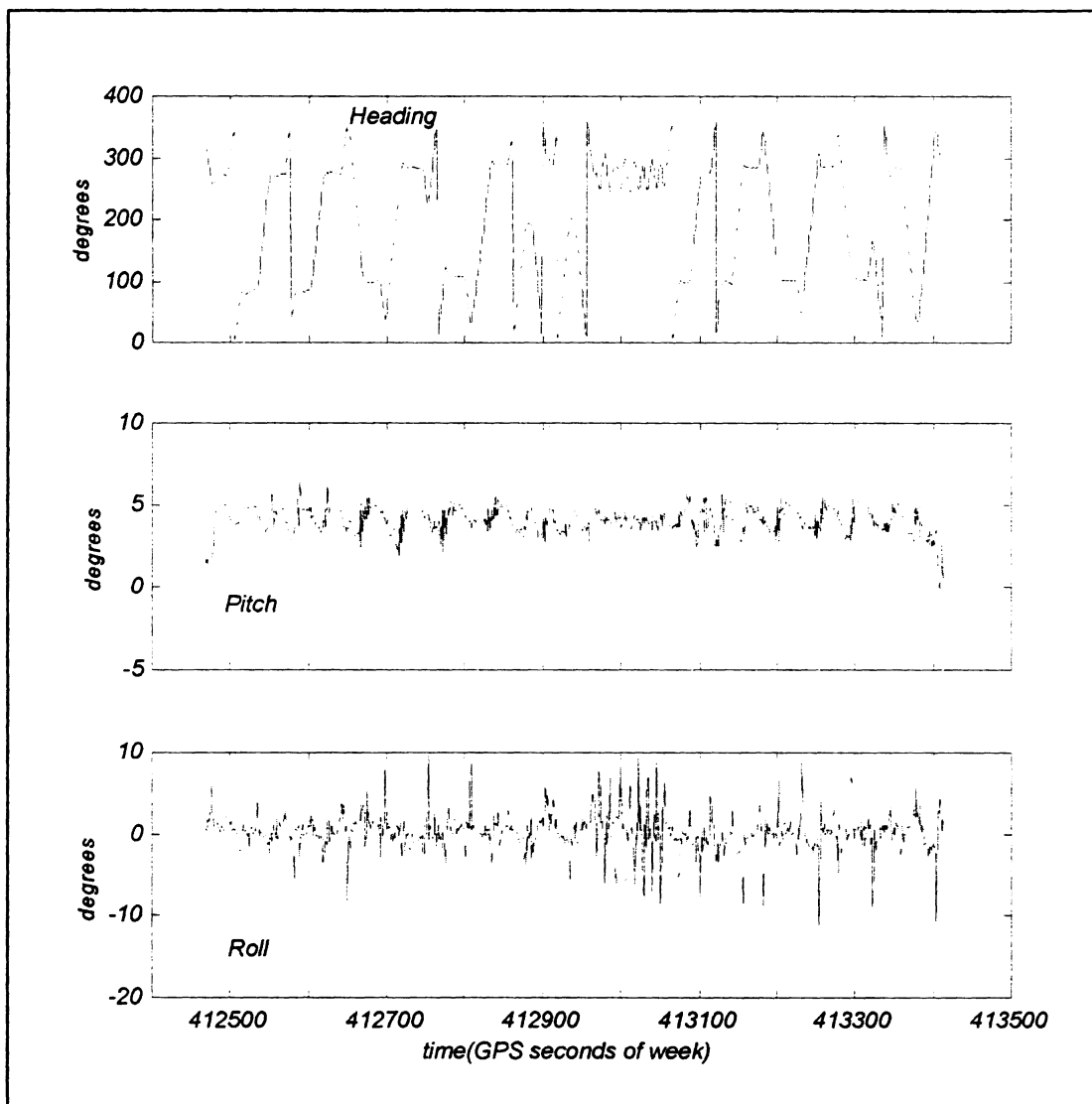


Figure B.3 - Heading, pitch and roll measured by the POS/MV 320 during period 3.

APPENDIX C

VESSEL TRAJECTORY

The next three figures show the vessel trajectory for each of the observation periods. The coordinates are referred to the base station installed at the Bedford Institute of Oceanography with the following WGS-84 coordinates:

Latitude = 44° 40' 57".27510 North	Stand. deviation = 0".004
Longitude = 63° 36' 42".34106 West	Stand. deviation = 0".003
Elip. height = 15.723 metres	Stand. deviation = 0.009 metres

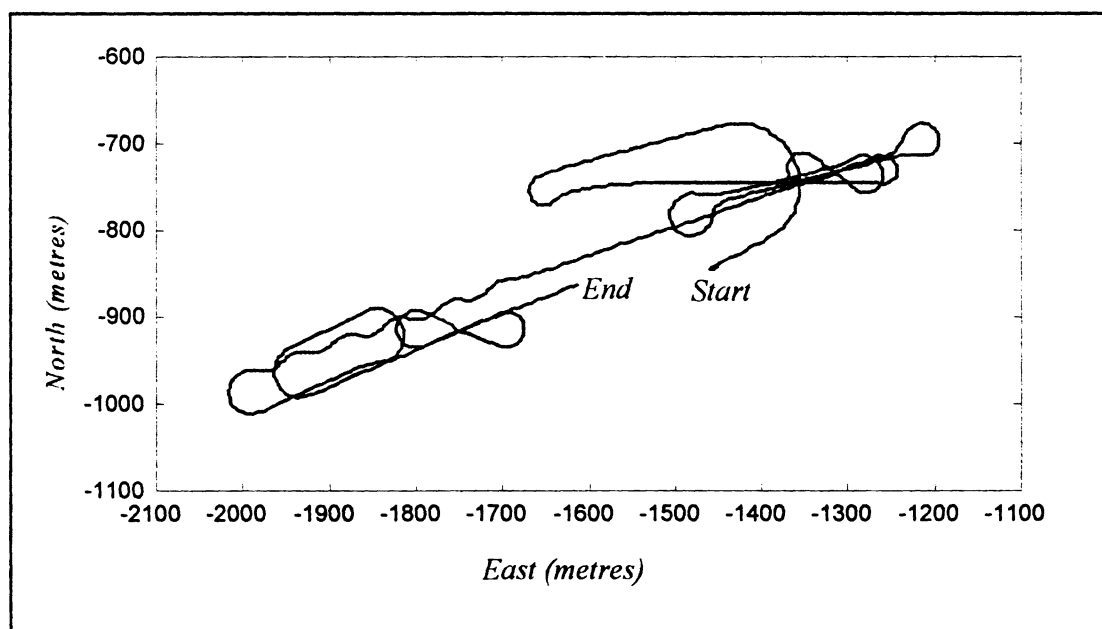


Figure C.1 - Vessel trajectory for period 1.

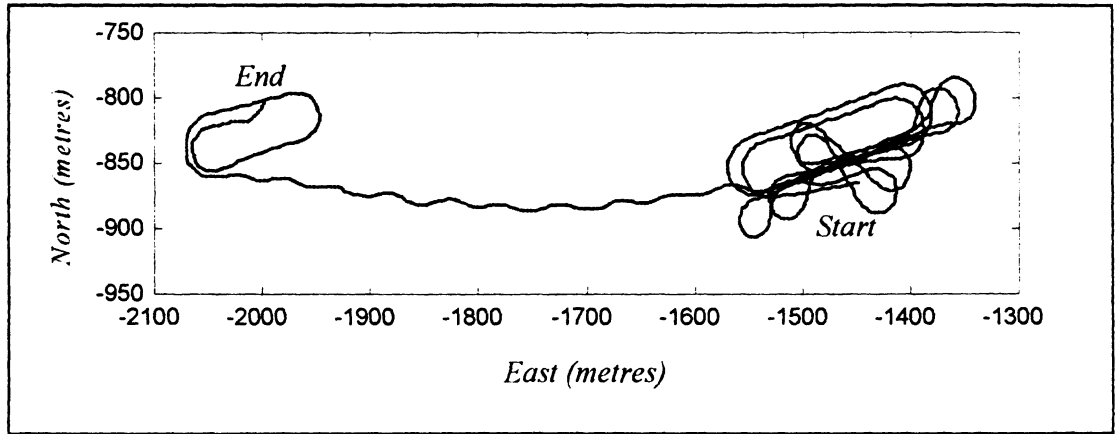


Figure C.2 - Vessel trajectory for period 2.

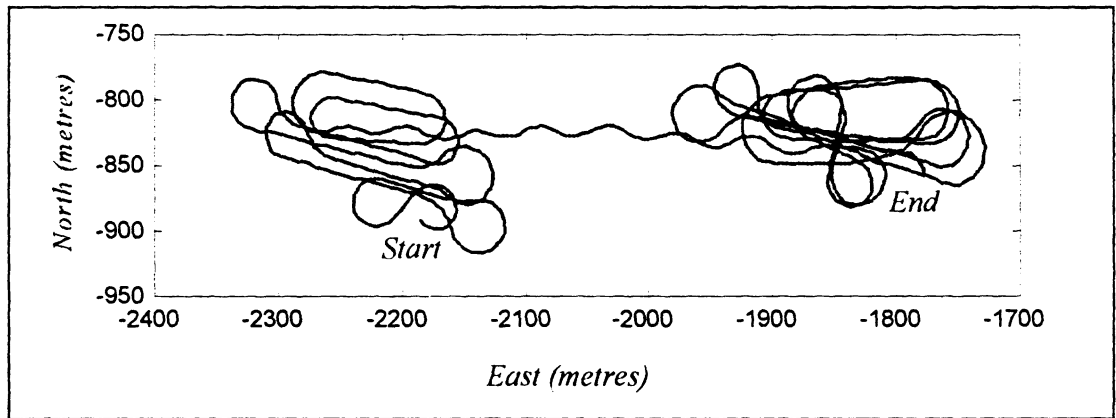


Figure C.3 - Vessel trajectory for period 3.

APPENDIX D

SATELLITE CONFIGURATION

Figures D.1, D.2 and D.3 show the satellite configuration for each of the three periods, when data from all the sensors (three vessel fixed GPS Ashtech antennas and POS/MV 320) were available (see Chapter 6). The legend is as follows: the numbers inside the circles stand for the GPS satellite PRN number, the azimuthal lines are separated by 15 degrees and the radial lines describe the satellite elevation, from 0 to 90 degrees with 30 degrees separation between consecutive lines. The satellite position in the plot is referred to its mean position during the observation period.

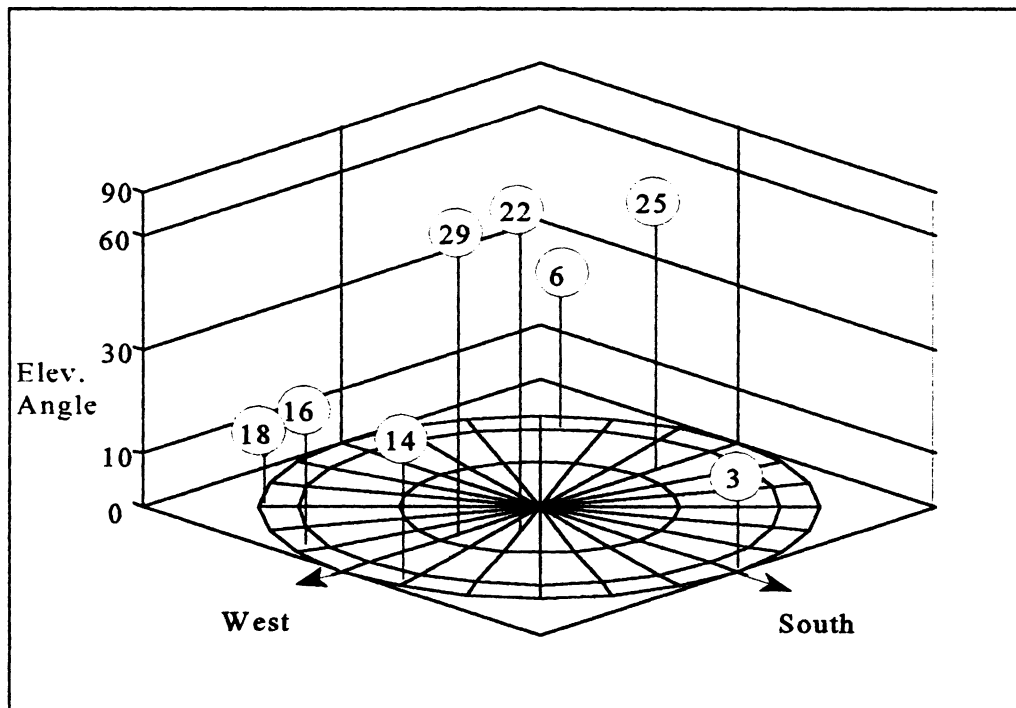


Figure D.1 - Satellite configuration for period 1.

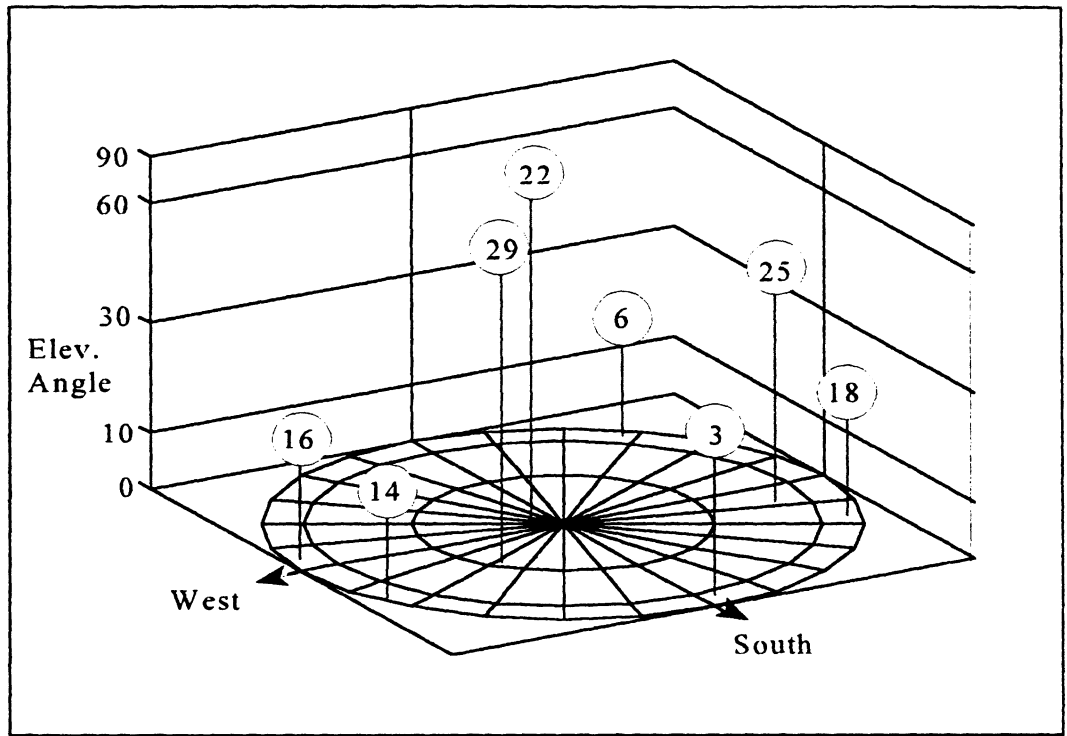


Figure D.2 - Satellite configuration for period 2.

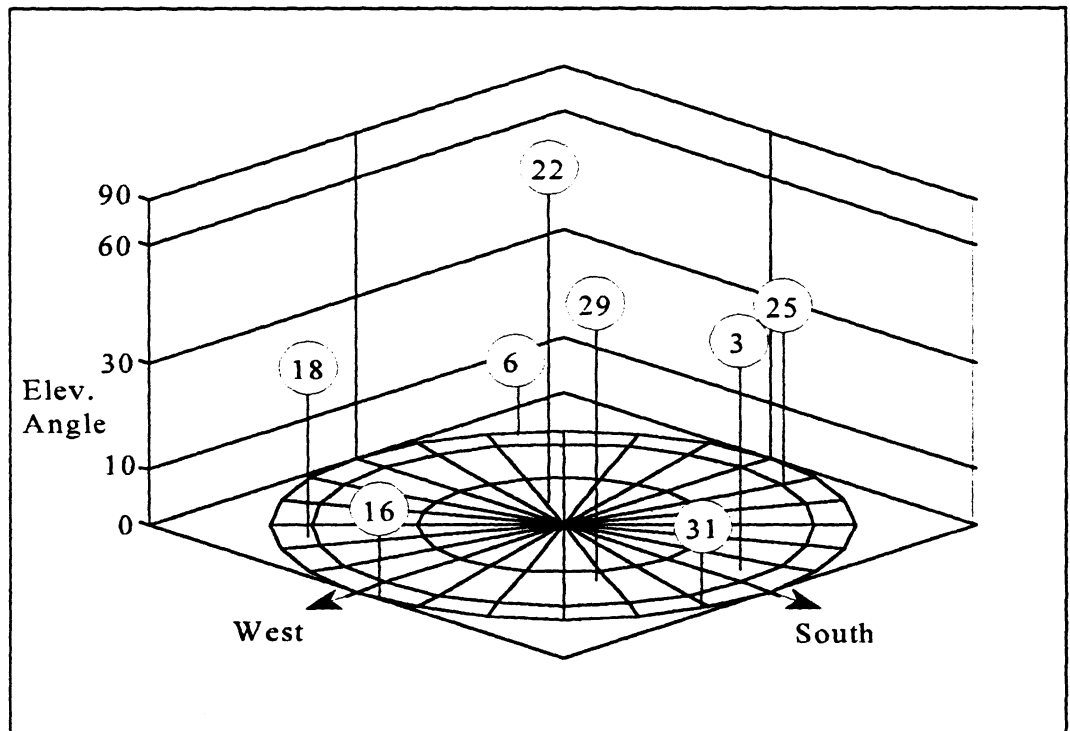


Figure D.3 - Satellite configuration for period 3.

Figure D.4 shows the PDOP and total number of satellites during each period of observation.

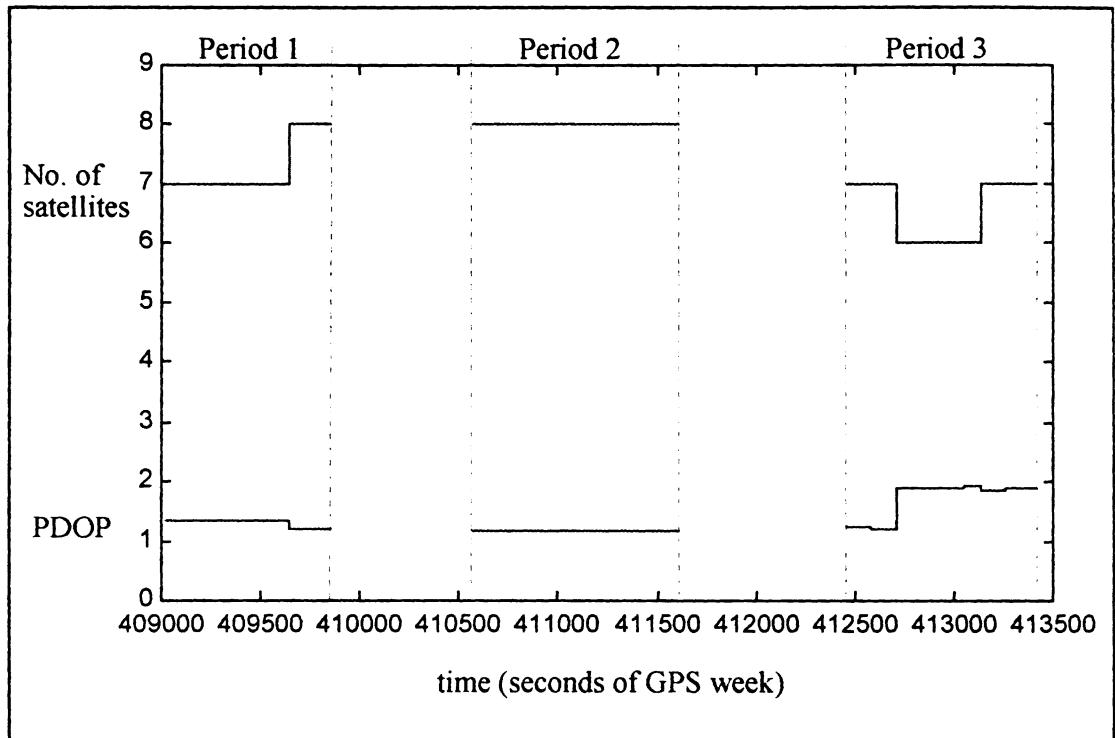


Figure D.4 - Total number of satellites and PDOP.

APPENDIX E

ATTITUDE DIFFERENCES BETWEEN GPS AND POS/MV 320

This appendix contains the plots for the heading, pitch and roll differences between GPS attitude results and POS/MV 320. In order to relate attitude differences with ship dynamics, plots of vessel speed and rate of change of heading are also represented.

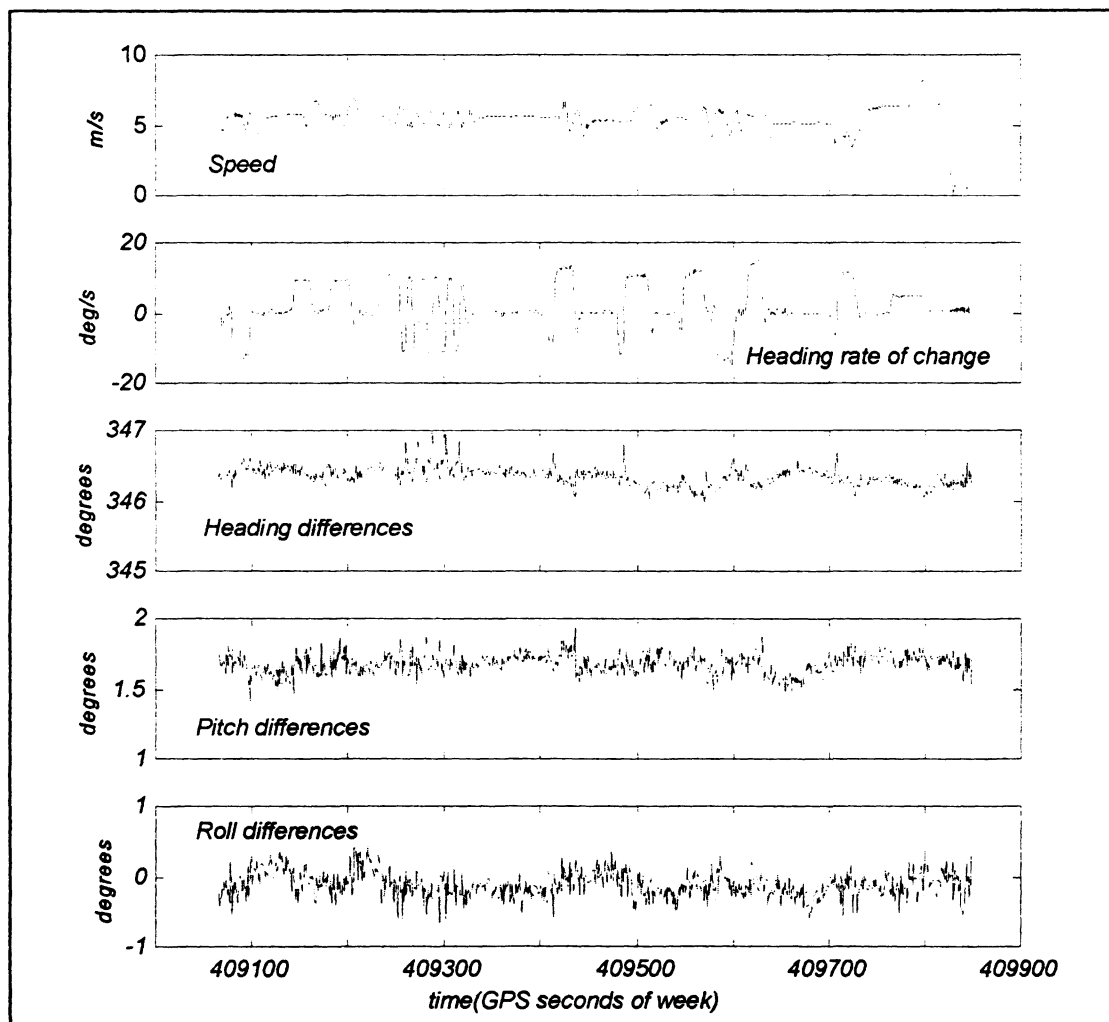


Figure E.1- Speed, rate of change of heading and attitude differences between POS/MV 320 and GPS during period 1.

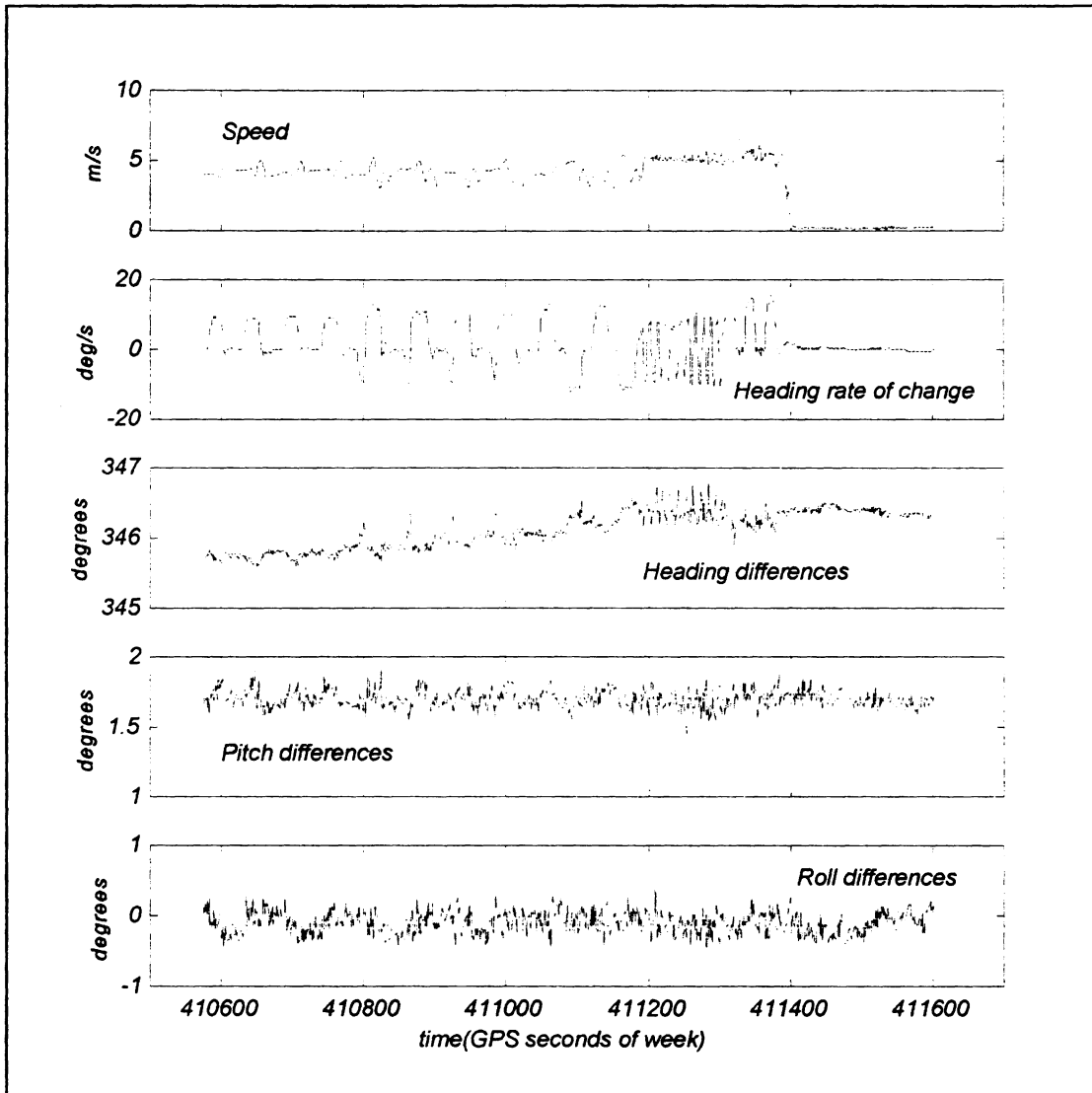


Figure E.2 - Speed, rate of change of heading and attitude differences between POS/MV 320 and GPS during period 2.

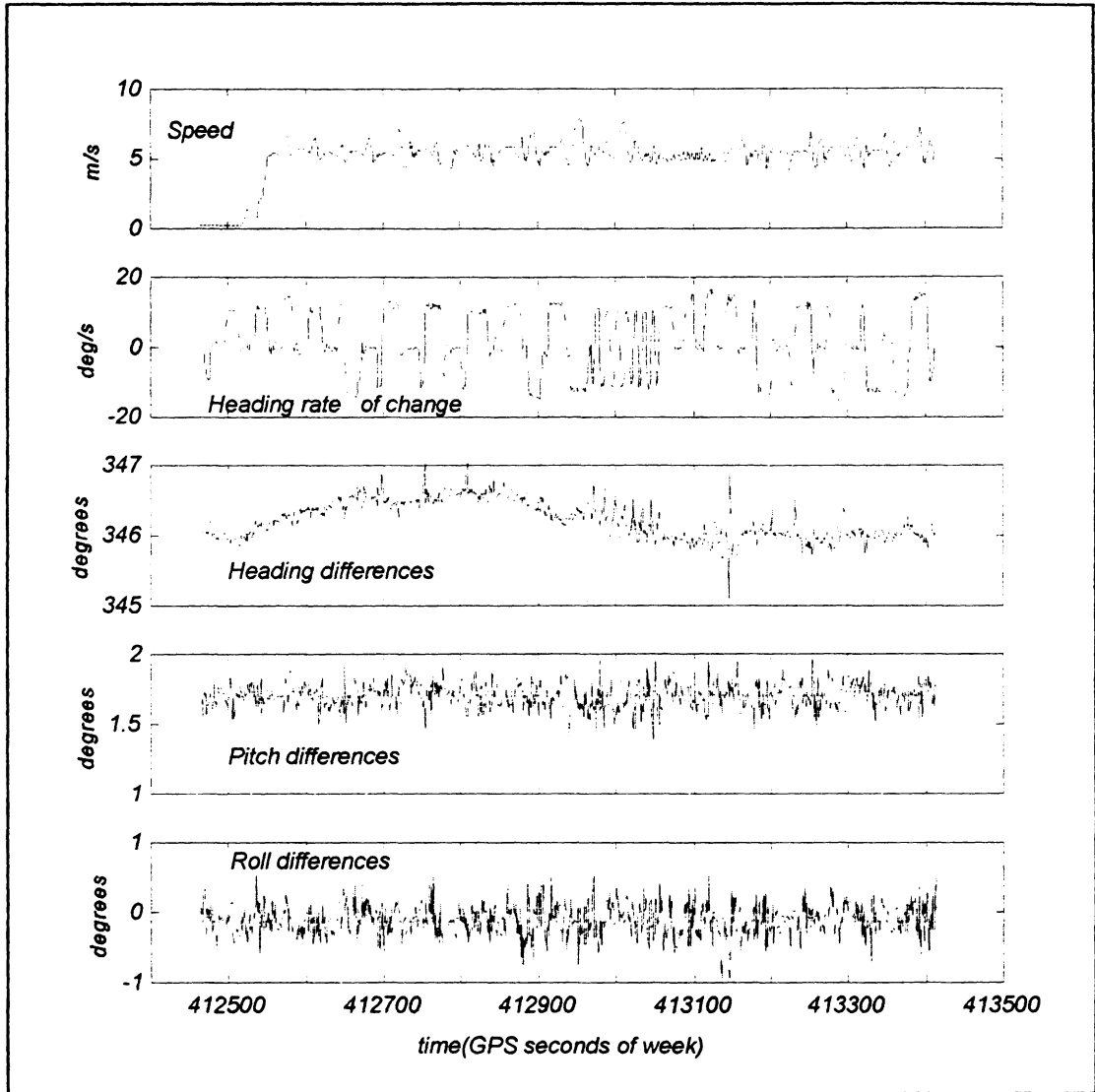


Figure E.3 - Speed, rate of change of heading and attitude differences between POS/MV 320 and GPS during period 3.

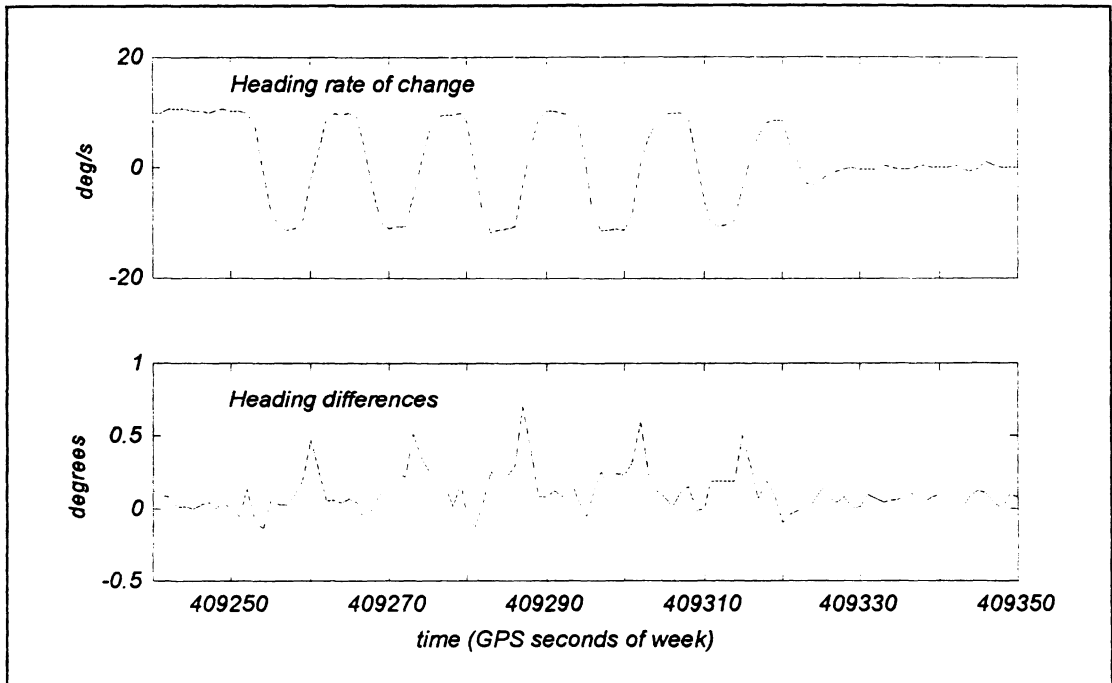


Figure E.4 - Rate of change of heading and heading differences, plot 1.

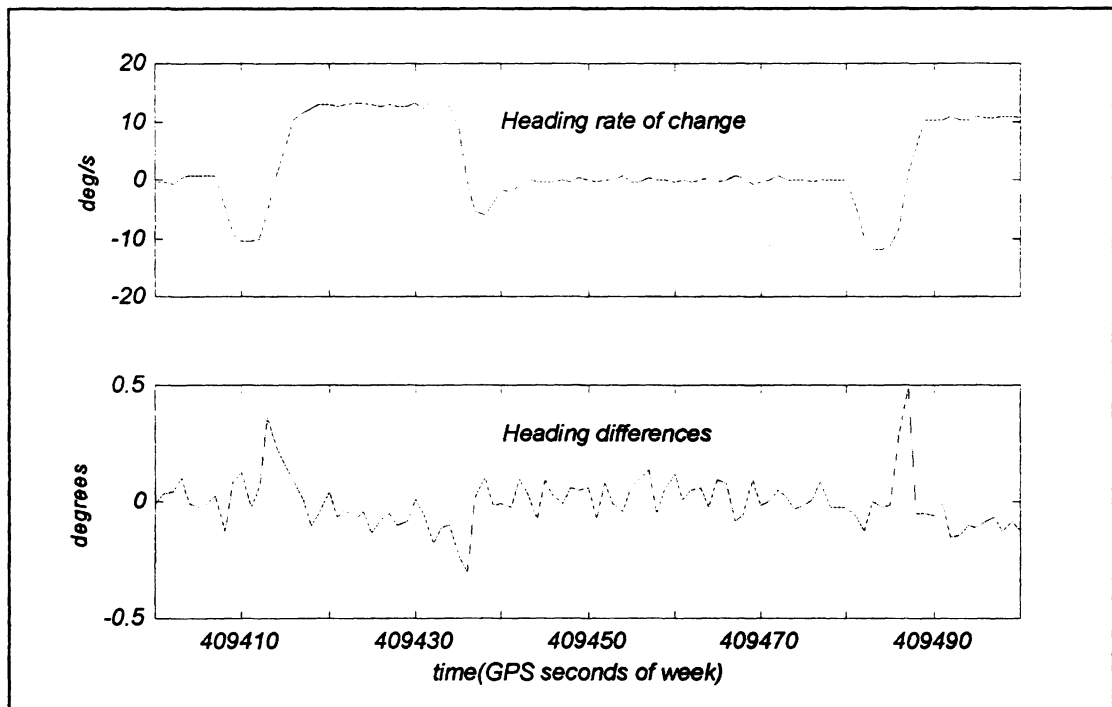


Figure E.5 - Rate of change of heading and heading differences, plot 2.

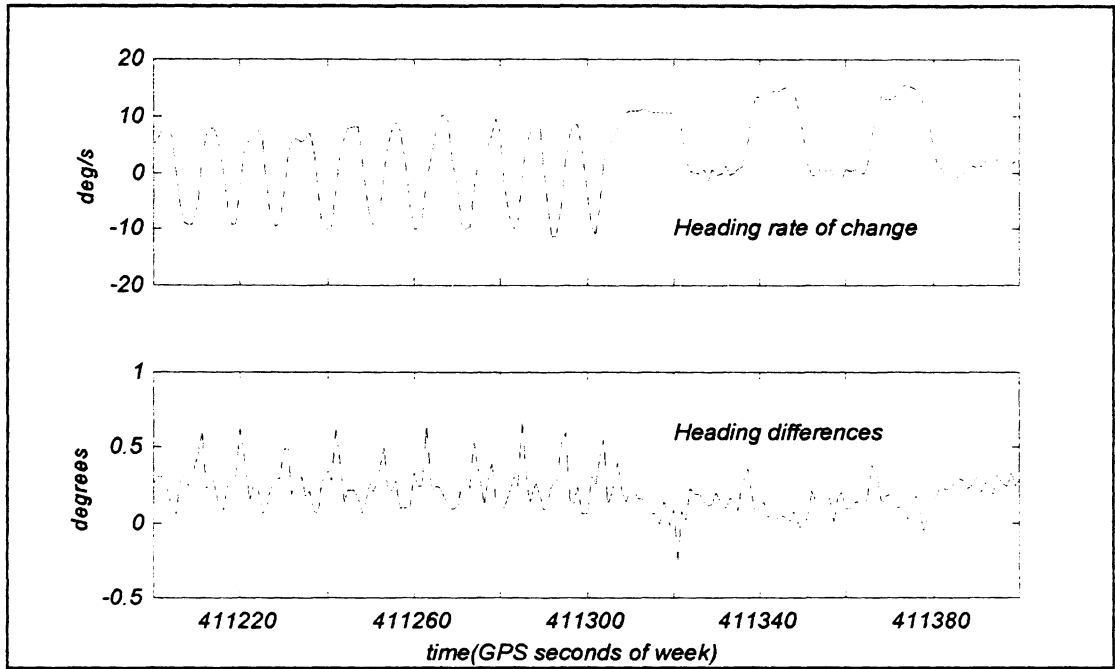


Figure E.6 - Rate of change of heading and heading differences, plot 3.

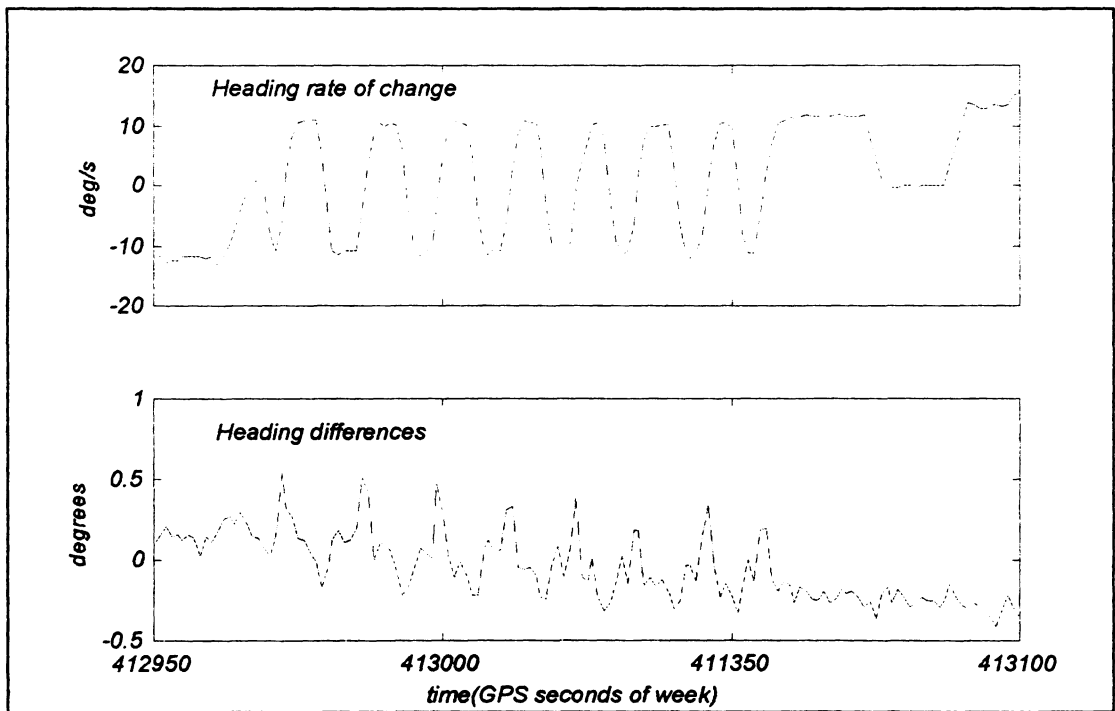


Figure E.7 - Rate of change of heading and heading differences, plot 4.

VITA

Candidate's full name: João Paulo Ramalho Marreiros

Place and date of birth: Lisbon, Portugal, on 22 July 1966

Permanent address: Rua Mousinho de Albuquerque,
Nº17, 2º Dº, Damaia,
2720 Amadora
Portugal

Schools attended: D. Pedro V High School, Lisbon, Portugal
(1978 - 1980)

Benfica High School, Lisbon, Portugal
(1980 - 1984)

Universities attended: Naval Academy, Almada, Portugal
Diploma in Naval Military Sciences
(1984 - 1989)

Hydrographic Institute, Lisbon, Portugal
Specialization Course in Hydrography
Certified with Category *A* from the International
Hydrographic Organization
(1991 - 1992)

University of Lisbon, Portugal
Faculty of Sciences, Department of Meteorology
Master's in meteorology (not concluded)
(1993 - 1995)

University of New Brunswick, Fredericton, Canada
Department of Geodesy and Geomatics Eng.
Master's of Engineering candidate (1995 - 1997)